NASA TM X-206

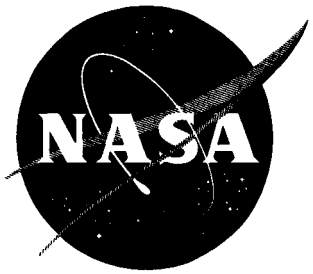

TECHNICAL MEMORANDUM

X-206

WIND-TUNNEL STUDIES AT SUBSONIC AND TRANSONIC SPEEDS OF A MULTIPLE-MISSION VARIABLE-WING-SWEEP AIRPLANE CONFIGURATION

By William J. Alford, Jr., Arvo A. Luoma,
and William P. Henderson

Langley Research Center
Langley Field, Va.

NATIONAL AERONAUTICS AND SPACE ADMINISTRATION

WASHINGTON

November 1959

NATIONAL AERONAUTICS AND SPACE ADMINISTRATION

TECHNICAL MEMORANDUM X-206

WIND-TUNNEL STUDIES AT SUBSONIC AND TRANSONIC SPEEDS OF A MULTIPLE-MISSION VARIABLE-WING-SWEEP AIRPLANE CONFIGURATION*

By William J. Alford, Jr., Arvo A. Luoma,
and William P. Henderson

SUMMARY

Wind-tunnel studies have been made to determine the aerodynamic characteristics of a variable-wing-sweep airplane configuration capable of performing multiple missions. The tests covered the Mach number range from 0.25 to 1.30 for the 75° wing-sweep condition but for other sweep angles was limited to a Mach number of 0.93. It was found that at subsonic speeds the longitudinal stability characteristics were essentially the same for both 25° and 75° of wing leading-edge sweep with no wing translation necessary and that the longitudinal control was adequate. There was a slight degree of instability at the higher lift coefficients which, however, does appear tolerable. The transonic aerodynamic-center shift was rather large and appears to be the most important aerodynamic problem. The lateral and directional stability and control appear satisfactory except possibly the lateral control in the low-sweep condition where the damping is high. For this condition it may be necessary to augment the roll control tail with wing-tip ailerons.

Author

INTRODUCTION

Reference 1 briefly summarizes the results of a wind-tunnel study at low speed aimed toward the development of a variable-sweep-aircraft configuration having satisfactory stability and control characteristics over a large sweep range and not requiring the wing translation which characterized previous variable-sweep aircraft. Such an aircraft could combine efficient supersonic cruise with good landing and take-off characteristics while avoiding the added complexity, weight, and performance

*Title, Unclassified.

penalties associated with wing translation. As discussed briefly in reference 1 an aircraft such as this would have desirable landing and take-off characteristics and be capable of performing both low and high altitude attack missions, combat air patrol missions, and as a supersonic transport its subsonic climb-out capability would alleviate the supersonic "bang" problem. In addition, the favorable range capability might reduce or eliminate the need for ferry tankers.

The configuration which finally evolved from the study exhibited almost identical low-speed longitudinal stability and control characteristics at 25° and 75° of sweep with a maximum static margin of only about $9\frac{1}{2}$ percent of the mean aerodynamic chord (including the moderate shift in center of gravity due to wing rotation) occurring at 50° of sweep, thereby eliminating the need for wing translation. This was accomplished, in the main, by providing a fixed portion of the wing ahead of the center of gravity. The instability contributed by this fixed portion increases as the rotating portion of the wing is swept back, due to the reduction in wing lift-curve slope and thereby tends to counteract the rearward shift of the rotating wing aerodynamic center. Adequate lateral and directional stability and control were also obtained throughout the sweep range and the lift-curve slope increased from about 0.045 to about 0.085 as the sweep decreased from 75° to 25°.

In view of the desirable low-speed characteristics of the configuration developed, the study was extended to high subsonic speeds for the complete sweep range and to transonic and supersonic speeds for the high sweep condition. The purpose of this paper therefore is to present the results of the high subsonic and transonic studies along with the complete results from the low-speed study. In addition to the basic configuration the low-speed study included tests of two canard tails to provide design information applicable to a possible retractable canard configuration. The supersonic results obtained at a Mach number of 2.01 are presented in reference 2 and therefore only the summary data will be repeated herein.

COEFFICIENTS AND SYMBOLS

The results are referred to the body-axis system except the lift and drag which are, of course, referred to the wind-axis system. (See fig. 1.) All coefficients are nondimensionalized with respect to the geometric characteristics associated with the maximum sweep condition. The moment center is located at 0.417 percent of the mean aerodynamic chord of the 75° sweep condition as shown in figure 2.

C_L lift coefficient, $\frac{\text{Lift}}{qS_w}$

C_D drag coefficient, $\frac{\text{Drag}}{qS_w}$

C_m pitching moment, $\frac{\text{Pitching moment}}{qS_w\bar{c}}$

C_l rolling-moment coefficient, $\frac{\text{Rolling moment}}{qS_wb}$

C_n yawing-moment coefficient, $\frac{\text{Yawing moment}}{qS_wb}$

C_Y side-force coefficient, $\frac{\text{Side force}}{qS_w}$

$C_{l_\beta} = \frac{\partial C_l}{\partial \beta}$, per deg

$C_{n_\beta} = \frac{\partial C_n}{\partial \beta}$, per deg

$C_{Y_\beta} = \frac{\partial C_Y}{\partial \beta}$, per deg

q dynamic pressure, lb/sq ft

R Reynolds number based on $\bar{c}$

S_w wing area (75° sweep condition), 1.916 sq ft

S_c canard-surface area, sq ft

$\bar{c}$ mean aerodynamic chord (75° sweep condition), 1.14 ft

b wing span (75° sweep condition), 1.89 ft

M Mach number

α angle of attack, deg

β angle of sideslip, deg

Λ	wing leading-edge sweep angle, deg
i_t	horizontal-tail deflection, deg
δ	deflection of left wing aileron or $i_{t,L} - i_{t,R}$ (for rolling tail)
C_{l_δ}	roll-control effectiveness parameter, per deg
C_{n_δ}	yawing-moment effectiveness parameter due to roll control, per deg
C_m/C_L	static margin, percent $\bar{c}$
C_{D_o}	drag at zero lift
C_{L_α}	lift-curve slope
$(L/D)_{max}$	maximum lift-drag ratio

L
7
7
0

MODEL AND TEST EQUIPMENT

Model

The model configuration tested was that referred to in reference 1 as configuration IV and a three-view drawing is presented in figure 2. The pivot point for the outer wing panels was located at approximately 56 percent of the semispan of the wing at $\Lambda = 75^\circ$. The wing panels had sweep angles of 12.5°, 25°, 50°, 62.5°, and 75°. The inboard panel was fixed at $\Lambda = 60^\circ$. The wing aspect ratio varied from 6.25 at 12.5° sweep to 1.88 at 75° sweep. The wing employed NACA 63_6A004.5 airfoil sections normal to the leading edge. The horizontal- and vertical-tail panels were identical in plan form. The all-movable horizontal tail, which was used for pitch control, was mounted on the body center line at -15° dihedral. Roll control could be provided by ailerons located at the wing tips or by differential deflection of the horizontal-tail panels. Two sizes of auxiliary canard surfaces were also tested. For tests with fixed transition narrow bands of No. 60 carborundum grains were placed along the 10-percent-chord lines of the lifting surfaces and around the fuselage at the 10-percent station.

Tunnels

The tests were made in the Langley high-speed 7- by 10-foot wind tunnel and the Langley 8-foot transonic pressure tunnel.

The Langley high-speed 7- by 10-foot tunnel is a rectangular solid-wall atmospheric tunnel capable of providing Mach numbers up to approximately 0.93 for the size model used in this investigation. The Langley 8-foot transonic pressure tunnel has a test section which is square in cross section. The upper and lower walls of the test section have longitudinal slots which permit continuous testing through the transonic speed range up to approximately $M = 1.30$. The total pressure of the flow in the tunnel can be varied.

Instrumentation

In both tunnels the model was internally instrumented with a six-component strain-gage balance and was sting mounted. Photographs of the model mounted on the sting in the Langley high-speed 7- by 10-foot tunnel are shown in figure 3. The data measured in the 7- by 10-foot tunnel were recorded on strip chart recording oscillographs while those in the Langley 8-foot transonic pressure tunnel were recorded electrically on punch cards.

TESTS, CORRECTIONS, AND ACCURACY

Tests

The major portion of the tests in the Langley high-speed 7- by 10-10-foot tunnel were made at a Mach number of 0.25 over an angle-of-attack range of -2° to 19°. The lateral and directional parameter tests were made at sideslip angles of -4° and 4°. A limited amount of data for Mach numbers from 0.60 to 0.93 were also obtained in the Langley high-speed 7- by 10-foot tunnel over a reduced angle-of-attack range.

The tests in the Langley 8-foot transonic pressure tunnel were made at Mach numbers generally from 0.80 to 1.30. The angle of attack varied from approximately -4° to the value corresponding to the wing load limit. The configurations with the horizontal tail deflected 0° and with the horizontal tail removed were tested at a total pressure of both 2,120 lb/sq ft (1.0 atmosphere) and 800 lb/sq ft (0.38 atmosphere). The lower total pressure was used to extend the angle-of-attack range of the tests. The other test configurations were investigated at a total pressure of 800 lb/sq ft. A limited amount of data were obtained at a total pressure of 1,000 lb/sq ft.

The tunnel air was dried sufficiently to avoid condensation effects. The tests were made at a stagnation temperature of 122° F. A plot of the average Reynolds number, based on $\bar{c}$, of the investigation against Mach number at the various test total pressures is given in figure 4. The variation of Reynolds number for the tests in the Langley high-speed 7- by 10-foot tunnel is also shown.

Corrections

Jet-boundary and blockage corrections as calculated by the methods of references 3 and 4, respectively, have been applied to the data measured in the solid-wall tunnel (high-speed 7- by 10-foot tunnel).

For the tests in the slotted-wall tunnel (8-foot transonic pressure tunnel) at subsonic speeds the interference effects of the tunnel boundary were considered negligible. At a Mach number of 1.3 the data were clear of the interference effects of wall-reflected disturbances. At Mach numbers of 1.03, 1.06, 1.13, and probably 1.2 the flow over the model was subject to influence by wall-reflected disturbances. Previous results have indicated that the interference effects of wall-reflected disturbances are small at a Mach number of 1.03. At Mach numbers of 1.06, 1.13, and 1.2 the magnitudes and slopes of the force and moment data obtained herein show no obvious irregularities or changes which can be ascribed to interference effects. The nose angle (total) of the fuselage was small, varying from 7.5° in the vertical plane to 14.3° in the horizontal plane. This small value of the nose angle would tend to make the interference effects of the wall-reflected fuselage-nose shock small. Also, the varying nose angle would spread out the interference effects axially on the model surface, and one might thereby expect a lessening of the interference effects on overall forces and moments. The results at Mach numbers of 1.06, 1.13, and 1.2 are probably adequate (as regards freedom from interference effects) for most applications.

At a Mach number of 1.3 the nose of the fuselage was located in a static-pressure gradient, requiring a small buoyancy correction to the drag data. This correction consisted of reducing the measured drag coefficients at a Mach number of 1.3 by 0.0010. At the other Mach numbers no buoyancy correction was required.

The base pressure was measured and all drag data were corrected to a base pressure equal to free-stream static pressure.

The angles of attack and sideslip were corrected for the deflection of the sting and balance under load. No sting interference corrections have been made to the data except to the extent of the partial correction for sting interference inherent in the base-pressure correction.

No corrections have been made to the data for bending of the model structural components under aerodynamic load.

Accuracy

The estimated accuracy of the quantities measured in the Langley high-speed 7- by 10-foot tunnel at $M = 0.25$ is as follows:

C_L	±0.009
C_D	0.0025
C_m	0.0010
C_l	0.0003
C_n	0.0004
α, deg	±0.1
β, deg	±0.1

The results at the higher Mach numbers would be more accurate because of the higher loads involved.

The estimated accuracy of the data from the Langley 8-foot transonic pressure tunnel at a total pressure of 1.0 atmosphere (2,120 lb/sq ft) is essentially the same as that obtained in tests at high subsonic speeds in the Langley high-speed 7- by 10-foot tunnel. The accuracy of the data at a total pressure of 800 lb/sq ft is poorer because of the smaller aerodynamic forces and moments acting on the model.

PRESENTATION OF RESULTS

Results at Low Speeds

A fairly complete study of the longitudinal aerodynamic characteristics was made at a Mach number of 0.25 for sweep angles of 12.5°, 25°, 50°, 62.5°, and 75° over a range of angles of attack from -2° to 19° in the Langley high-speed 7- by 10-foot tunnel. The basic data are presented in figures 5 to 19 according to the following outline:

	Figure
Effect of sweep angle	
Basic configuration ($i_t = 0°$)	5
Basic configuration (horizontal tail off)	6
Basic configuration with small canard ($i_t = 0°$)	7
Basic configuration with small canard (horizontal tail off)	8
Basic configuration with large canard ($i_t = 0°$)	9
Basic configuration with large canard (horizontal tail off)	10

Results at High Subsonic Speeds

A series of tests limited to low angles of attack were made at Mach numbers up to 0.93 in the Langley high-speed 7- by 10-foot tunnel to determine the effect of sweep throughout the probable Mach number range for wing rotation. The results are presented in figures 20 and 21.

Results at Transonic Speeds

A rather complete set of tests were made with the high-sweep configuration ($\Lambda = 75^\circ$) in the Langley 8-foot transonic pressure tunnel and the basic data are presented in figures 22 to 27 according to the following outline:

ANALYSIS OF RESULTS

Results at Low Speeds

Since the results obtained at a Mach number of 0.25 have been discussed in reference 1 only a few observations will be made here. From figure 5 it can be seen that the 12.5° and 25° sweep conditions have essentially the same lift and drag characteristics. However, since the 25° sweep condition provides longitudinal stability characteristics which are very similar to those provided by the 75° condition it would appear that the 25° condition should be considered as the low-sweep condition. Some degree of instability is evident at the higher lift coefficients but comparisons with contemporary airplane configurations indicate that these characteristics are probably tolerable. However, if this instability should prove to be a problem a careful tailoring of stall control devices should provide an adequate solution. In addition to the fact that the longitudinal stability is essentially the same for both the high- (75°) and low-sweep (25°) conditions it is pertinent to note that the maximum aerodynamic-center shift relative to the 25° sweep condition occurred in the intermediate sweep angles and corresponded to $6\frac{1}{2}$ percent of the mean aerodynamic chord (fig. 21). This extremely small shift eliminates the need for wing translation and thereby avoids the added complexity, weight, and performance penalities associated with this wing translation.

The maximum trimmed lift-drag ratios increased from 7.1 at a sweep angle of 75° (fig. 13) to 10.8 at a sweep angle of 12.5° (fig. 11). The lift coefficient developed at a reasonable landing attitude of 15° was approximately 0.25 higher at 25° sweep than at 75° sweep. This, plus the fact that flaps should be more effective at the lower sweep, points to a considerable reduction in the landing speed.

The lateral and directional stability and control characteristics (figs. 18 and 19) appear satisfactory except possibly the roll control provided by the tail for the low-wing-sweep condition where the damping is high. Wing-tip ailerons may be necessary to augment this condition.

Results at High Subsonic Speeds

Inasmuch as the transition from one sweep condition to the other would, in all probability, be made at moderate or high subsonic Mach numbers, additional tests were made in the Langley high-speed 7- by 10-foot tunnel to determine the effect of sweep angle on the longitudinal stability characteristics at high subsonic speeds. Tests were made at Mach numbers up to 0.93 for an angle-of-attack range limited by the

strength of the model and the basic data are presented in figure 20. For the two design conditions (25° and 75° wing sweep), data were obtained with both free and fixed transition. For the limited angle-of-attack range covered, the effect of fixing transition was mainly limited to an increase in minimum drag. The effect of wing sweep angle on the longitudinal stability characteristics at several subsonic Mach numbers is summarized in figure 21 where the slope of the pitching-moment curves $C_{m_{C_L}}$ (at low lift coefficients) are presented as a function of sweep angle. If the center of gravity is assumed to be invariant with sweep angle and fuel consumption and to lie at the moment reference (see fig. 2) the values presented in figure 21 represent the static margin of the aircraft. The results indicate that the effect of sweep on the static margin is essentially independent of Mach number for Mach numbers up to 0.80. As the Mach number is increased to 0.91 there is an increase in the static margin for the 25° sweep condition of about 4 percent of the mean aerodynamic chord of the 75° wing. This increase in static margin due to Mach number decreases as the sweep increases. For a constant Mach number the largest change in static margin encountered in rotating the wing from 25° sweep to 75° sweep occurred at 50° sweep and amounted to only about $6\frac{1}{2}$ percent of the mean aerodynamic chord.

L 7 7 0

Results at Transonic Speeds

Tests in the Langley 8-foot transonic pressure tunnel were made only for the high-speed configuration (75° sweep).

Lift characteristics.- The variation of lift coefficient with angle of attack at transonic speeds is quite similar to that encountered at low speeds in that there is a substantial change in slope in a small range of angles of attack near 4°. (See fig. 22, for example.) At angles of attack below and above this range, the variation of lift coefficient with angle of attack was essentially linear. The lift-curve slope increased between lift coefficients of 0 and 0.4 by about 30 percent at subsonic speeds and by about one-half that amount at supersonic speeds.

Figure 28 presents the lift-curve slope at zero lift coefficient as a function of Mach number for the complete configuration. The lift-curve slope at zero lift coefficient increased by about 15 percent between a Mach number of 0.60 and the supersonic Mach numbers (fig. 28). The lift-curve slope measured at a Mach number of 2.01 (ref. 2) is also shown in figure 28.

Pitching-moment characteristics.- The variation of pitching-moment coefficient with lift coefficient is generally nonlinear. (See fig. 22, for example.) Decreases in stability, tending toward pitch-up characteristics, are evident at intermediate lift coefficients at the lower

Mach numbers. Except possibly for the case $M = 0.6$ the unstable tendencies are minor and for Mach numbers above about 0.90 the nonlinearities consisted mainly of gradual increases in stability with increasing lift coefficient. Since the 75° sweep phase of the various missions of such an aircraft would, in all probability, involve Mach numbers considerably above 0.60 it would appear that the variation of pitching moment with lift coefficient is satisfactory.

It will be noted that increases in tunnel pressure results in reductions in stability. It is believed that this reduction is due to increased aeroelastic effects rather than Reynolds number changes.

The increase in stability with increasing Mach number is apparent in figures 22 to 25 and is summarized in figure 28. In figure 28 the longitudinal stability parameter $C_{m_{C_L}}$ is presented as a function of Mach number and it will be noted that the increase with Mach number in the transonic range corresponds to about a 10-percent increase in static margin (based on $\bar{c}$). The value measured at a Mach number of 2.01 (ref. 2) is also presented and indicates an additional 11-percent increase in static margin. This increase in stability is undesirable and devices such as extendable canard surfaces or a variable dihedral horizontal tail may have to be resorted to.

Drag characteristics.- In the fairing of the drag data test points greater weight was given to the results at a total pressure of 2,120 lb/sq ft than to those at the lower total pressures, because of the better drag accuracy at the total pressure of 2,120 lb/sq ft.

The transonic drag-coefficient rise for the configuration with a horizontal-tail incidence of 0° amounted to 0.006 (fig. 29). The variation of the maximum lift-drag ratio with Mach number for both the zero stabilizer condition and the trimmed condition are also shown in figure 29. The trim value of maximum lift-drag ratio varied from 8.2 at a Mach number of 0.80 to about 6.0 at a Mach number of 1.3. The corresponding horizontal-tail incidence for trim varied from -1.3° to -4.5°, and the lift coefficient for trim from 0.20 to 0.26.

At a Mach number of 2.01 a trimmed value of lift-drag ratio of about 5.3 was obtained. In view of the fact that no attempt was made to obtain the optimum configuration from a supersonic performance standpoint, this lift-drag ratio appears to be reasonable for the wind-tunnel Reynolds numbers. It must be kept in mind, however, that no air inlets or canopy were incorporated on this model.

Lateral control.- Differential deflection of the horizontal-tail panels was used for lateral control and the basic results obtained for 5° deflections are presented in figure 27. The results indicate that the

roll effectiveness is relatively independent of angle of attack and Mach number. The variation of C_{l_δ} and C_{n_δ} $(\delta = i_{t,L} - i_{t,R})$ with Mach number at $\alpha = 0^\circ$ from the transonic tests is presented in figure 30 along with values from the tests at low subsonic and supersonic speeds. The value C_{l_δ} varies from approximately 0.00075 at $M = 0.25$ to about 0.00056 at $M = 2.01$. The variation of C_{n_δ} is also shown in figure 30 and it will be noted that it varies from about 0.0009 at $M = 0.25$ to about 0.0005 at $M = 2.01$. The differential tail appears to offer sufficient roll control and yawing moments in the direction to augment the roll. The large magnitudes of the yawing moments may present a problem, however.

CONCLUDING REMARKS

The wind-tunnel studies discussed herein indicate that a variable-sweep-airplane configuration can be designed such that the subsonic longitudinal stability characteristics will be essentially the same for both 25° and 75° of wing leading-edge sweep without the use of wing translation. This is accomplished, in the main, by providing a fixed portion of the wing ahead of the center of gravity. The instability contributed by this fixed portion increases, as the rotating portion of the wing is swept back, due to the reduction in wing lift-curve slope and thereby tends to counteract the rearward shift of the rotating wing aerodynamic center. Tests at transonic and supersonic speeds for the 75° sweep condition indicated a rather large rearward aerodynamic-center shift but the trimmed lift-drag ratios were still relatively high, with a value of 5.3 being obtained at a Mach number of 2.01. This increase in stability at supersonic speeds could, of course, be reduced by the use of extendable canard surfaces or by a variable dihedral horizontal tail.

The longitudinal control is adequate for all conditions and the lateral and directional stability and control appear satisfactory except possibly the lateral control in the low-sweep condition where the damping is high. For this condition it may be necessary to augment the roll control tail with wing-tip ailerons.

Langley Research Center,
National Aeronautics and Space Administration,
Langley Field, Va., September 11, 1959.

REFERENCES

1. Alford, William J., Jr., and Henderson, William P.: An Exploratory Investigation of the Low-Speed Aerodynamic Characteristics of Variable-Wing-Sweep Airplane Configurations. NASA TM X-142, 1959.

2. Spearman, M. Leroy, and Foster, Gerald V.: Stability and Control Characteristics at a Mach Number of 2.01 of a Variable-Wing-Sweep Configuration With Outboard Wing Panels Swept Back 75°. NASA TM X-32, 1959.

3. Gillis, Clarence L., Polhamus, Edward C., and Gray, Joseph L., Jr.: Charts for Determining Jet-Boundary Corrections for Complete Models in 7- by 10-Foot Closed Rectangular Wind Tunnels. NACA WR L-123, 1945. (Formerly NACA ARR L5G31.)

4. Herriot, John G.: Blockage Corrections for Three-Dimensional-Flow Closed-Throat Wind Tunnels, With Consideration of the Effect of Compressibility. NACA Rep 955, 1950. (Supersedes NACA RM A7B28.)

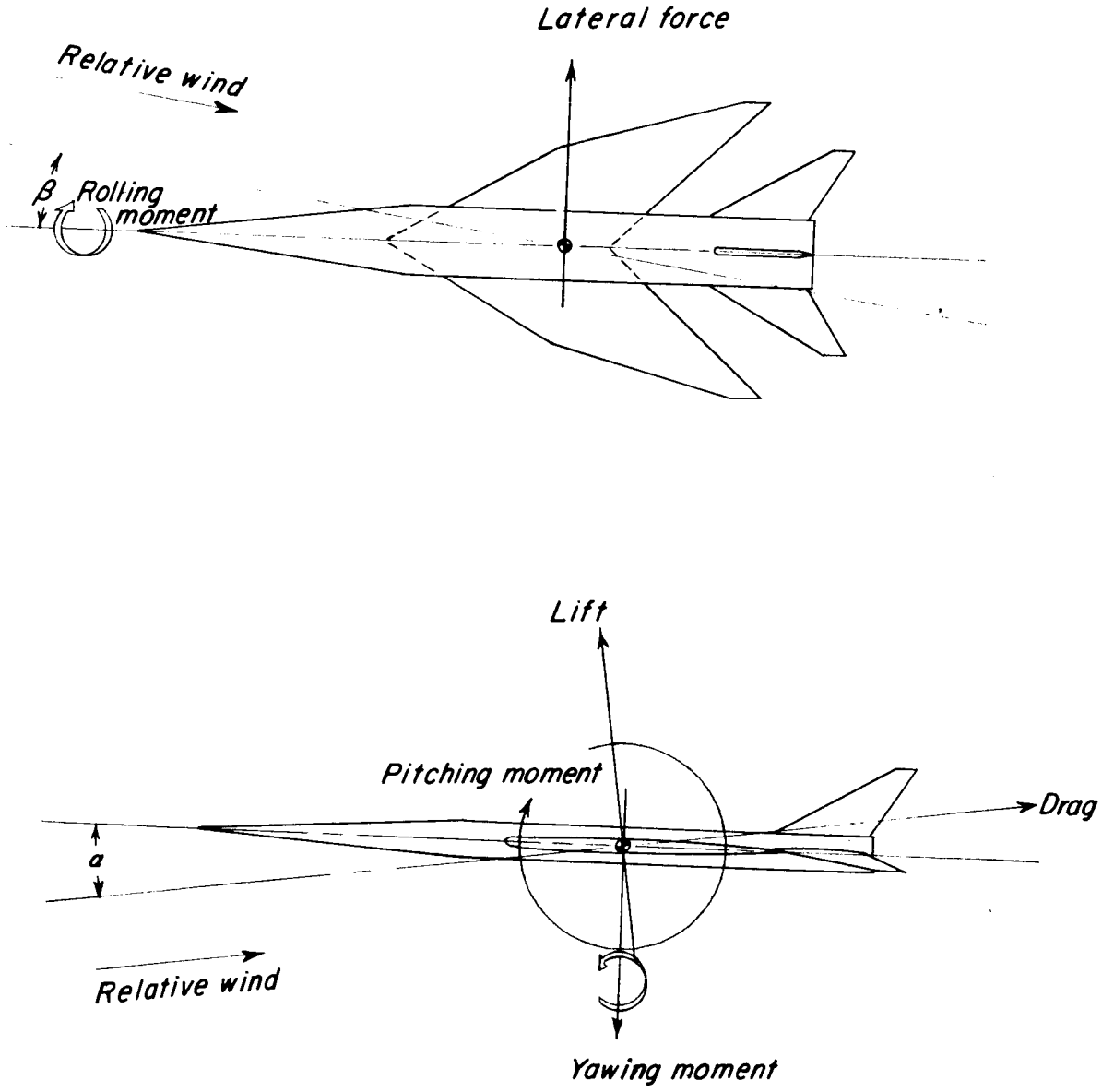

Figure 1.- System of axes used showing positive direction of forces, moments, and angles.

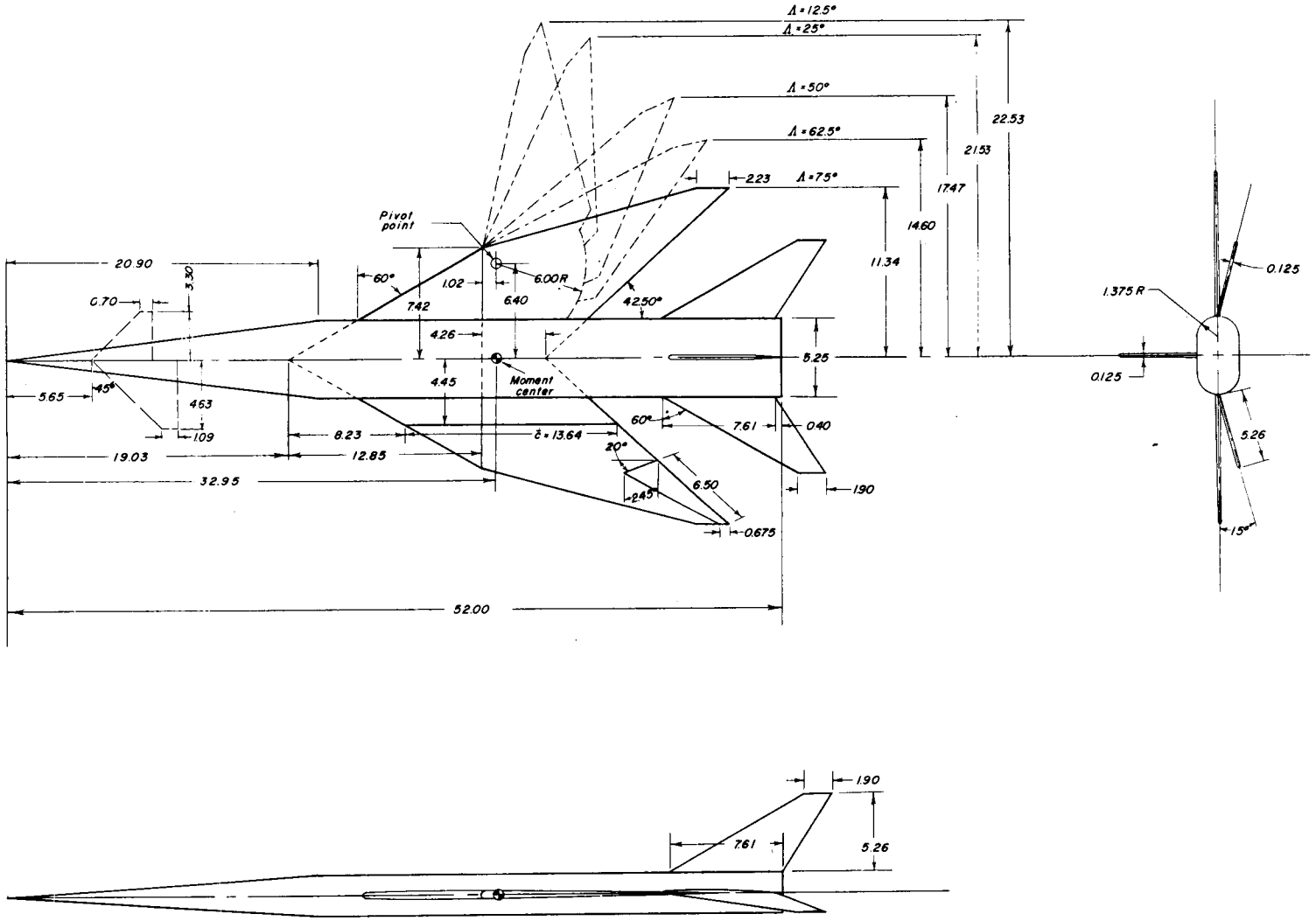

Figure 2.- Drawing of the variable-sweep configuration. All dimensions are in inches.

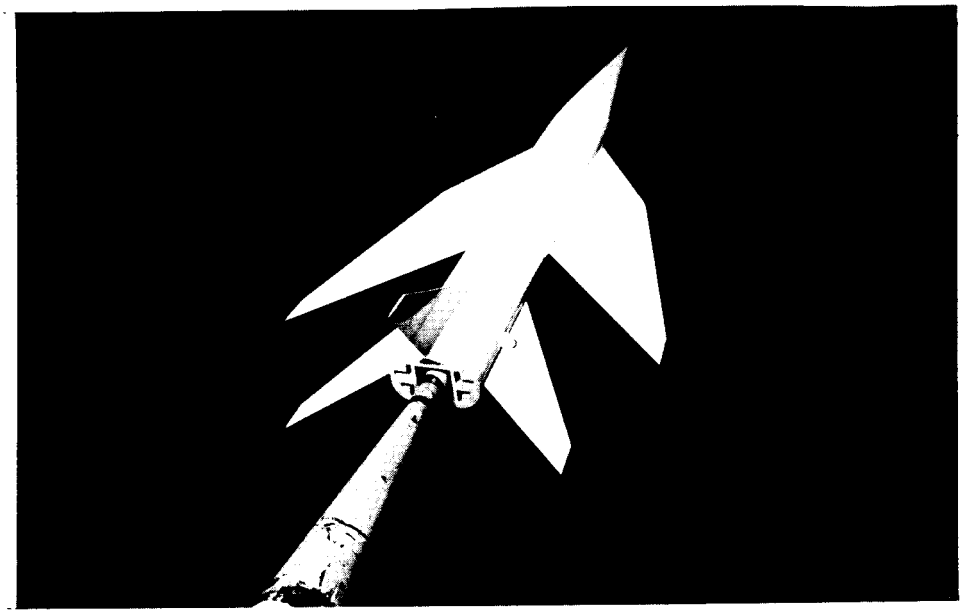

(a) $\Lambda = 75^{\circ}$. L-59-2044

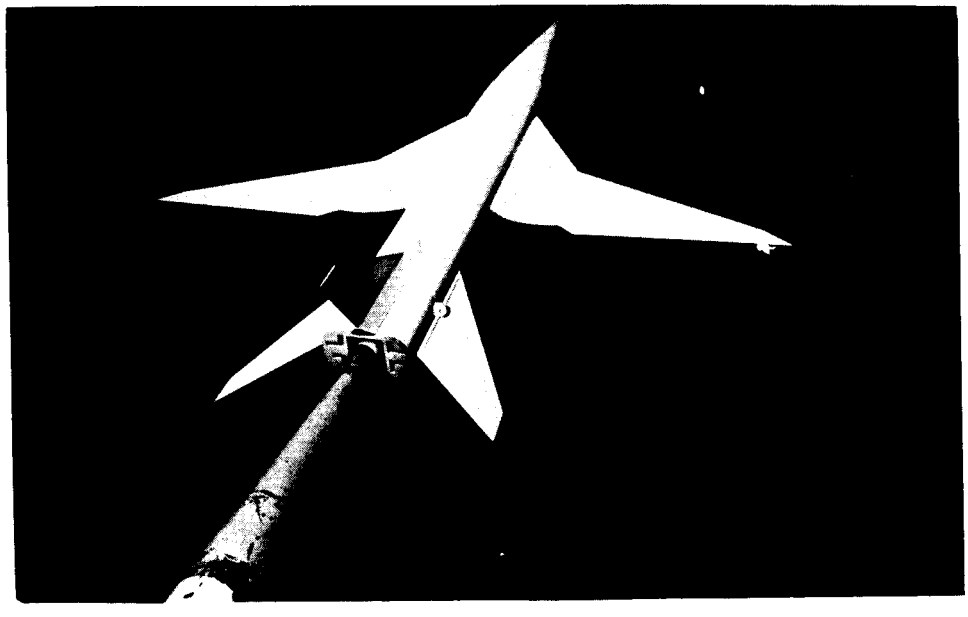

(b) $\Lambda = 25^{\circ}$. L-59-2045

Figure 3.- Photographs of the variable-sweep configuration sting mounted in the Langley 7- by 10-foot wind tunnel.

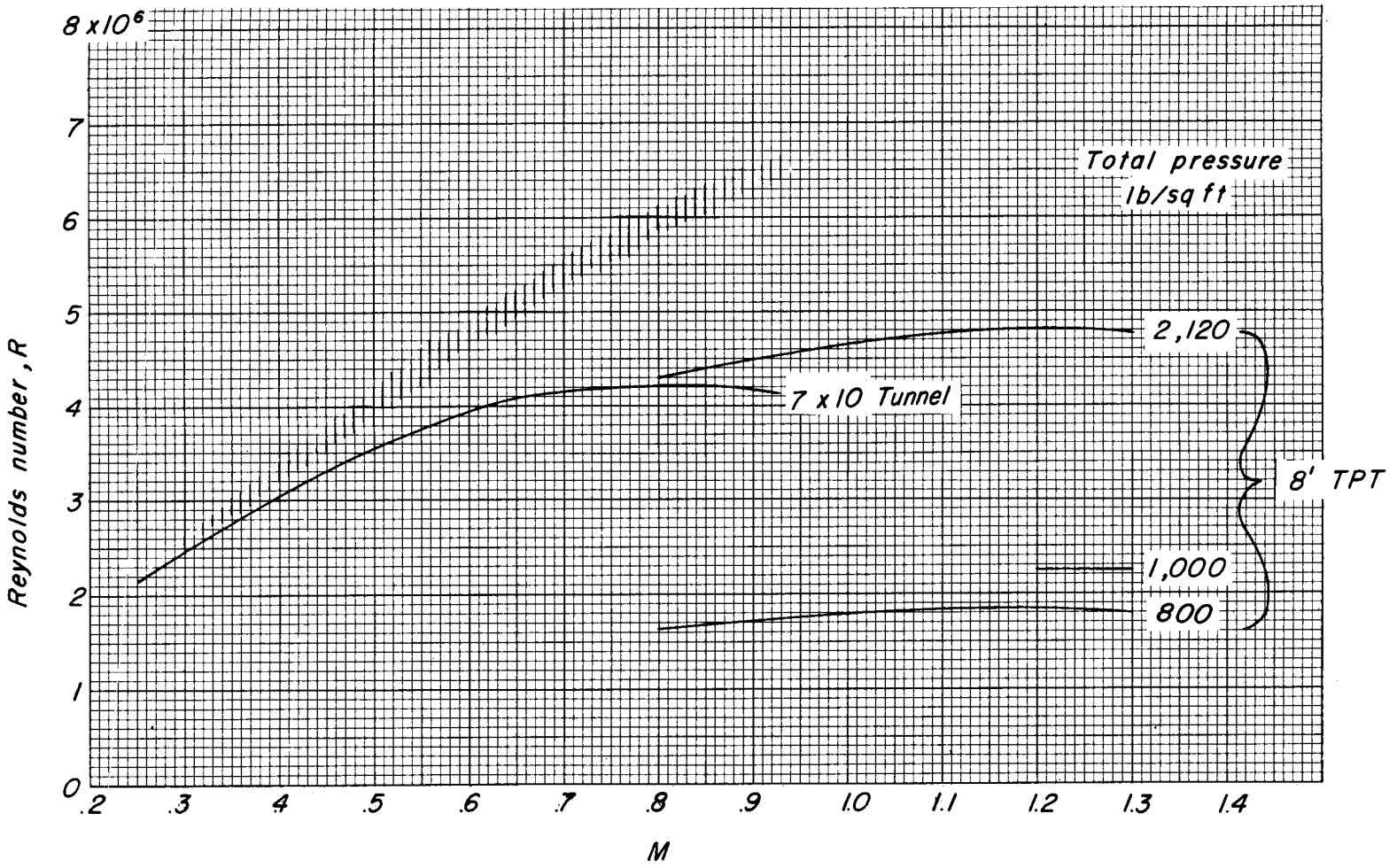

Figure 4.- Variation of Reynolds number (based on wing mean aerodynamic chord of 13.64 inches) with Mach number in test of model in the Langley 7- by 10-foot tunnel and the Langley 8-foot transonic pressure tunnel.

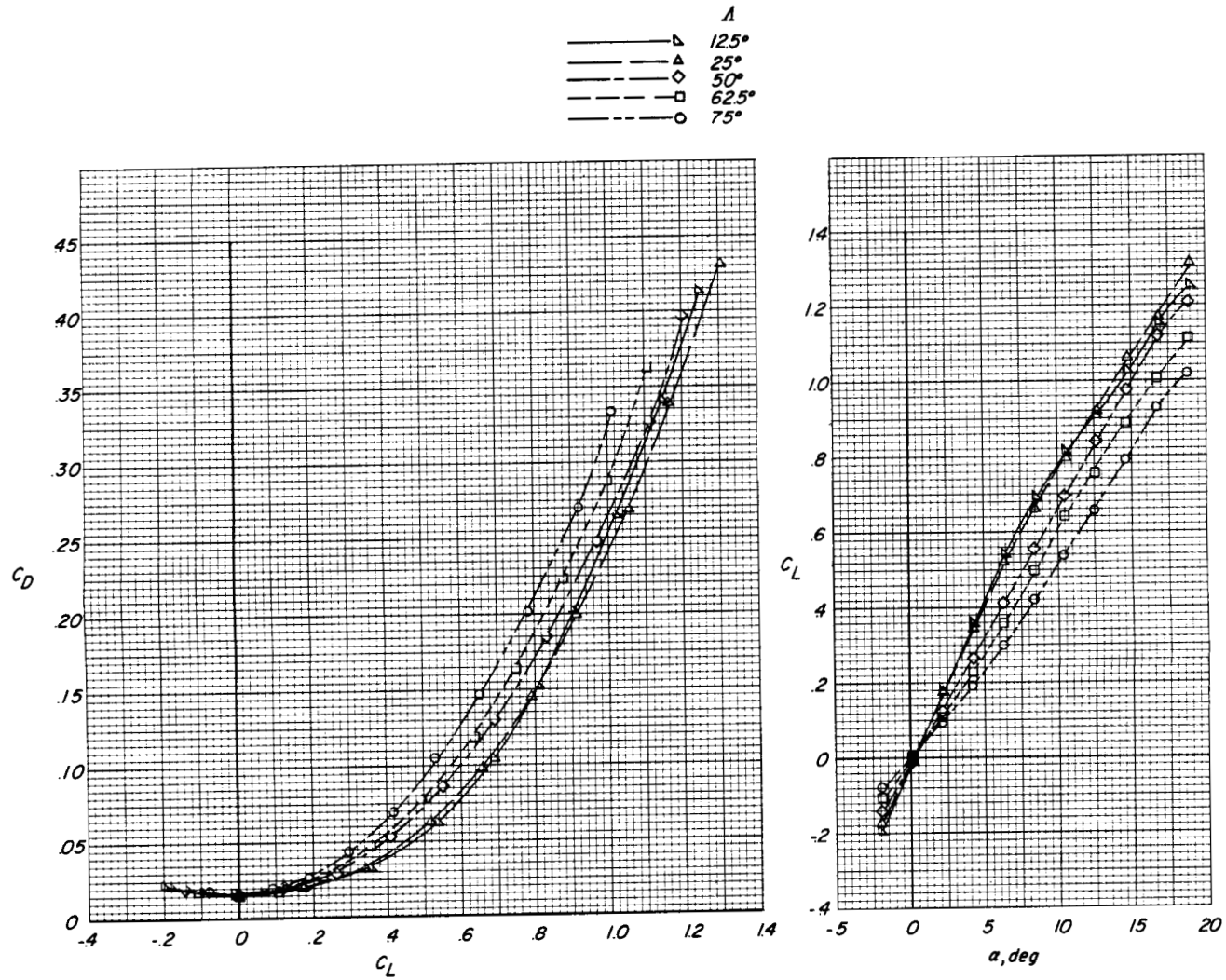

Figure 5.- Effect of wing leading-edge sweep angle on the longitudinal aerodynamic characteristics. Horizontal tail $i_t = 0^o$; M = 0.25.

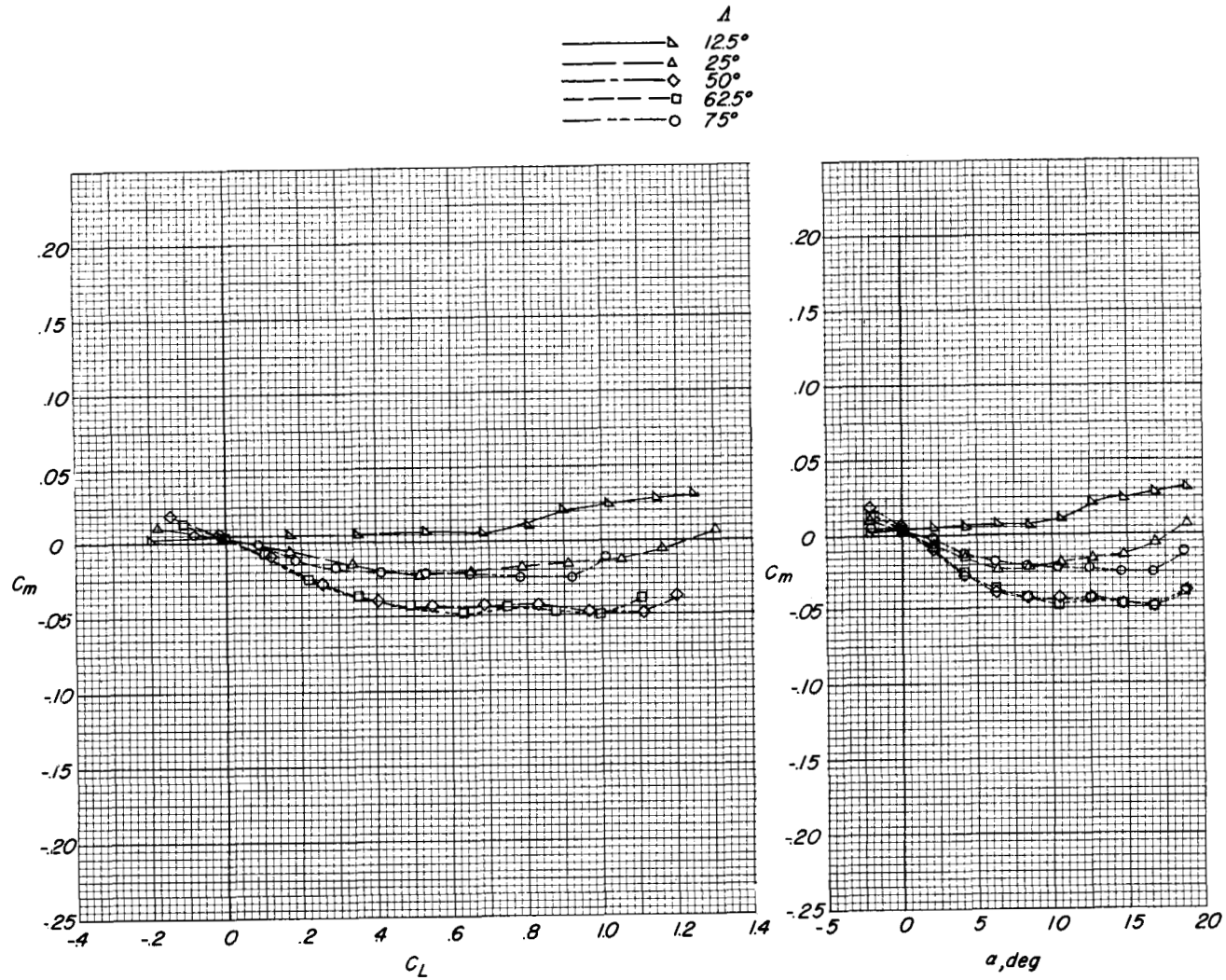

Figure 5.- Concluded.

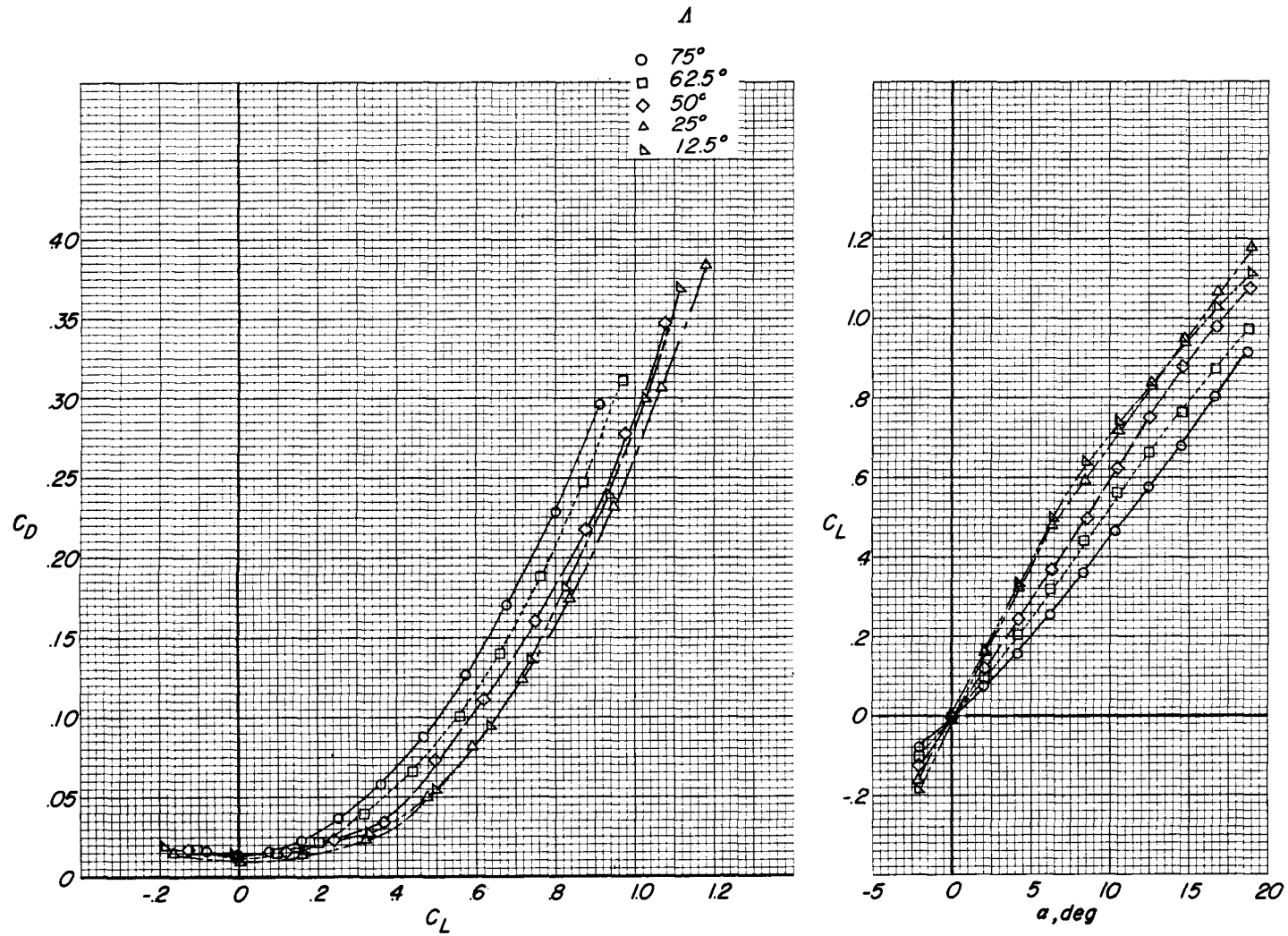

Figure 6.- Effect of wing leading-edge sweep angle on the longitudinal aerodynamic characteristics. Horizontal tail off; M = 0.25.

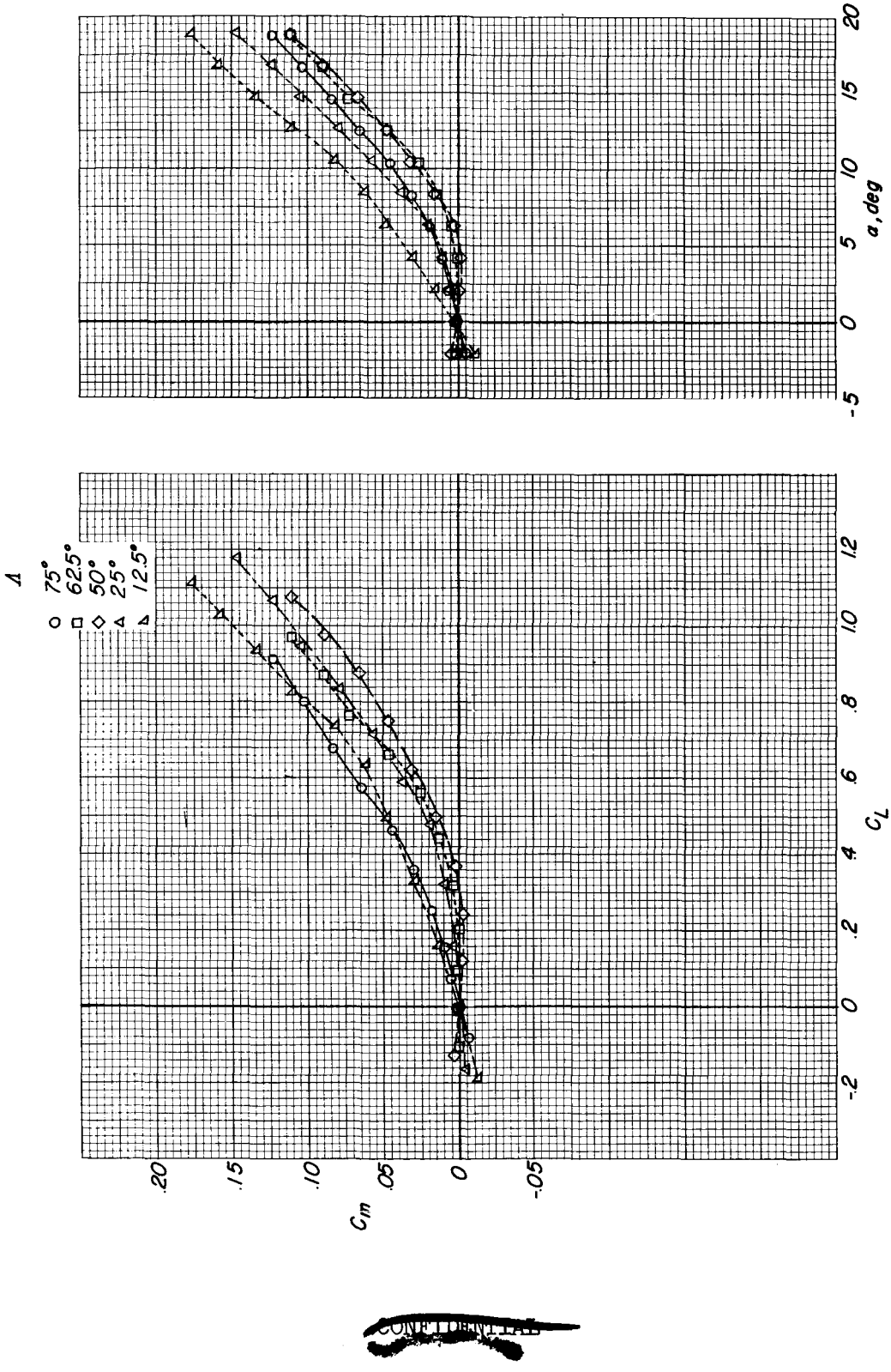

Figure 6.- Concluded.

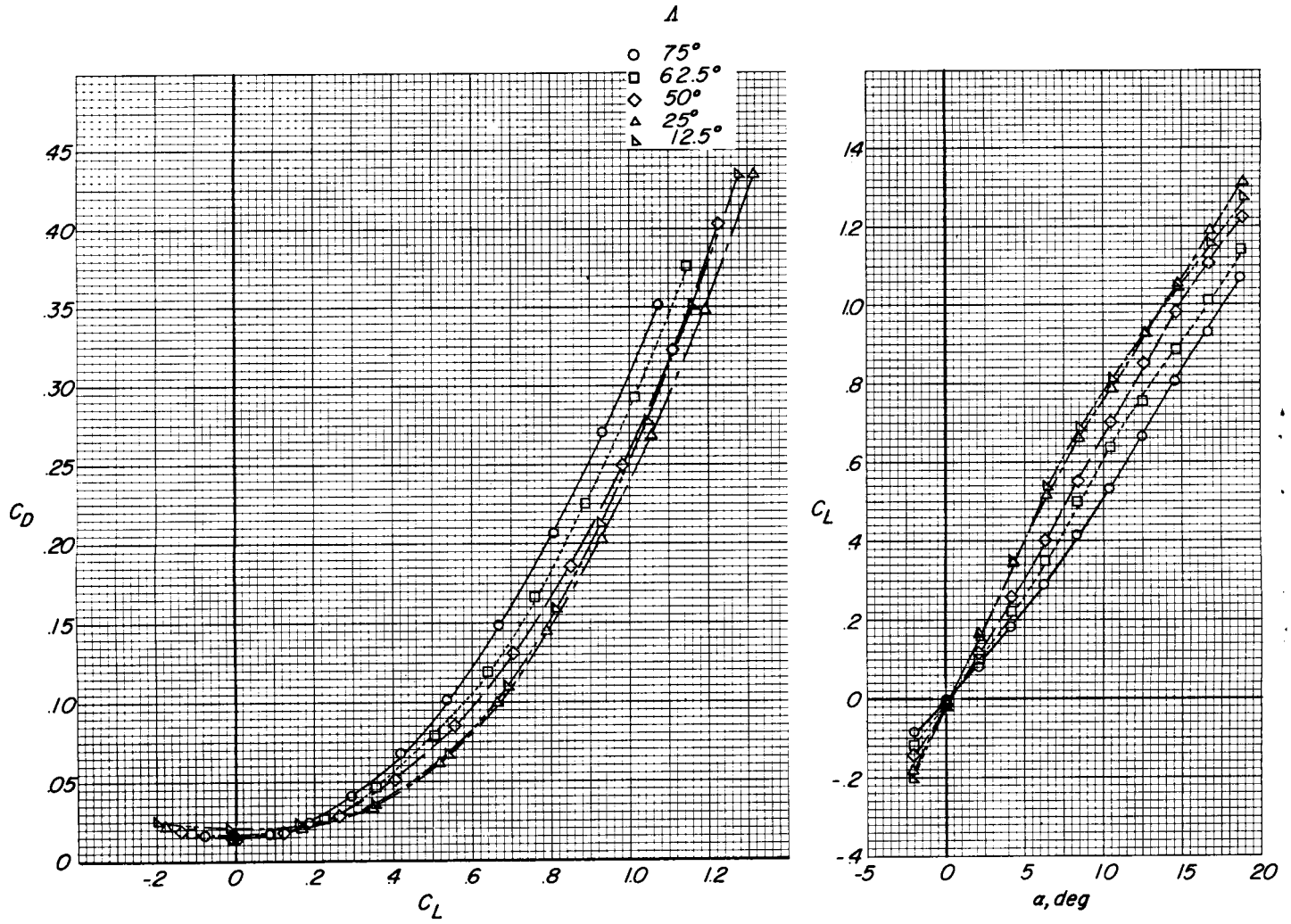

Figure 7.- Effect of wing leading-edge sweep angle on the longitudinal aerodynamic characteristics. Canard $S_c/S_w = 0.06$; horizontal tail $i_t = 0^o$; M = 0.25.

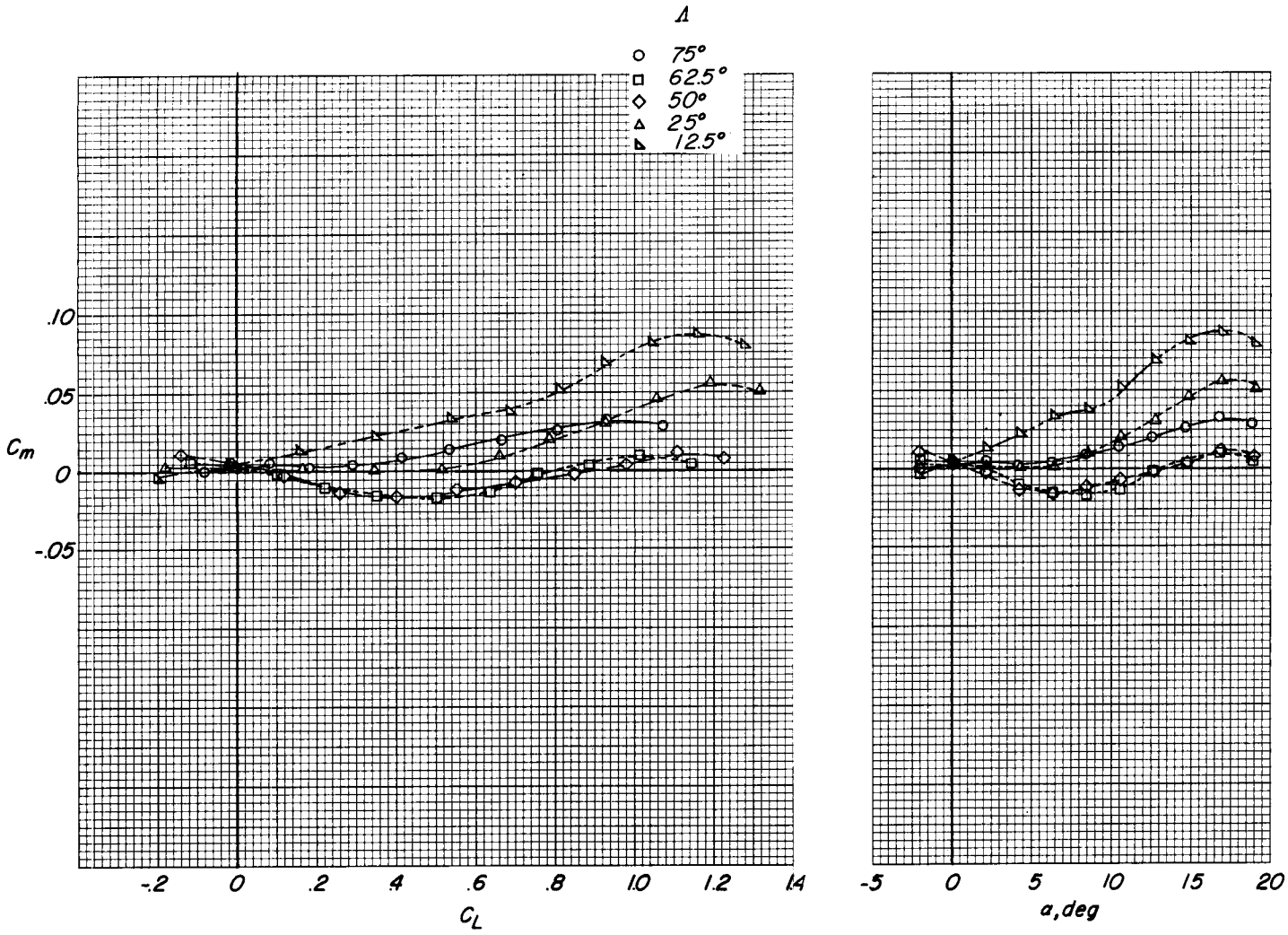

Figure 7.- Concluded.

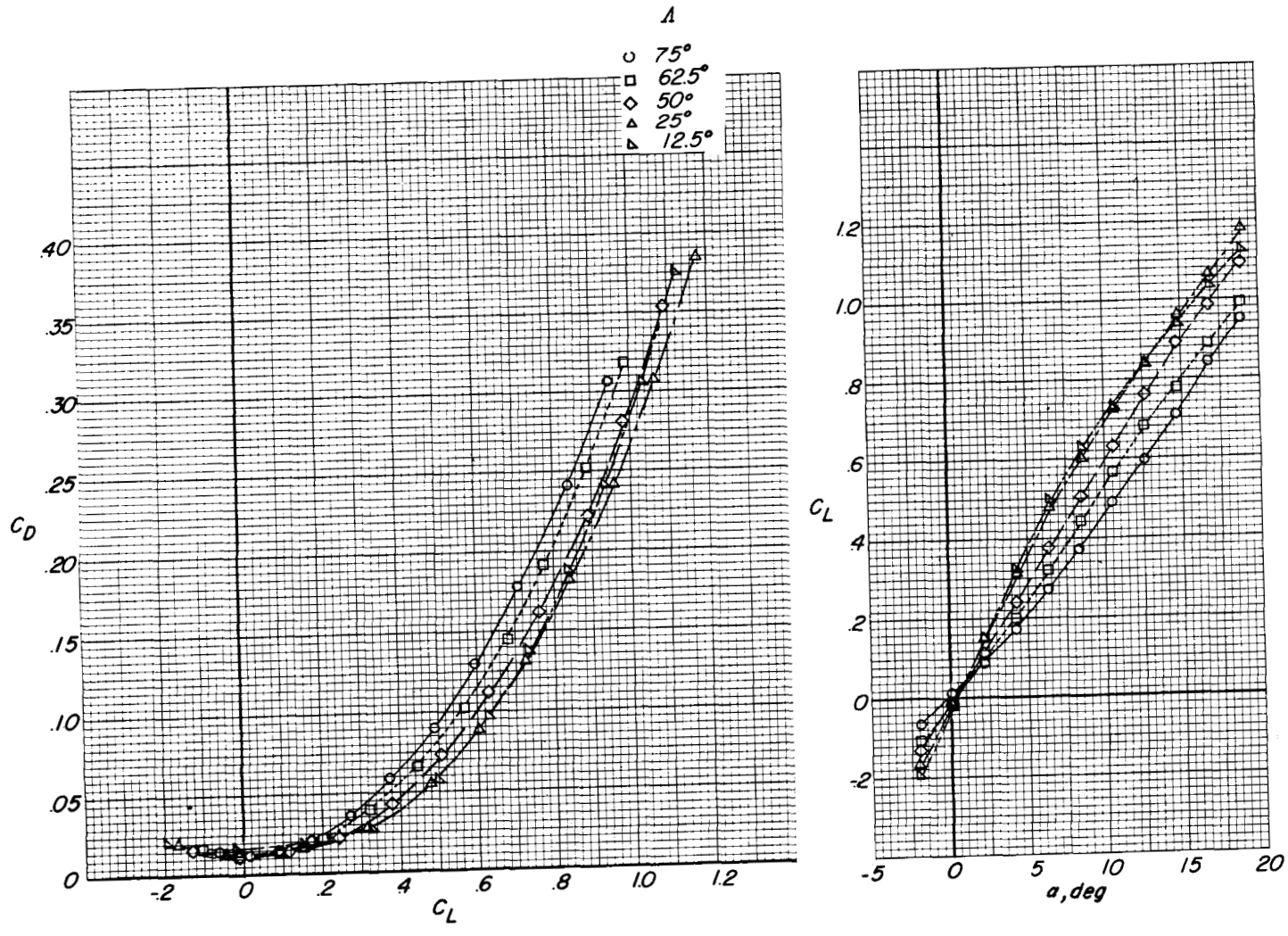

Figure 8.- Effect of wing leading-edge sweep angle on the longitudinal aerodynamic characteristics. Canard S_c/S_w = 0.06; horizontal tail off; M = 0.25.

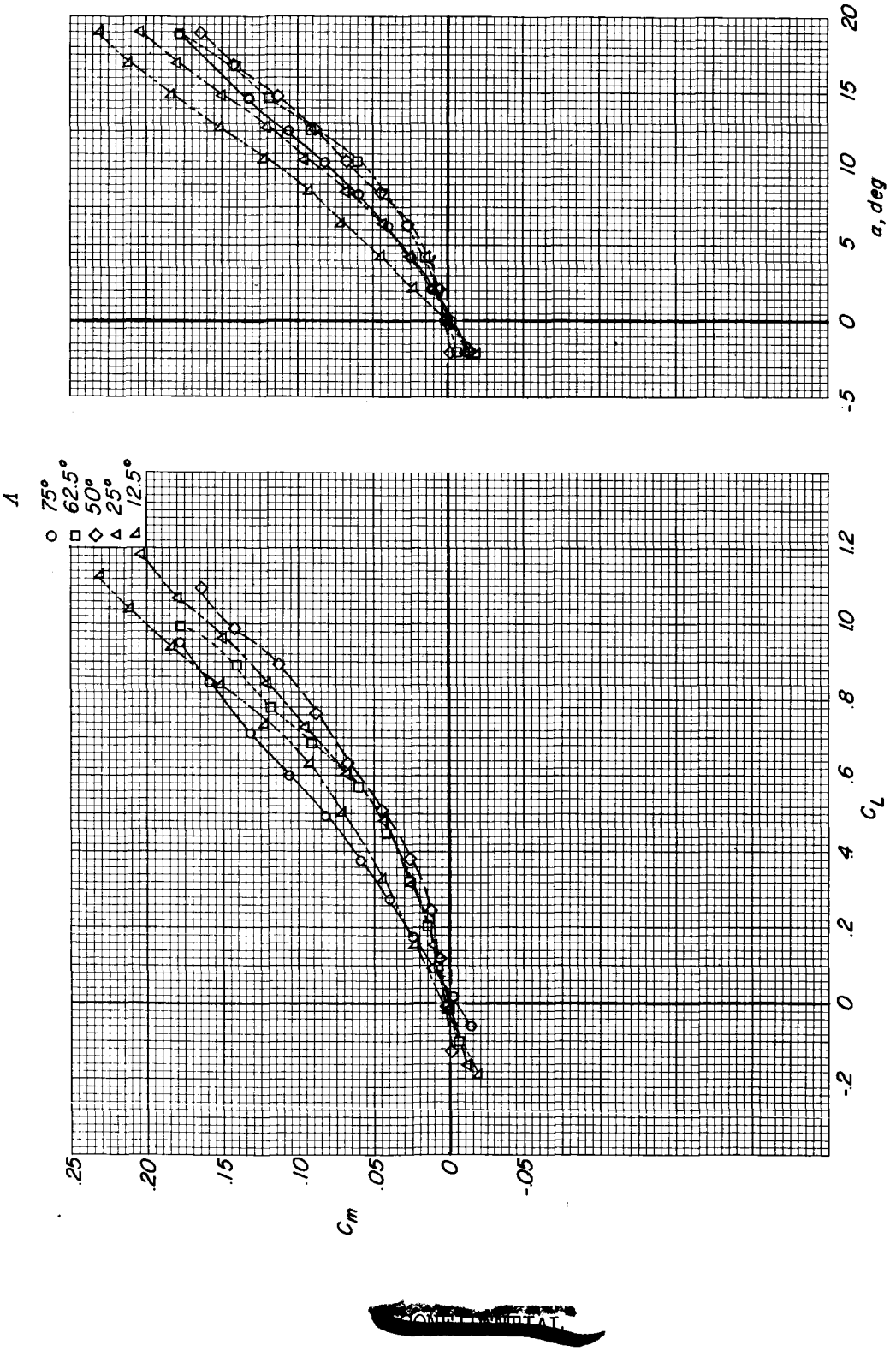

Figure 8.- Concluded.

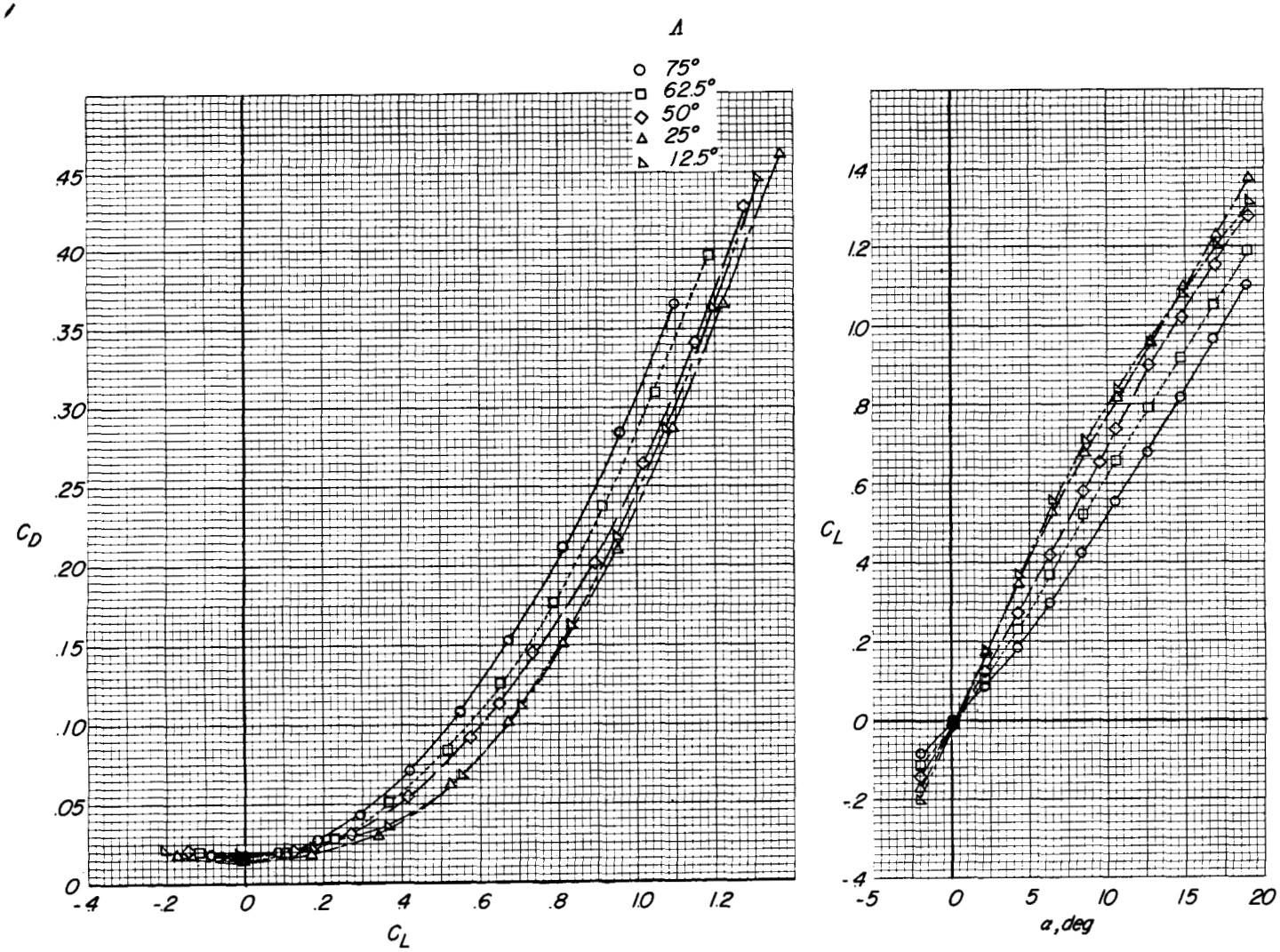

Figure 9.- Effect of wing leading-edge sweep on the longitudinal aerodynamic characteristics. Canard $S_c/S_w = 0.12$; horizontal tail $i_t = 0^o$; M = 0.25.

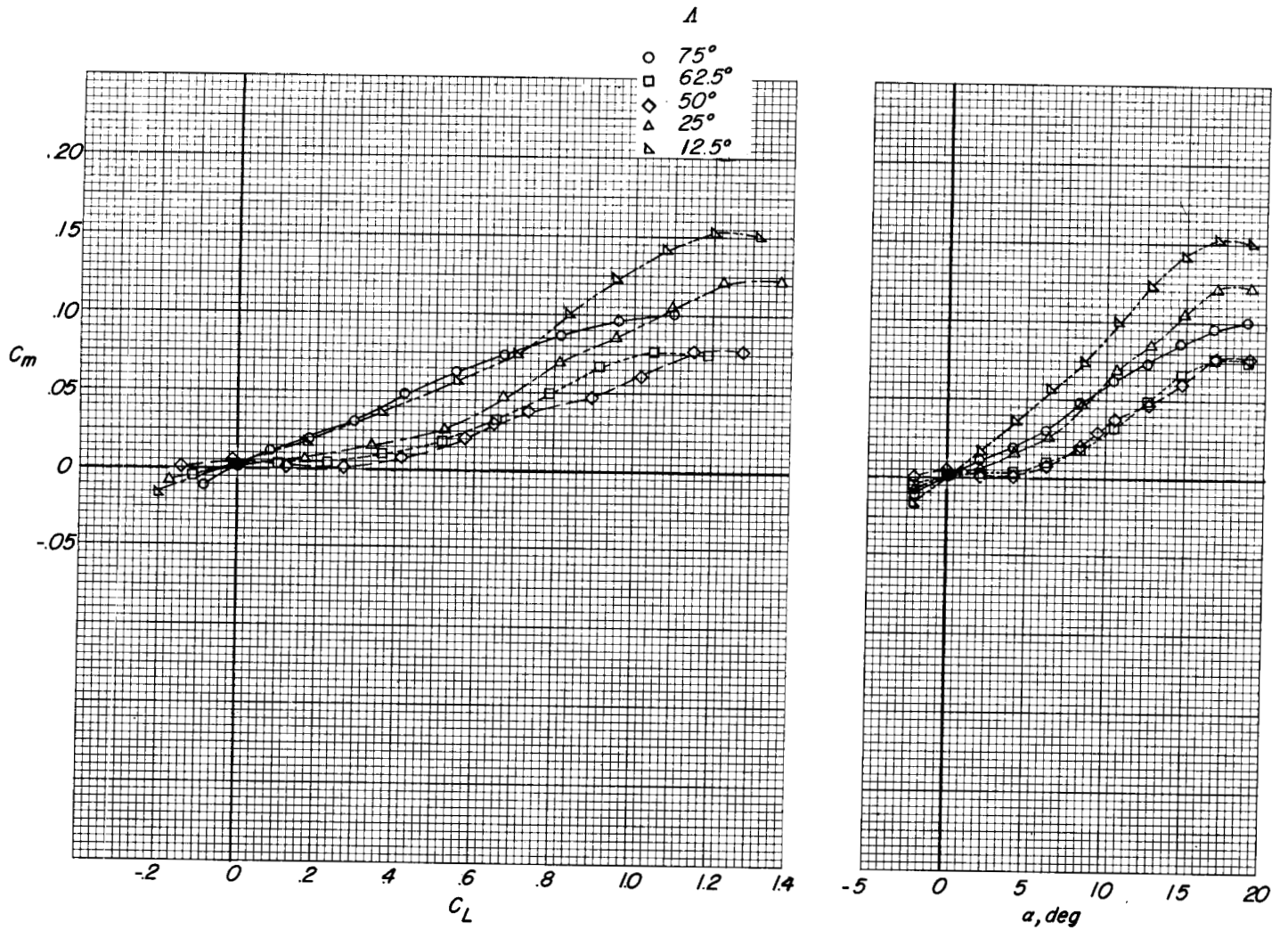

Figure 9.- Concluded.

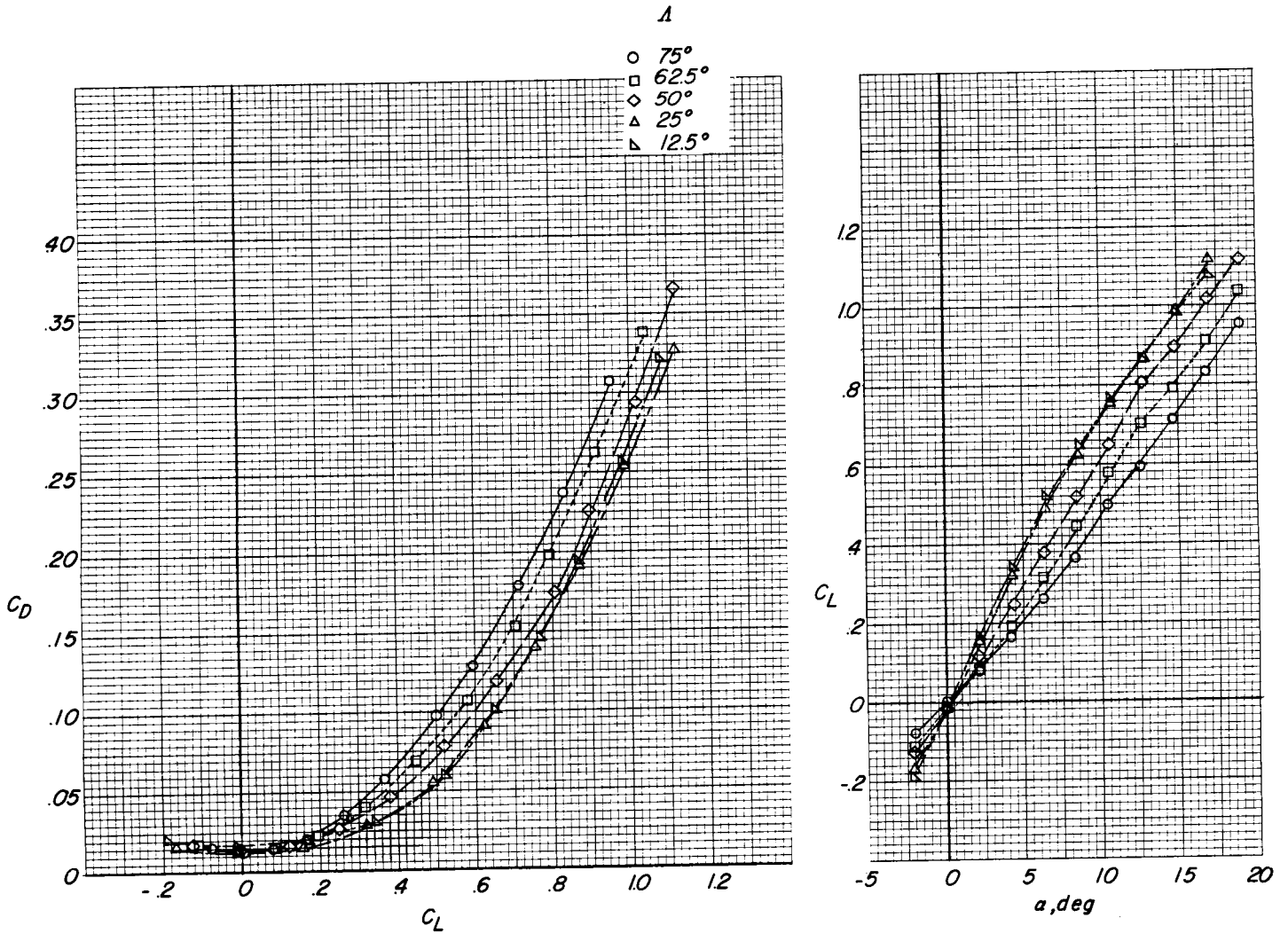

Figure 10.- Effect of wing leading-edge sweep angle on the longitudinal aerodynamic characteristics. Canard S_c/S_w = 0.12; horizontal tail off; M = 0.25.

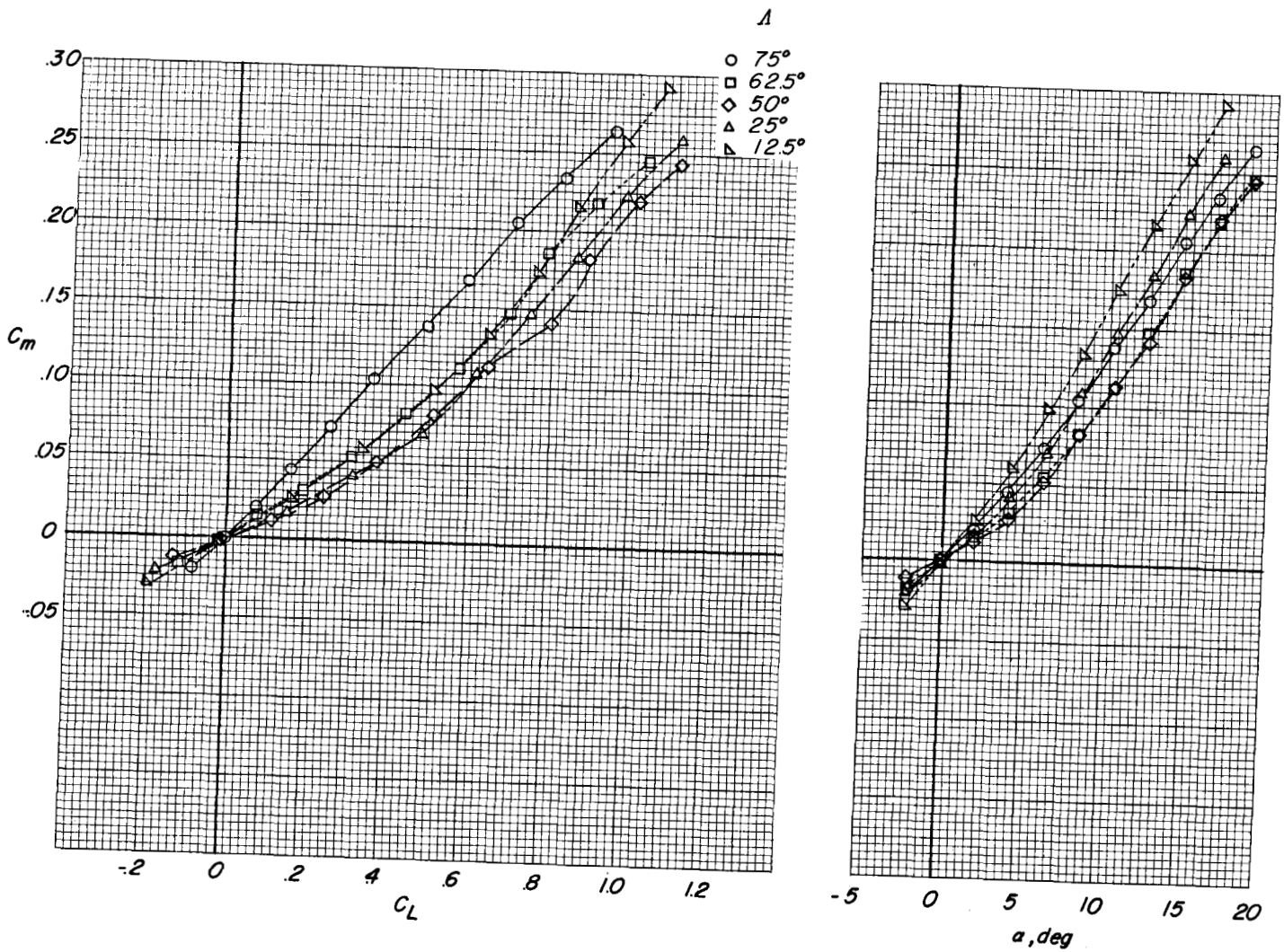

Figure 10.- Concluded.

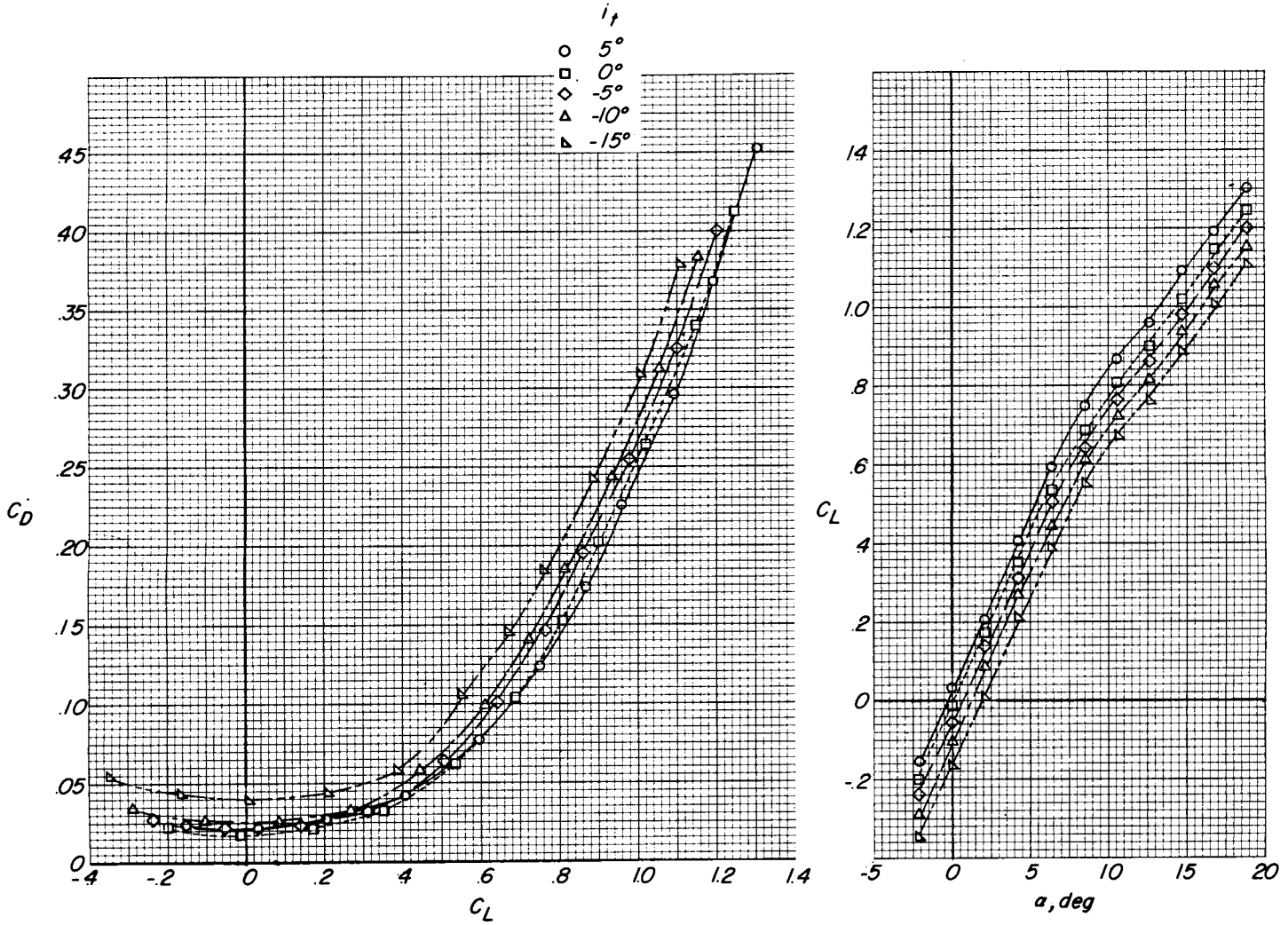

Figure 11.- Effect of horizontal-tail incidence on the longitudinal aerodynamic characteristics. $\Lambda = 12.5^{\circ}$; M = 0.25.

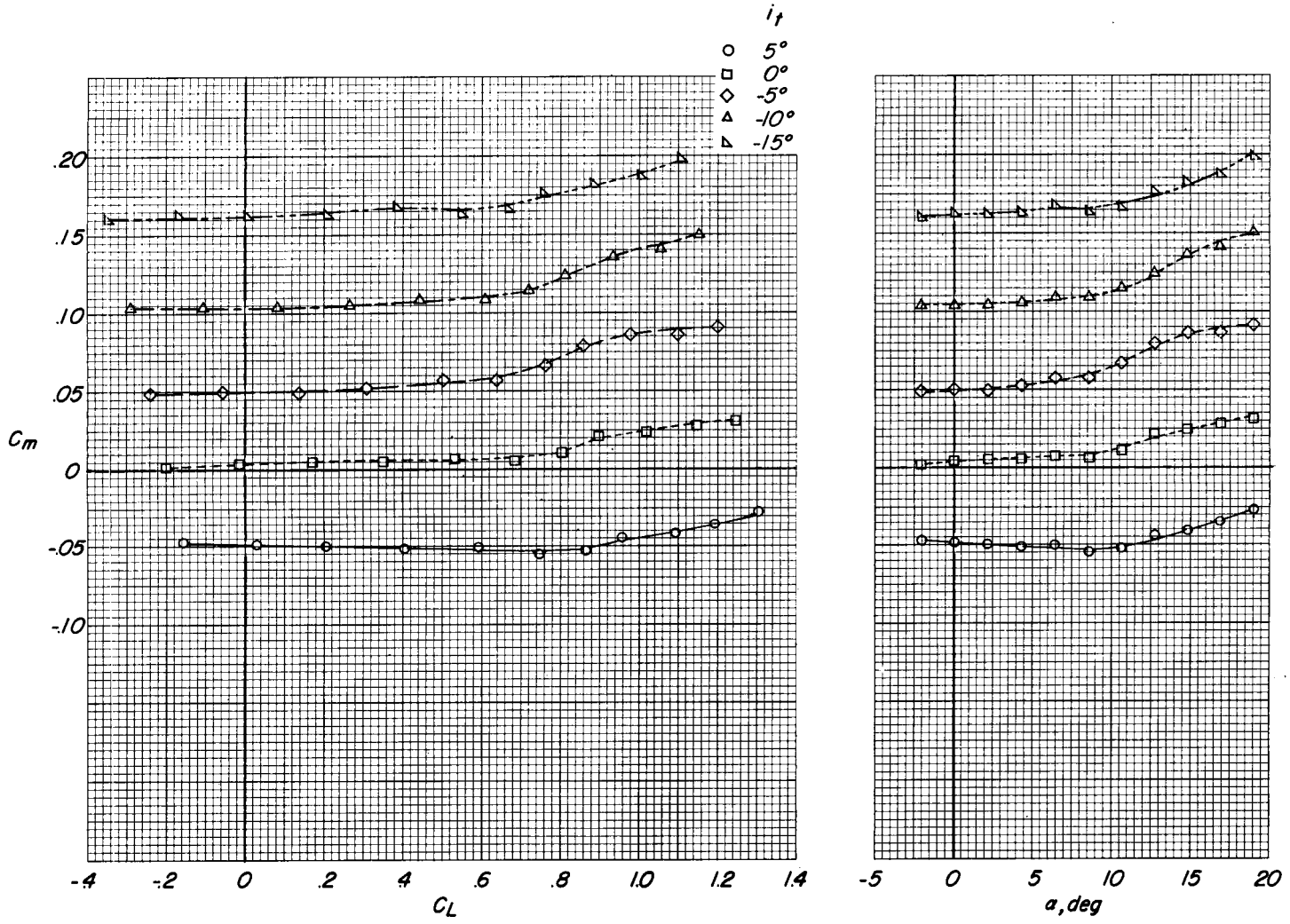

Figure 11.- Concluded.

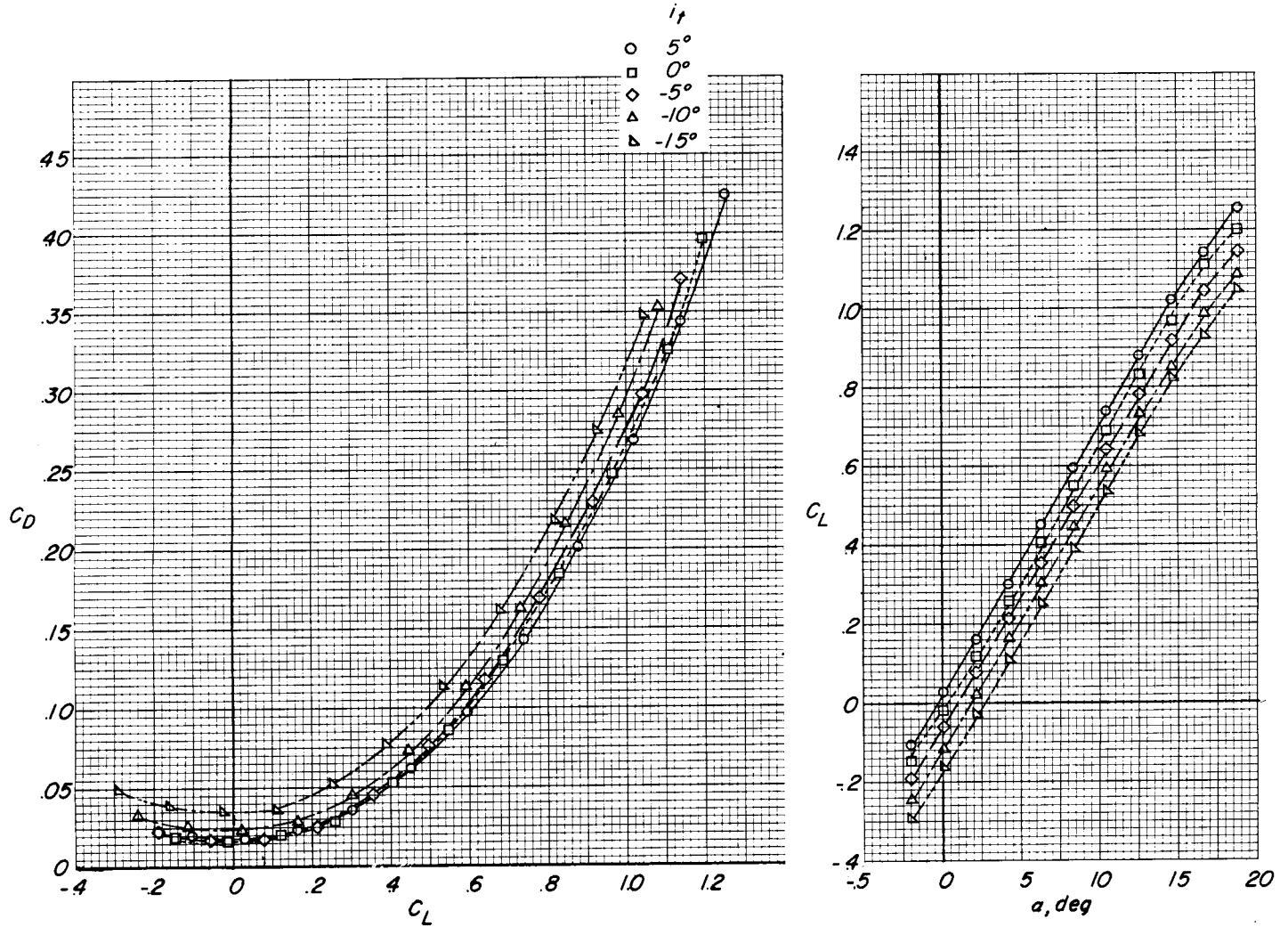

Figure 12.- Effect of horizontal-tail incidence on the longitudinal aerodynamic characteristics. $\Lambda = 50^{\circ}$; M = 0.25.

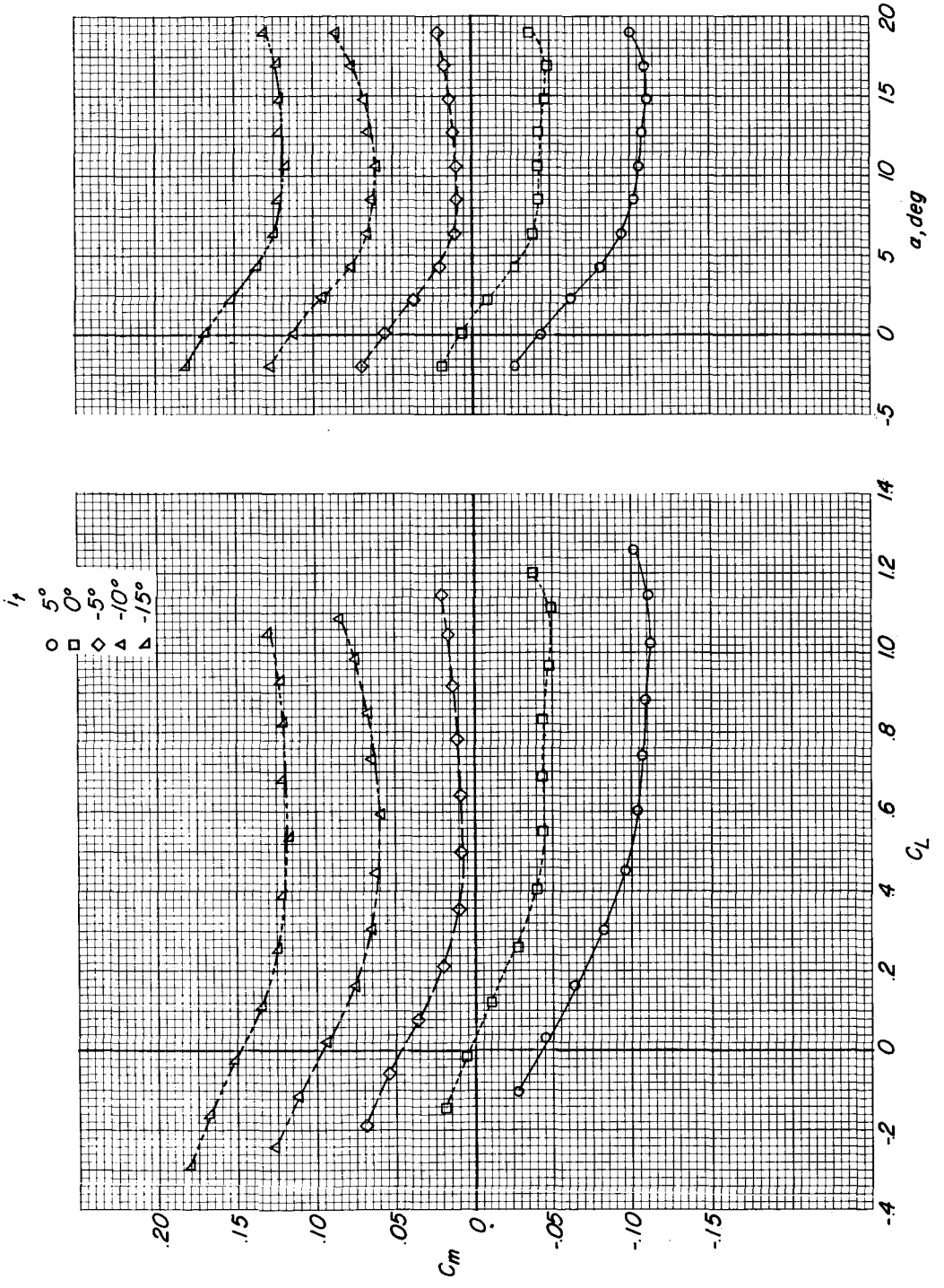

Figure 12.- Concluded.

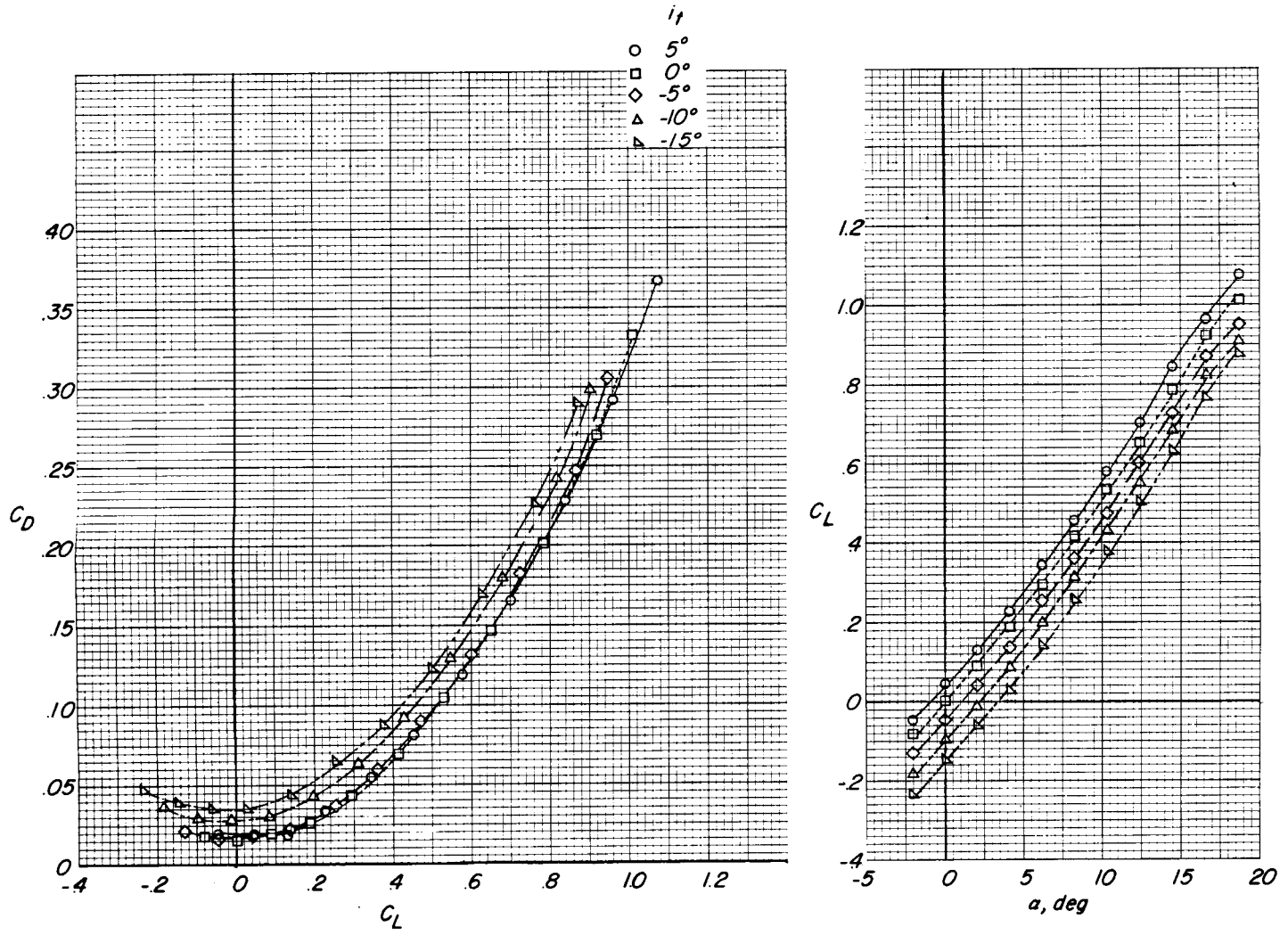

Figure 13.- Effect of horizontal-tail incidence on the longitudinal aerodynamic characteristics. $\Lambda = 75^{\circ}$; M = 0.25.

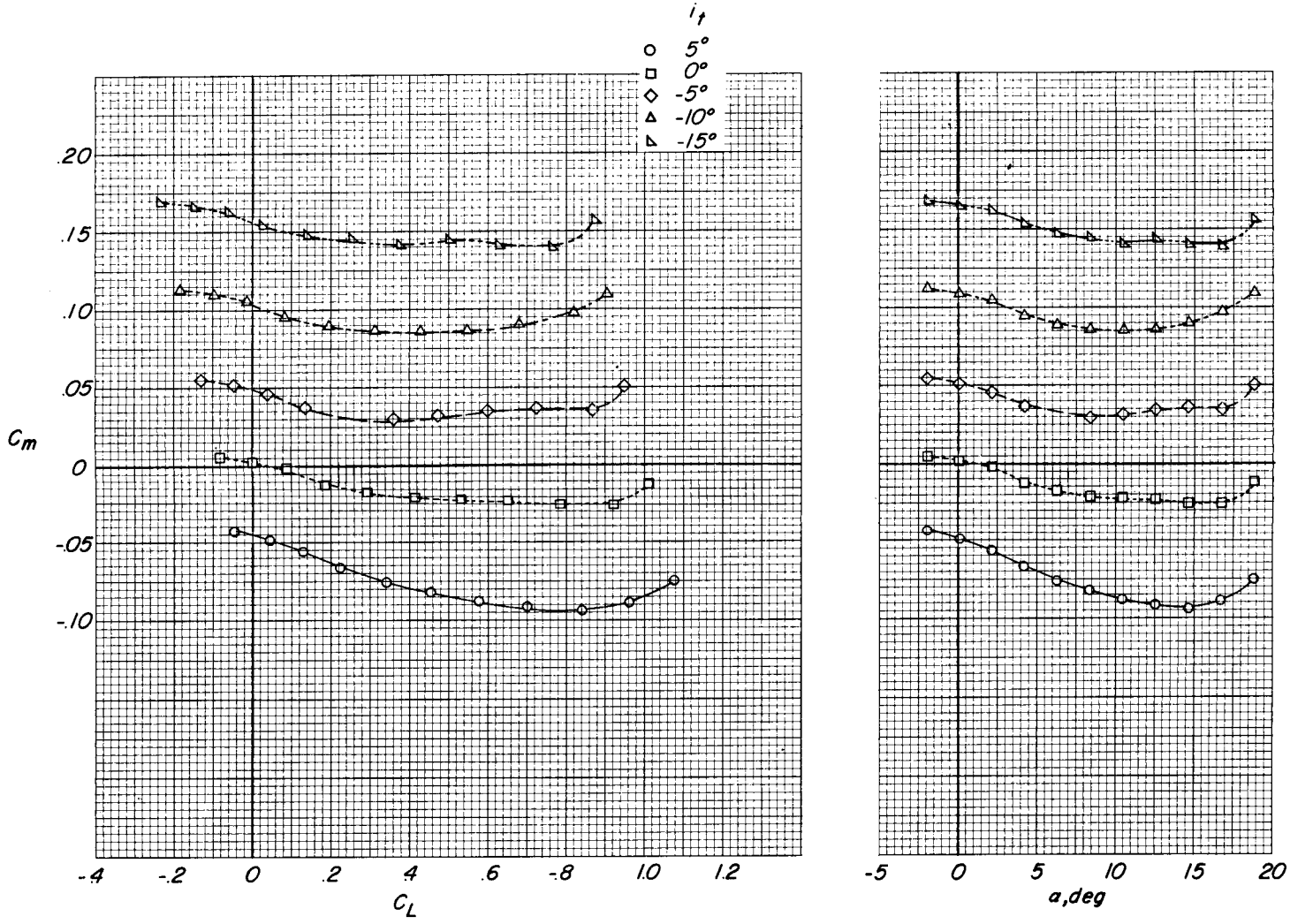

Figure 13.- Concluded.

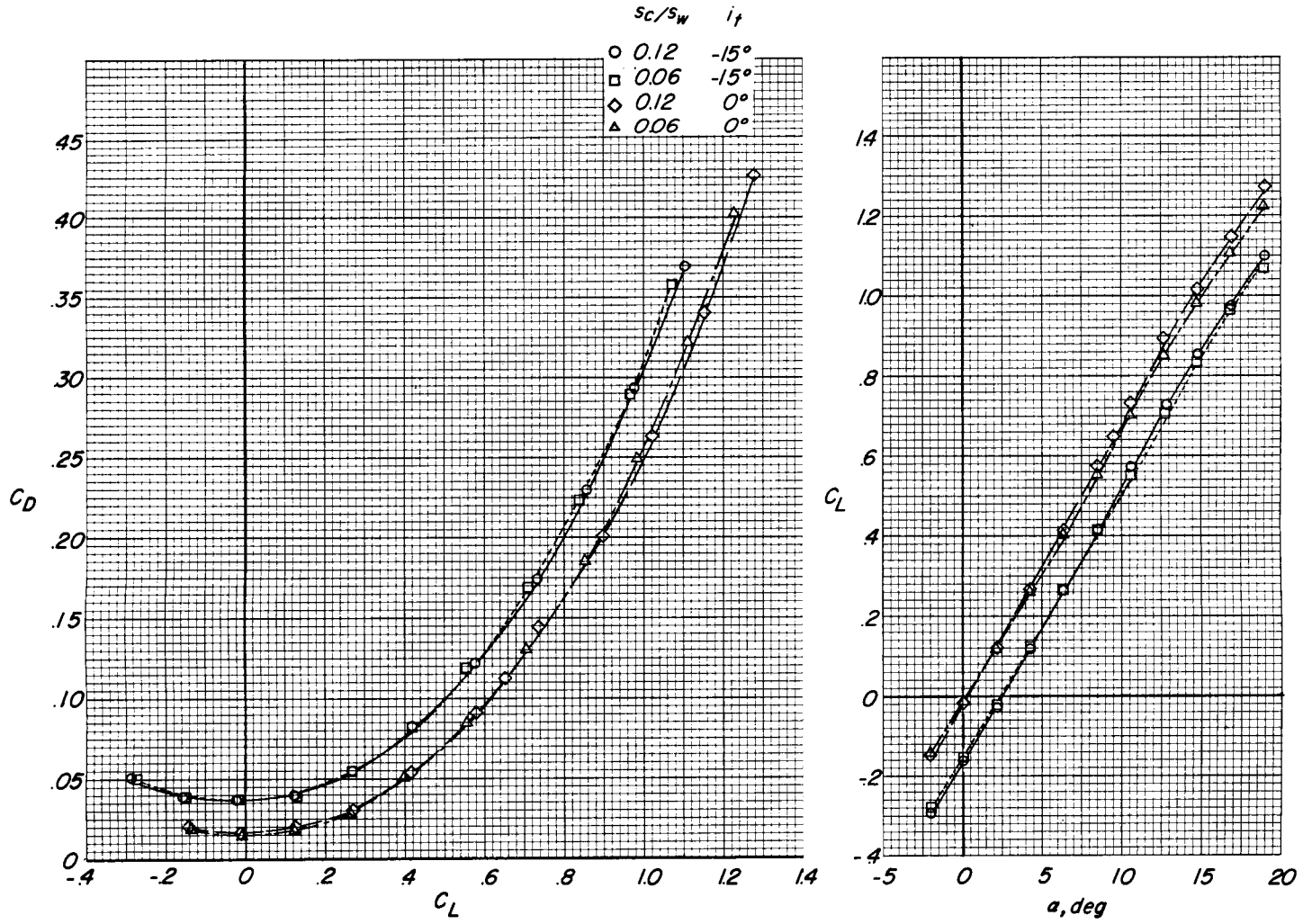

Figure 14.- Effect of horizontal-tail incidence with canard on the longitudinal aerodynamic characteristics. $\Lambda = 50^{\circ}$; M = 0.25.

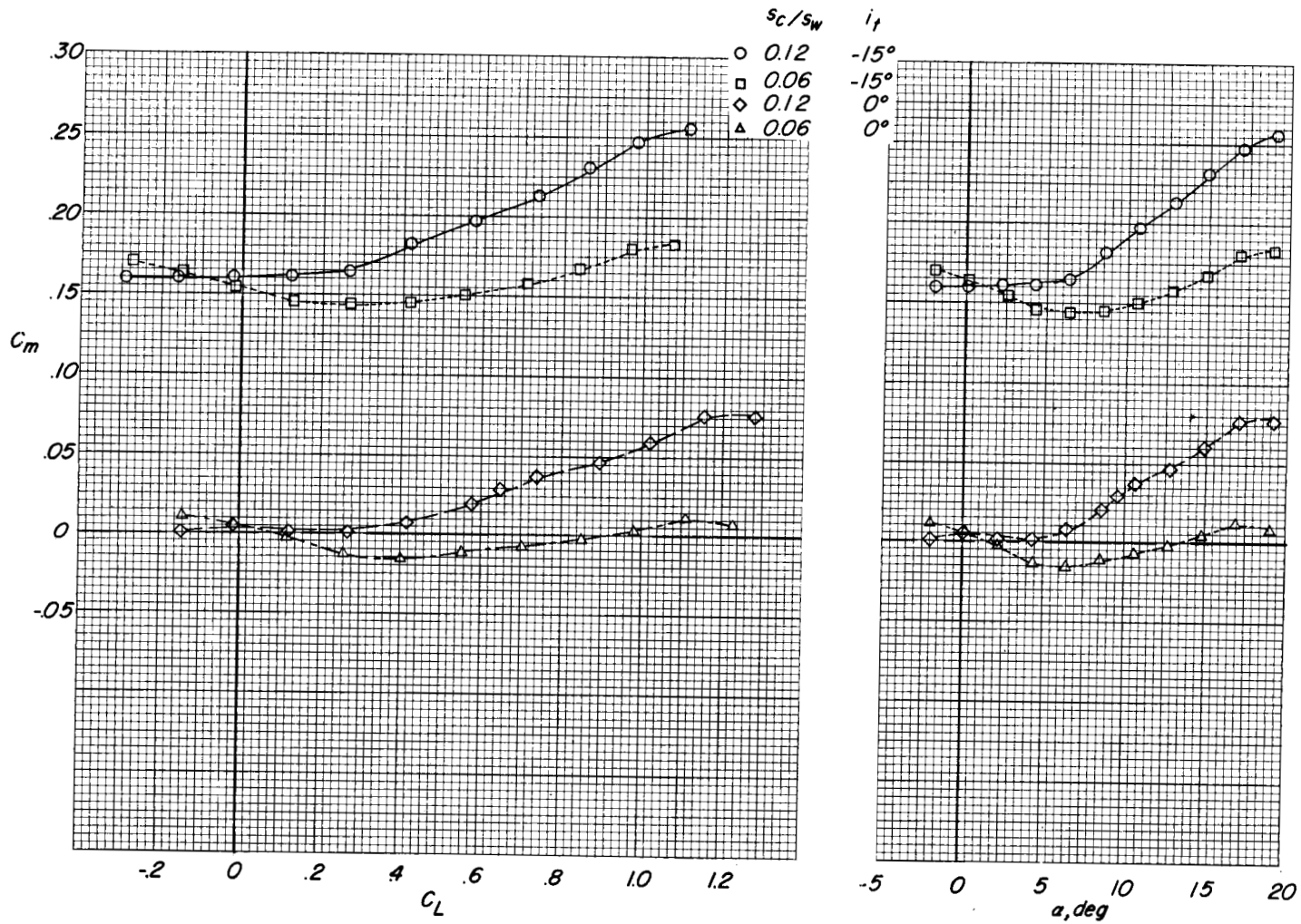

Figure 14.- Concluded.

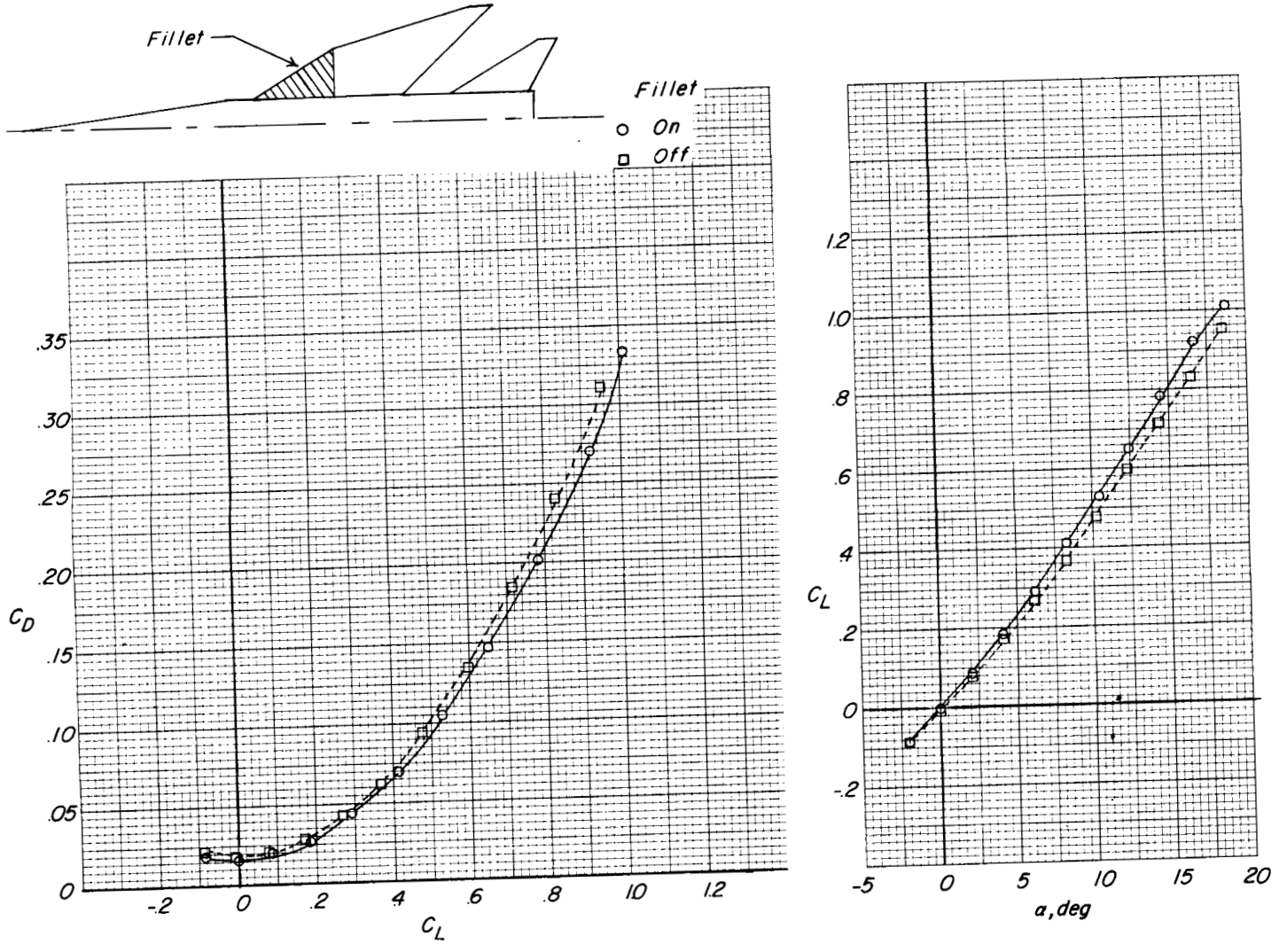

Figure 15.- Effect of the leading-edge fillet on the longitudinal aerodynamic characteristics. $\Lambda = 75^\circ$; M = 0.25.

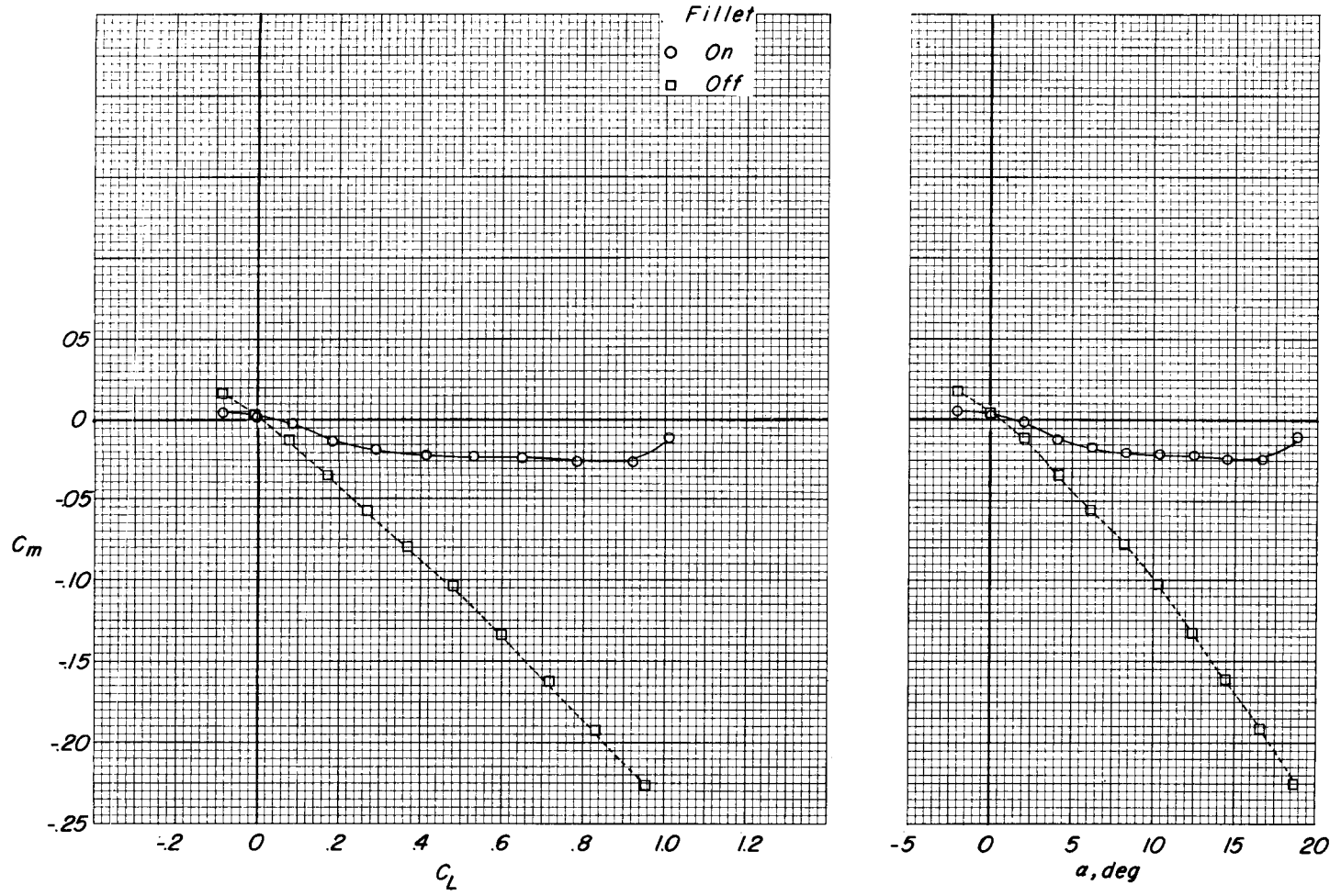

Figure 15.- Concluded.

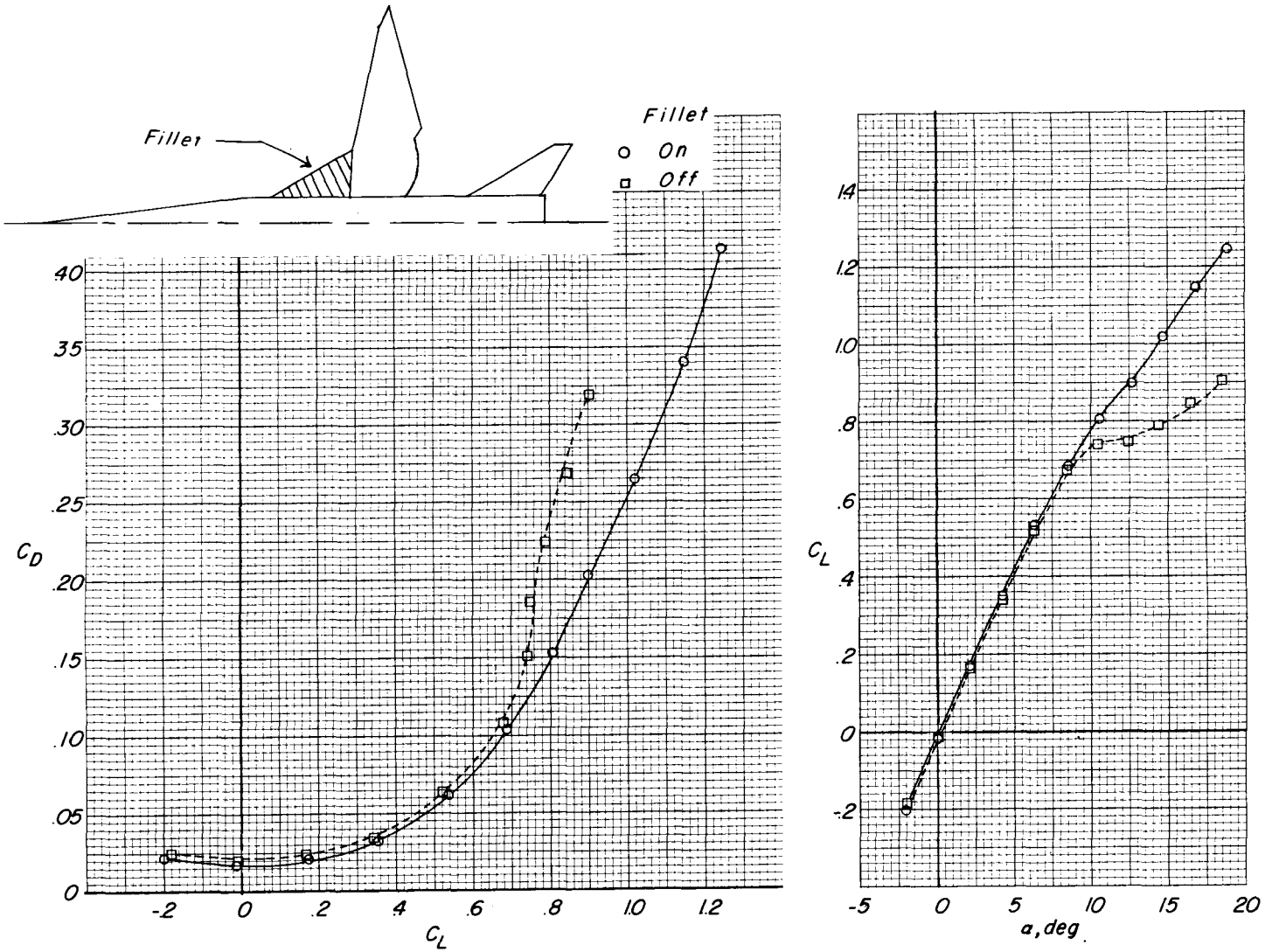

Figure 16.- Effect of the leading-edge fillet on the longitudinal aerodynamic characteristics. $\Lambda = 12.5^{\circ}$; M = 0.25.

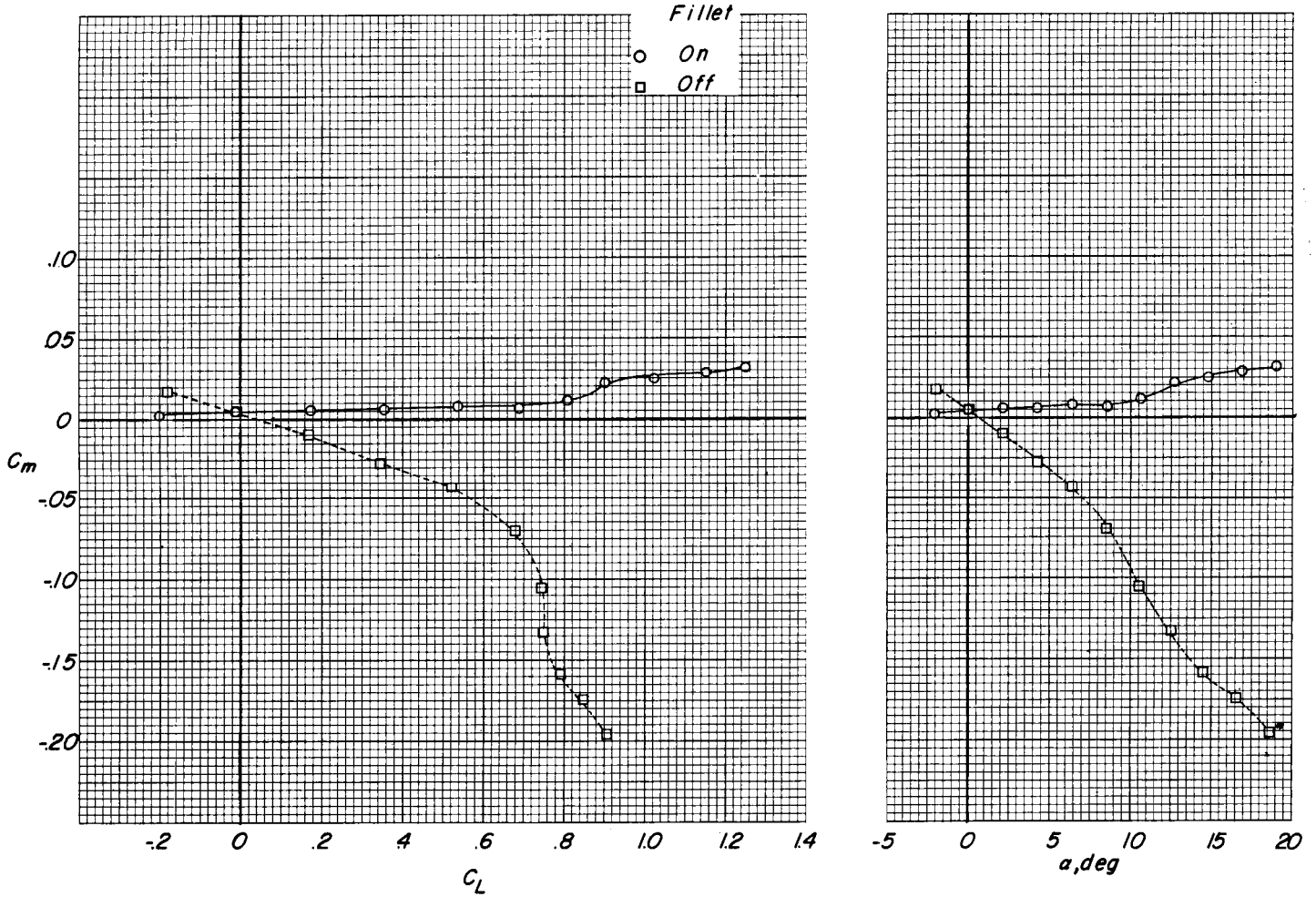

Figure 16.- Concluded.

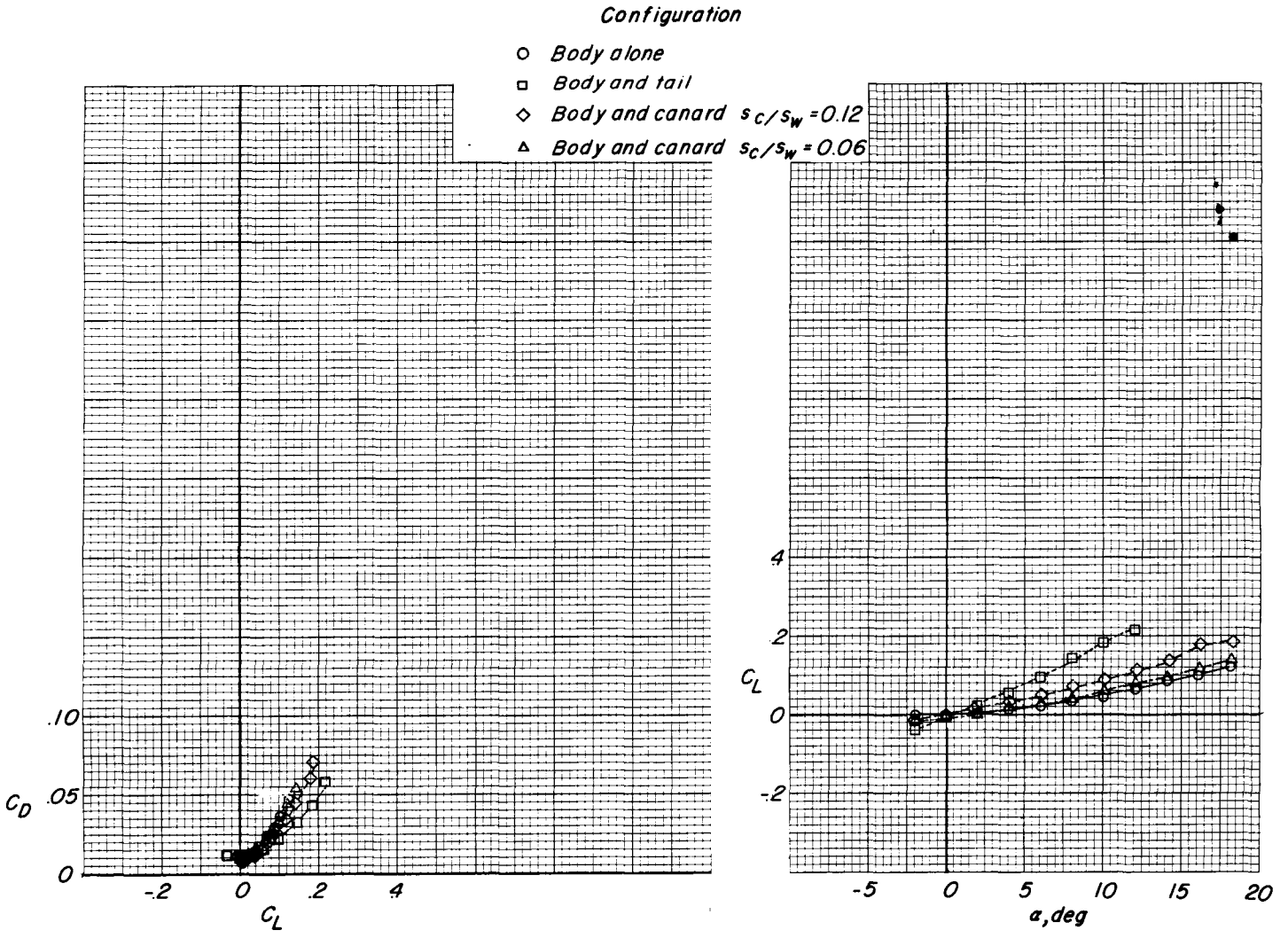

Figure 17.- Effect of breakdown tests on the longitudinal aerodynamic characteristics. M = 0.25.

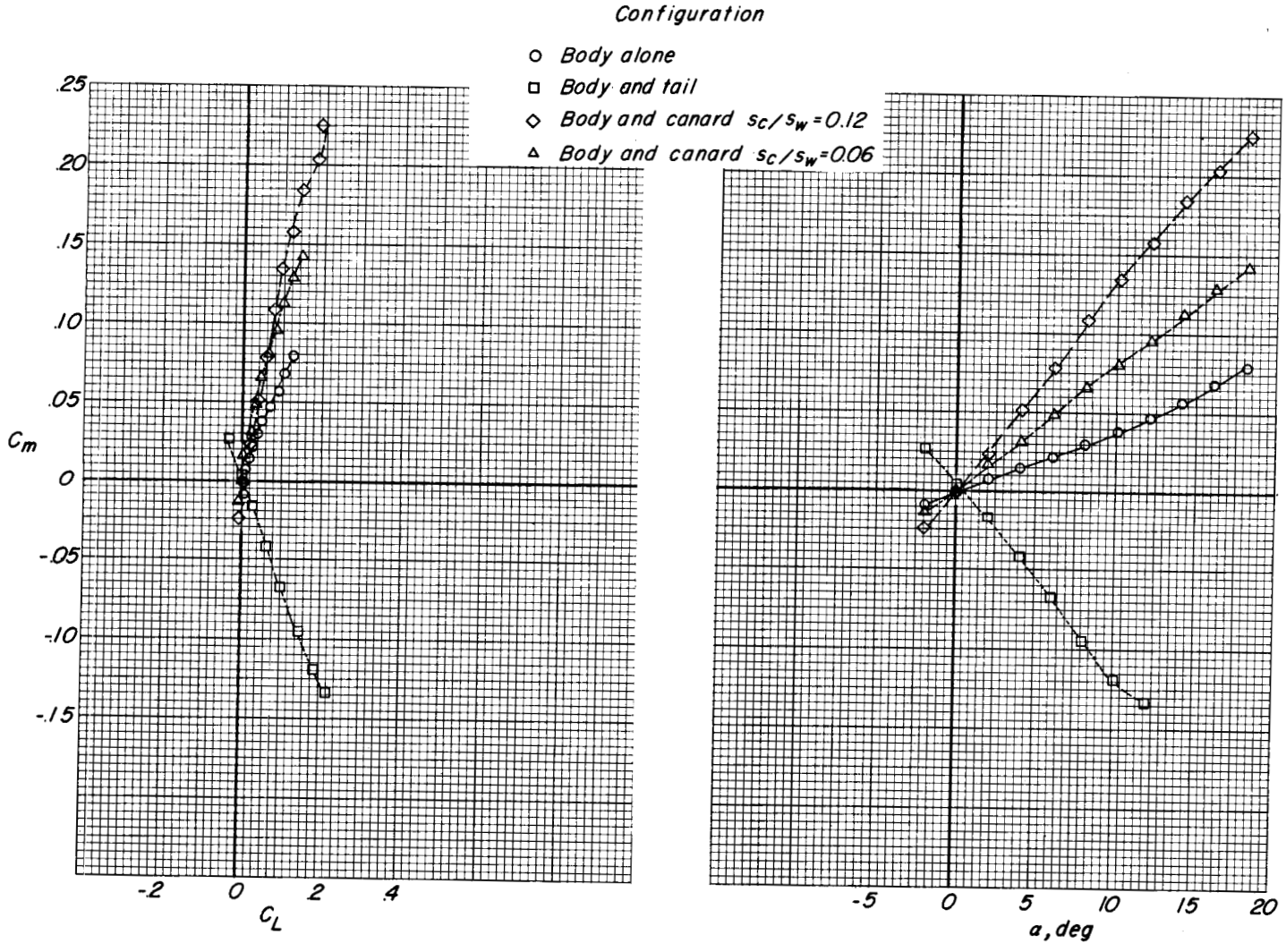

Figure 17.- Concluded.

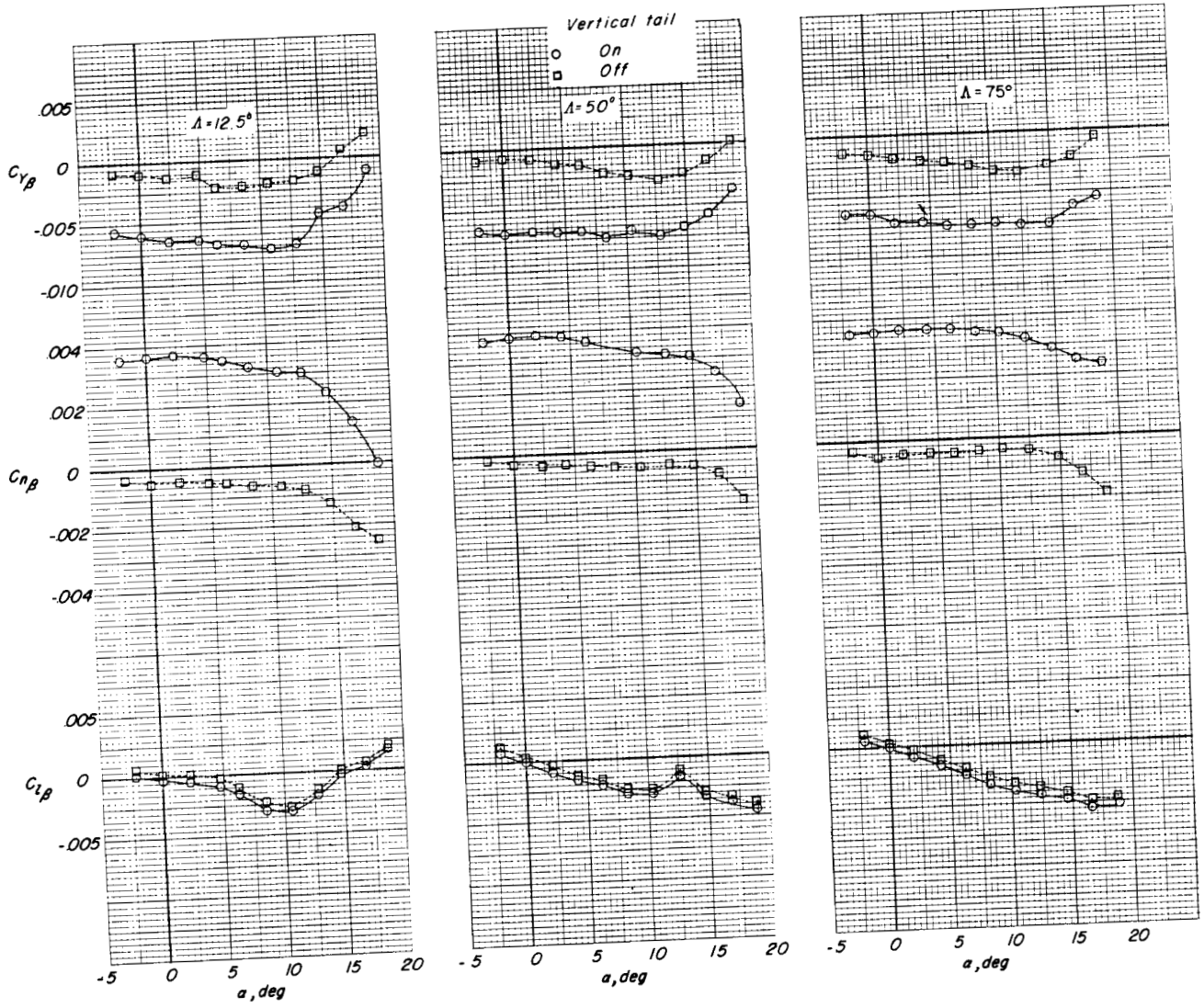

Figure 18.- Lateral and directional stability characteristics. M = 0.25.

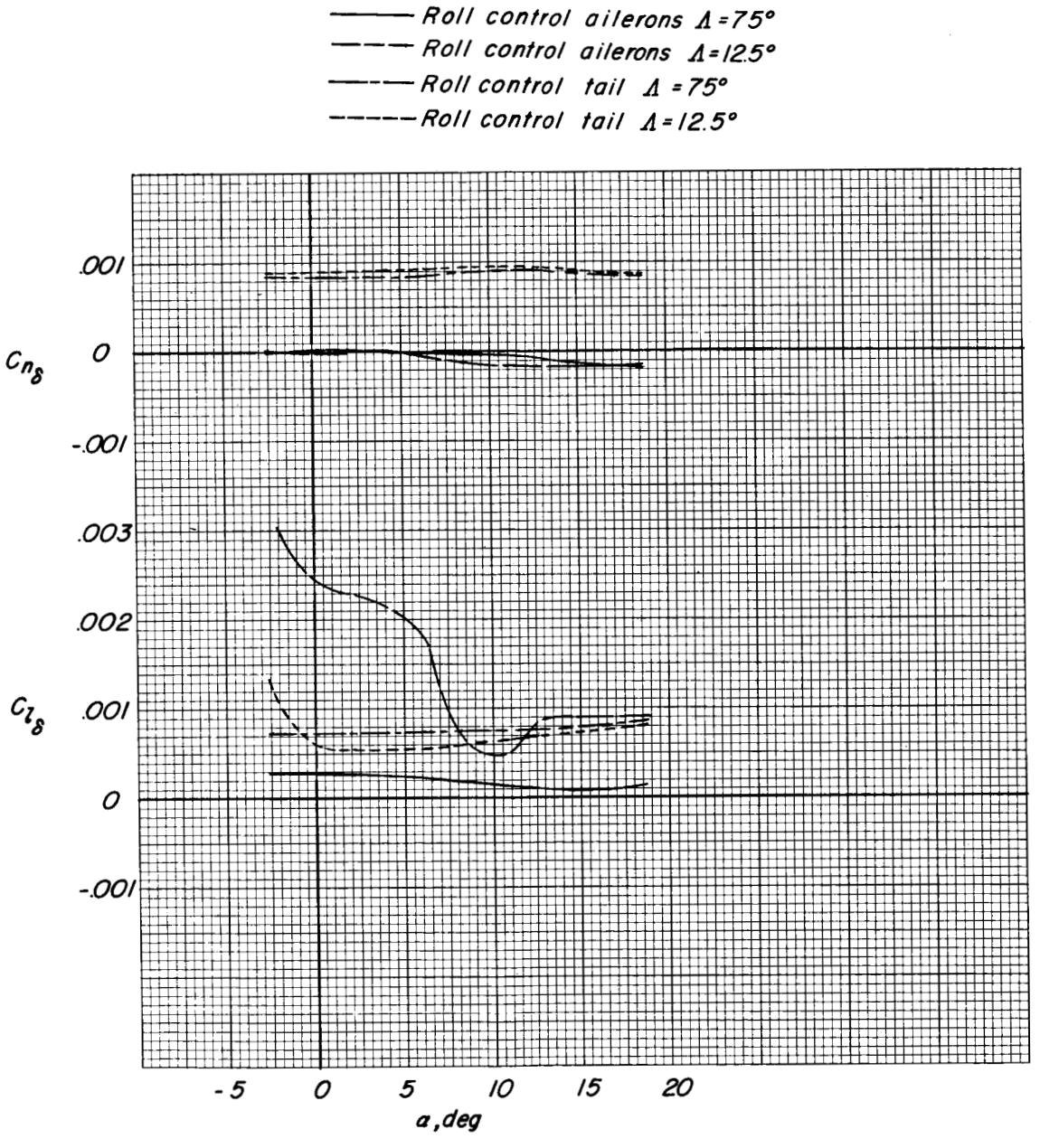

Figure 19.- Lateral control characteristics. M = 0.25.

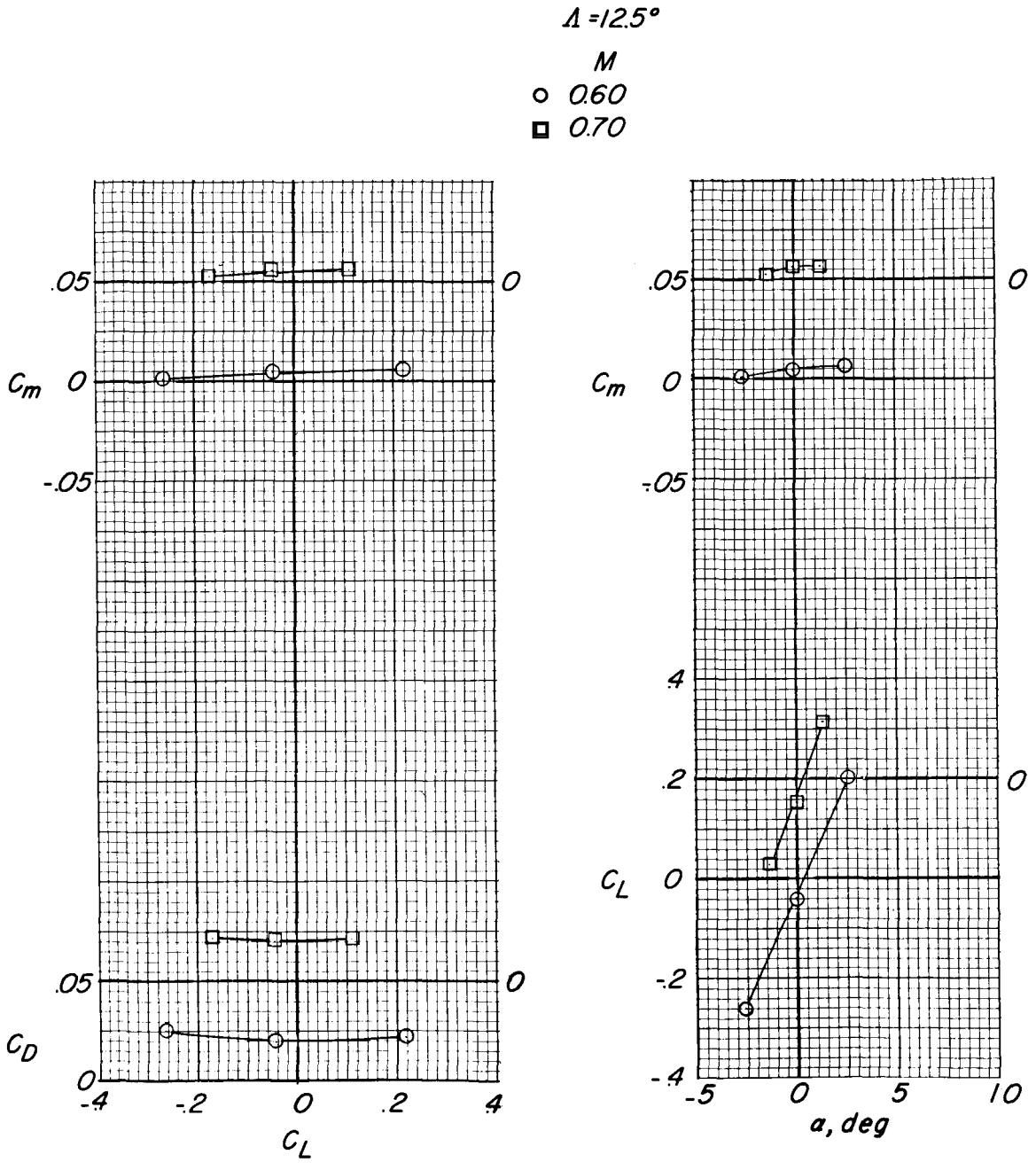

(a) $\Lambda = 12.5^{\circ}$; transition off.

Figure 20.- Mach number effects on the longitudinal aerodynamic characteristics.

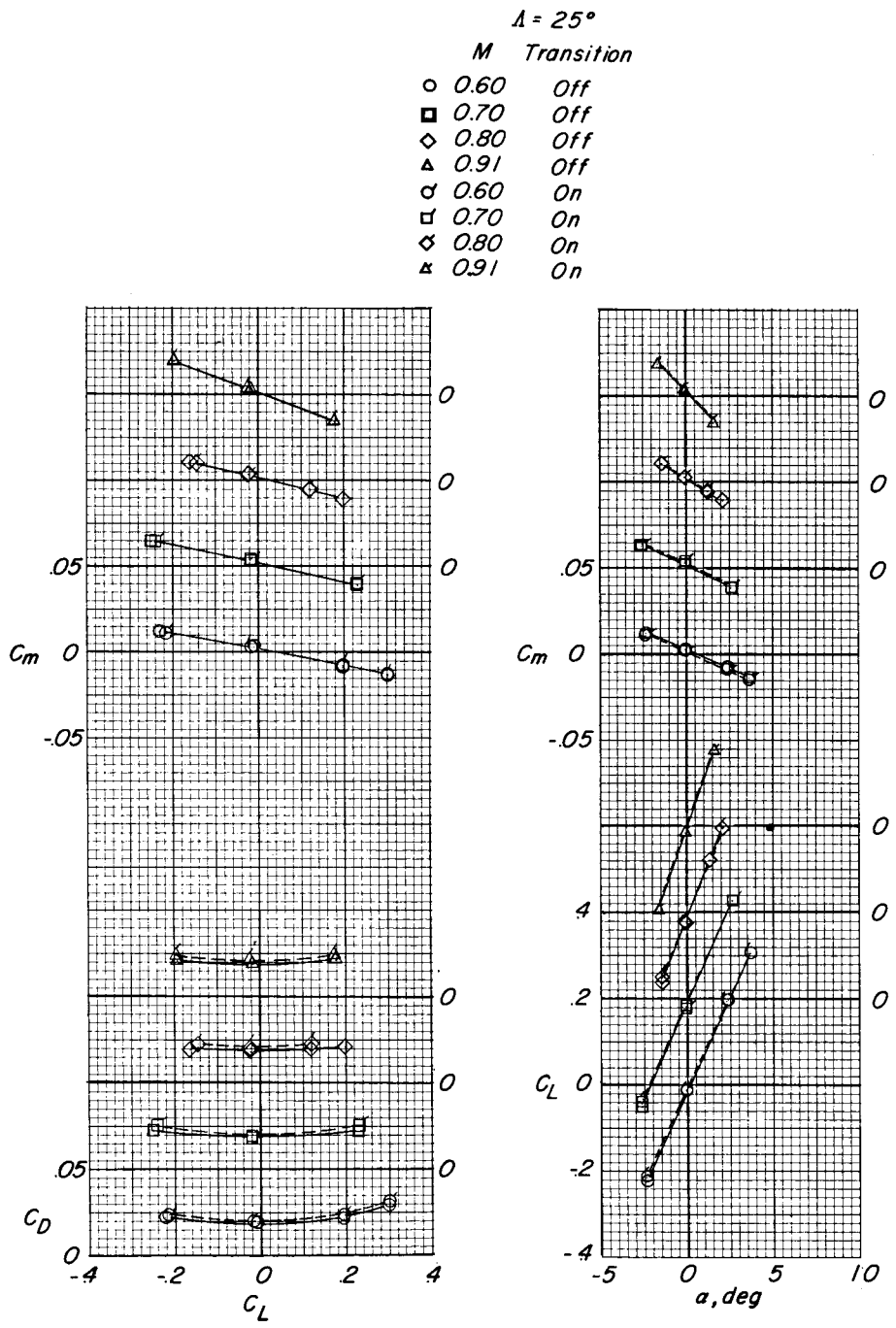

(b) $\Lambda = 25^{\circ}$; transition on and off.

Figure 20.- Continued.

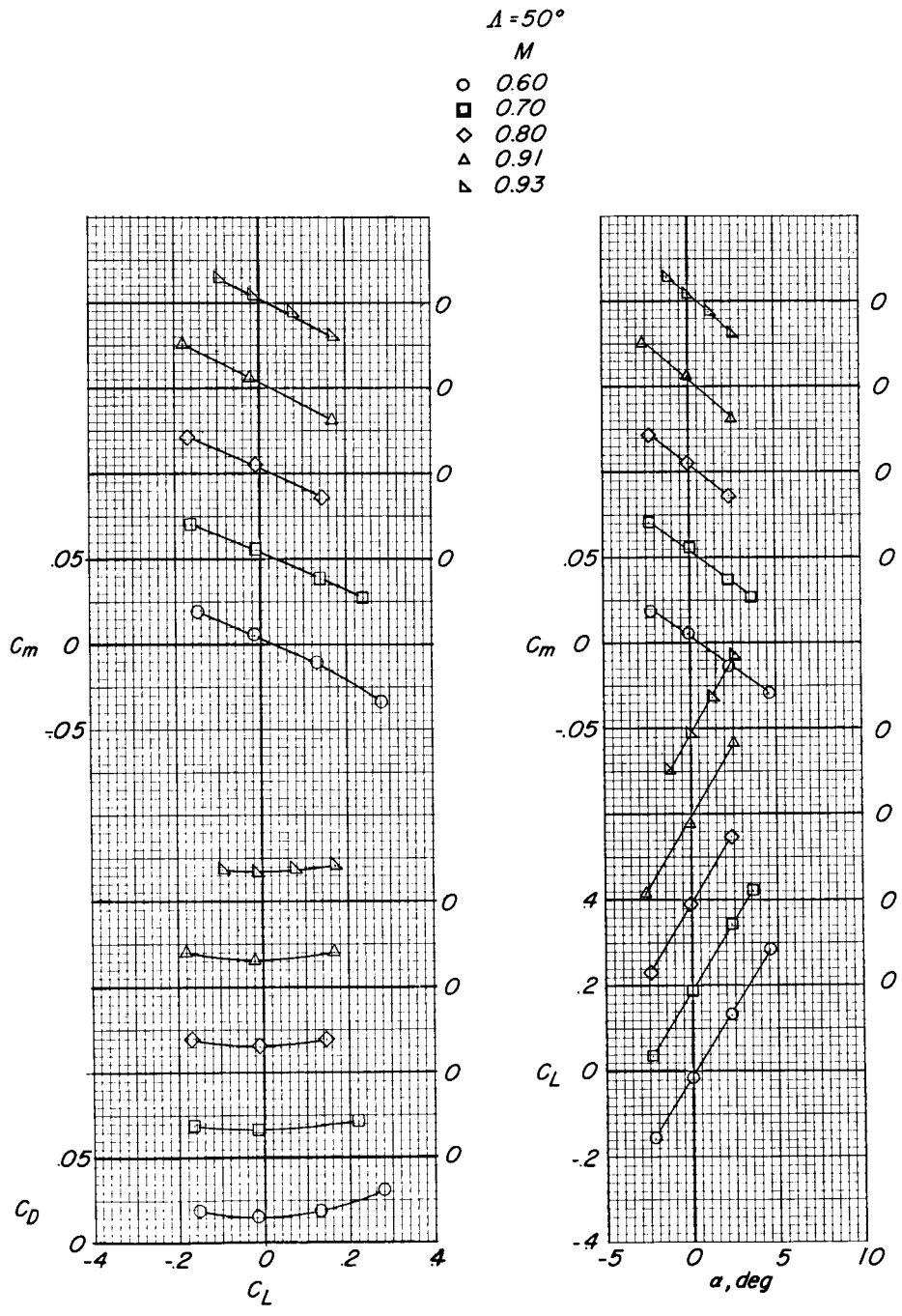

(c) $\Lambda = 50^{\circ}$; transition off.

Figure 20.- Continued.

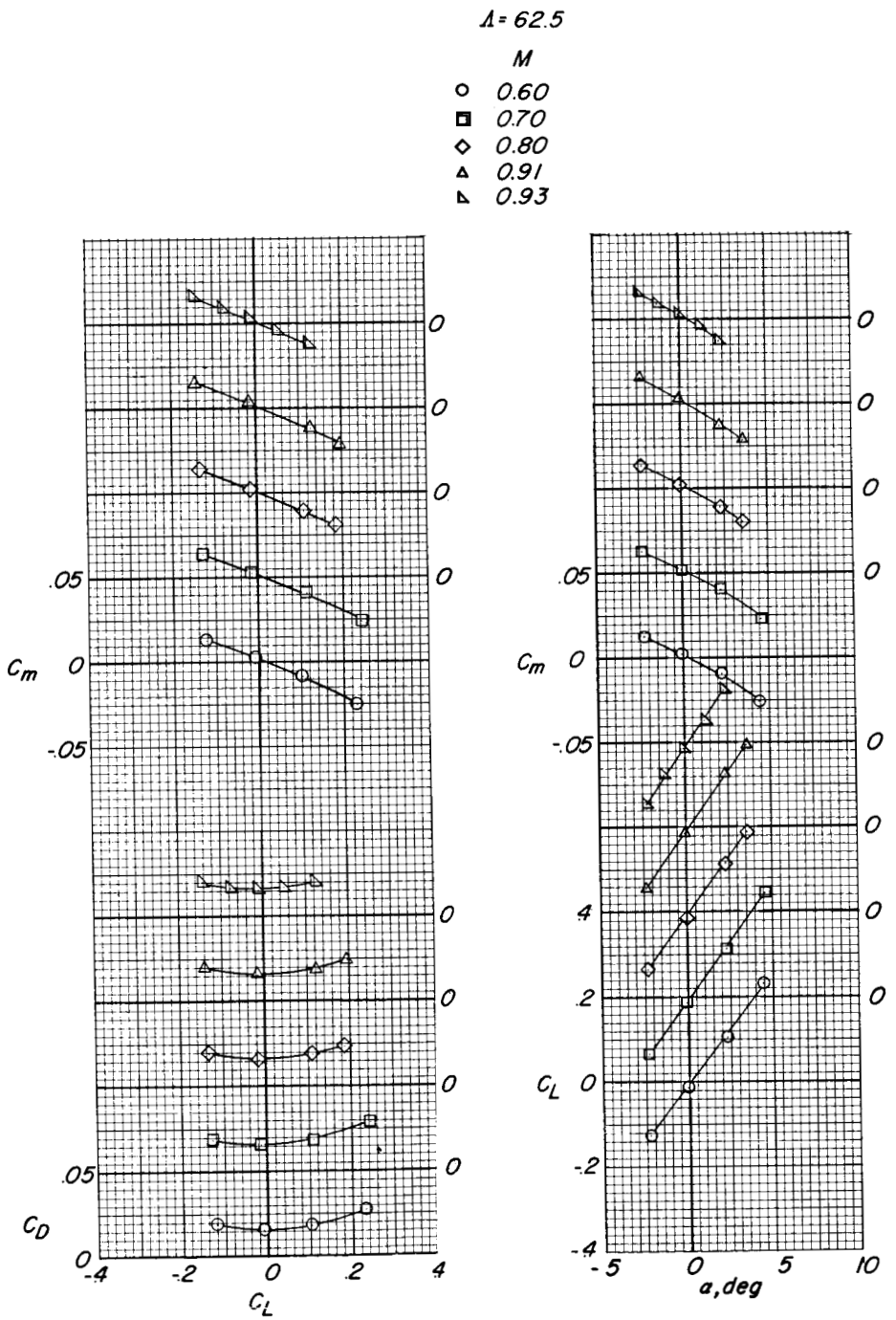

(d) $\Lambda = 62.5^{\circ}$; transition off.

Figure 20.- Continued.

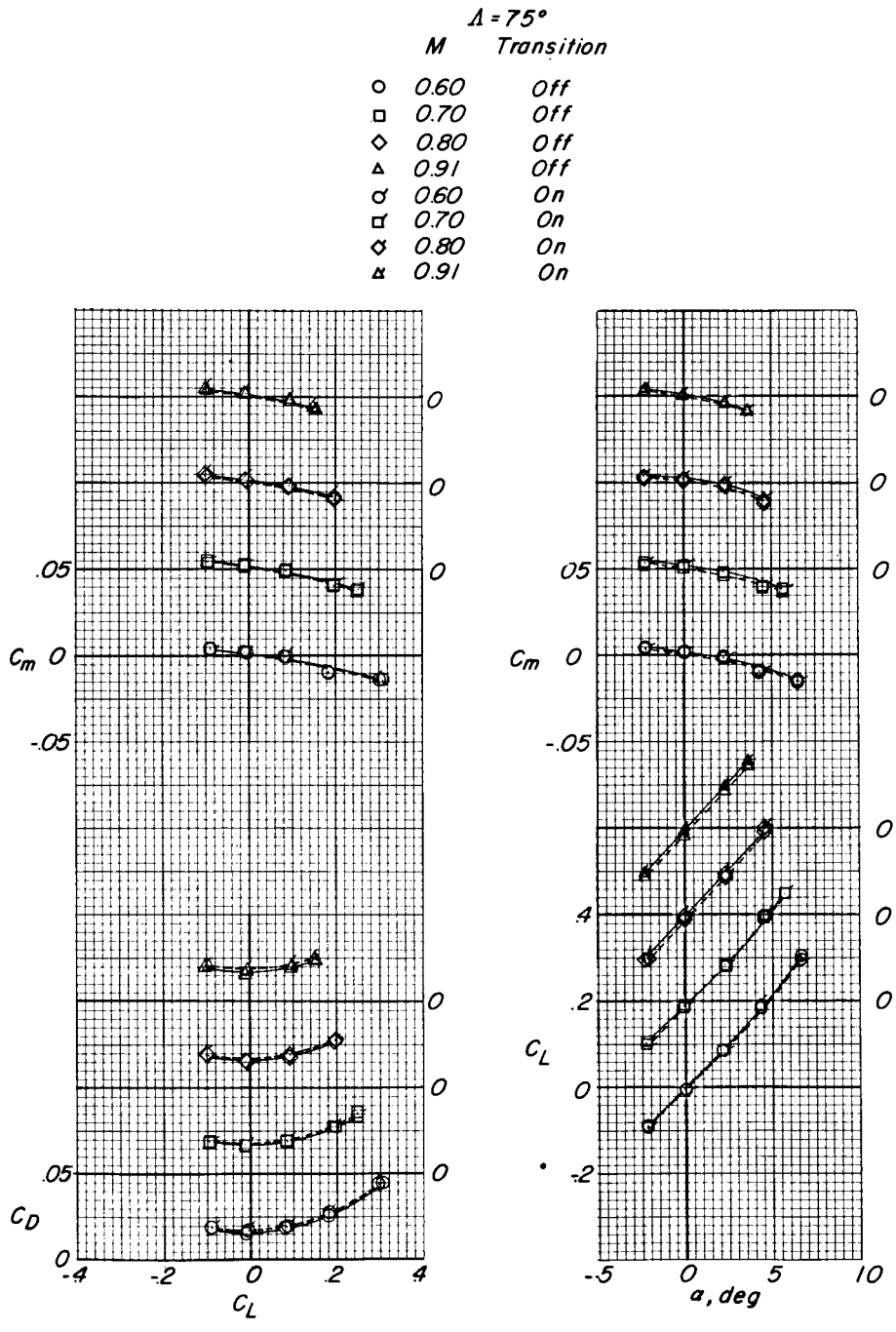

(e) Λ = 75°; transition on and off.

Figure 20.- Concluded.

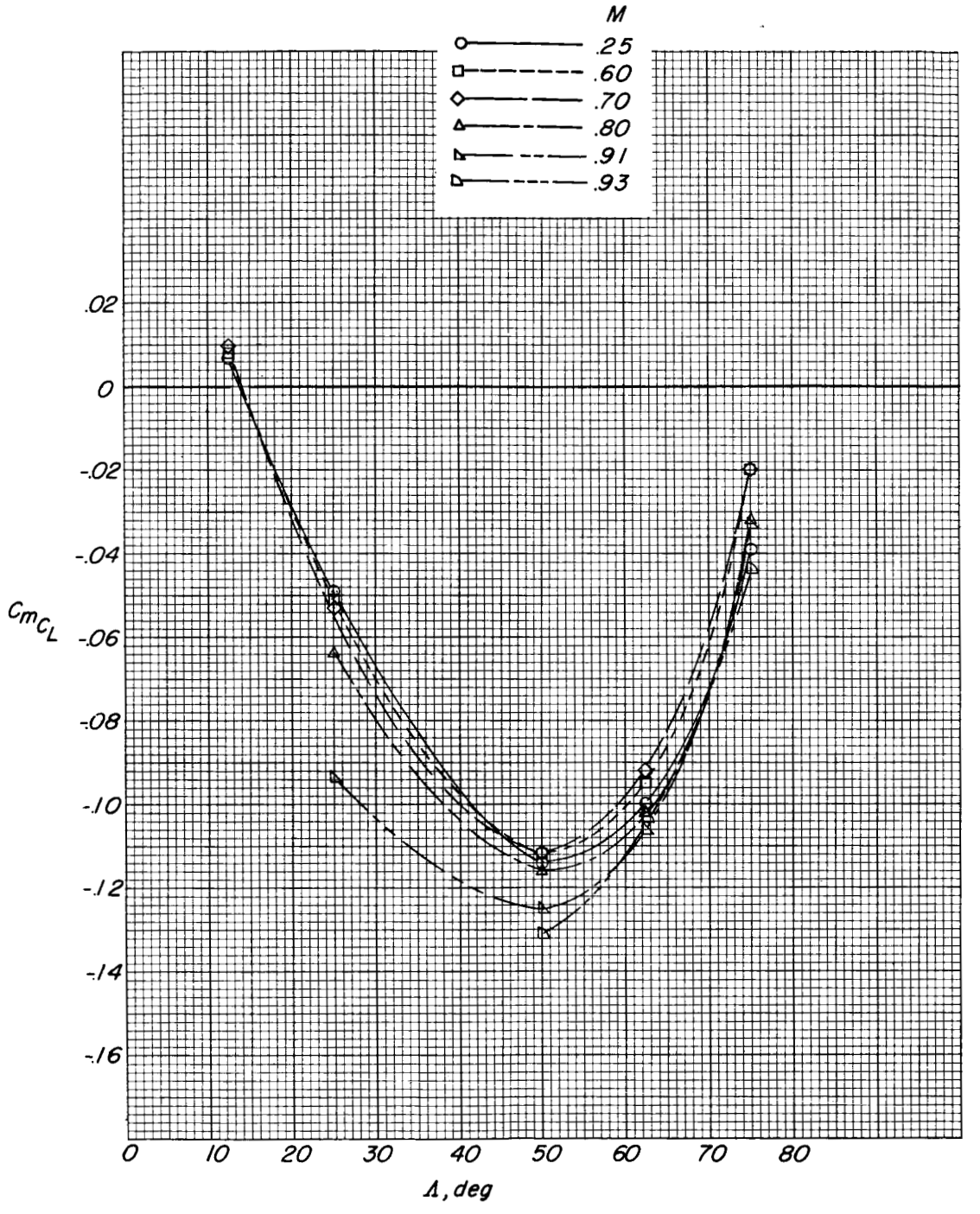

Figure 21.- Effect of wing leading-edge-sweep angle on the longitudinal stability for several Mach numbers.

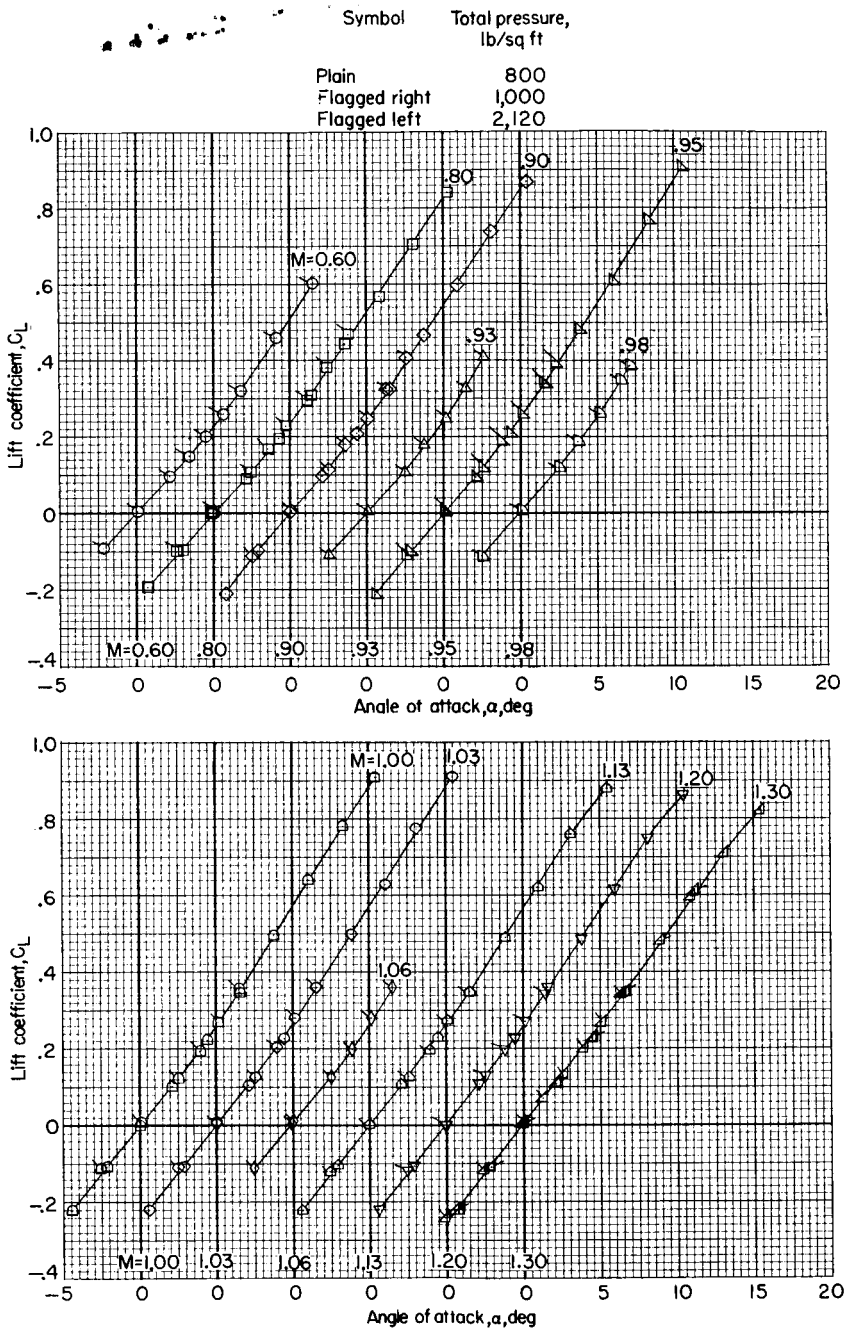

(a) C_L against α.

Figure 22.- Longitudinal aerodynamic characteristics. $\Lambda = 75^\circ$; $i_t = 0^\circ$; $\beta = 0^\circ$; Langley 8-foot transonic pressure tunnel.

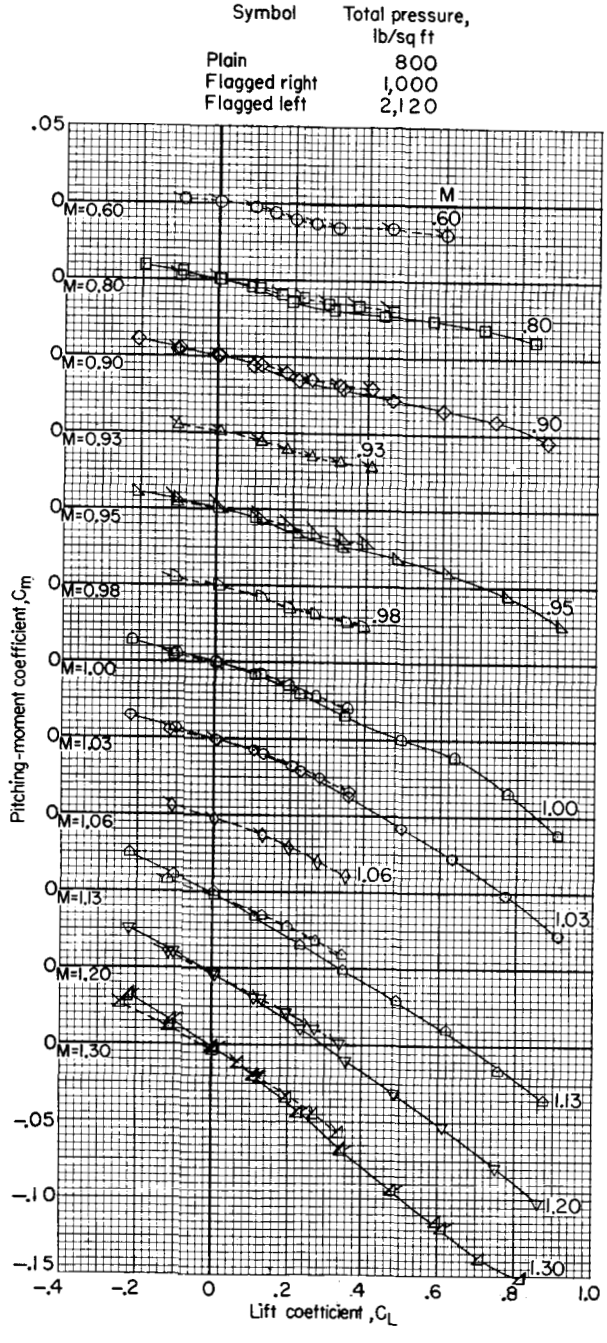

(b) C_m against C_L.

Figure 22.- Continued.

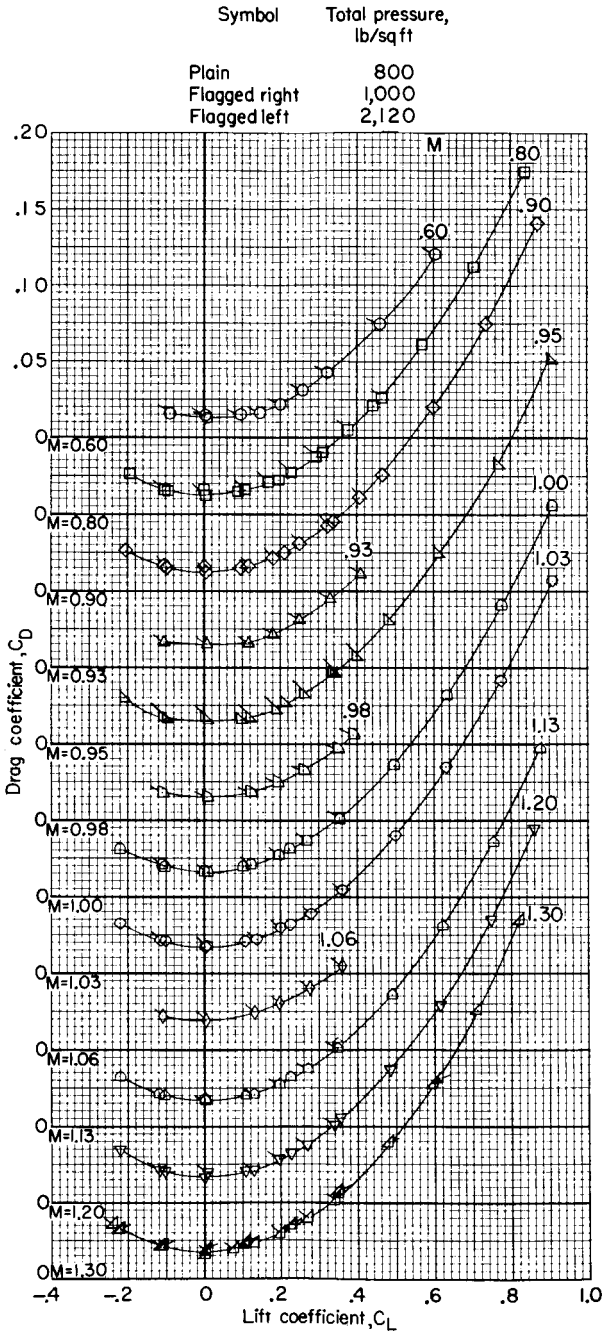

(c) C_D against C_L.

Figure 22.- Concluded.

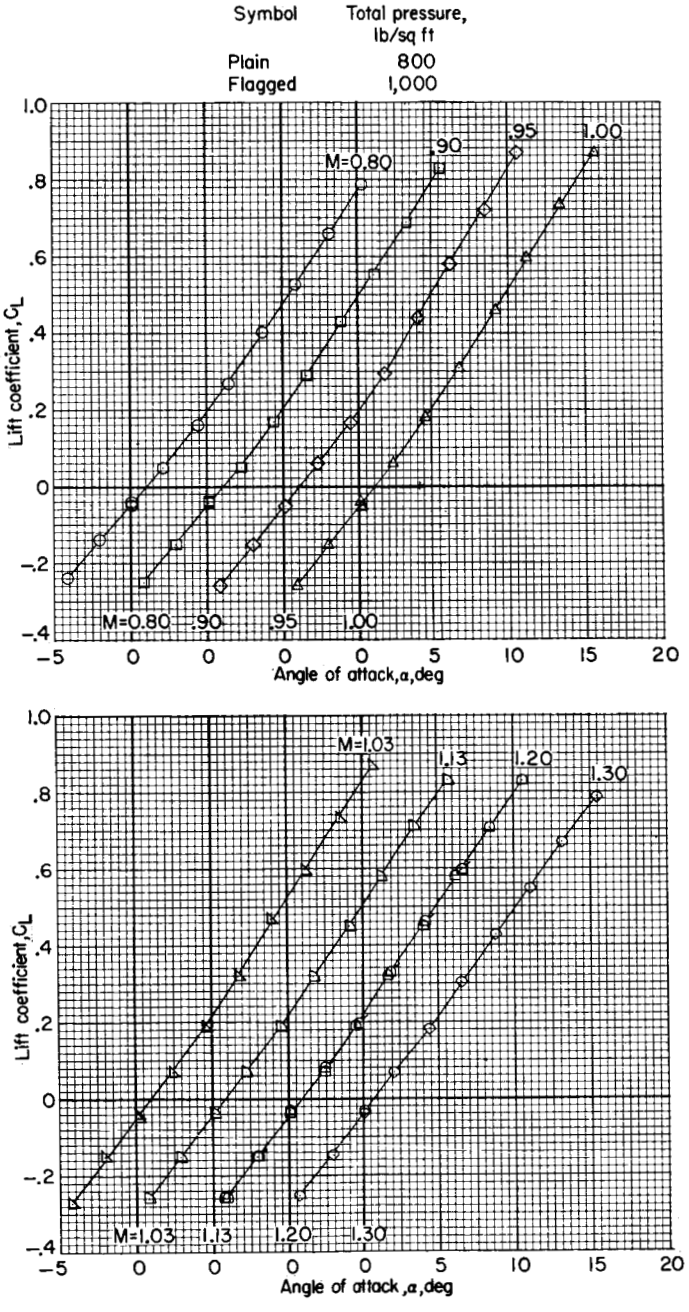

(a) C_L against α.

Figure 23.- Longitudinal aerodynamic characteristics. $\Lambda = 75^\circ$; $i_t = -5^\circ$; $\beta = 0^\circ$; 8-foot transonic pressure tunnel.

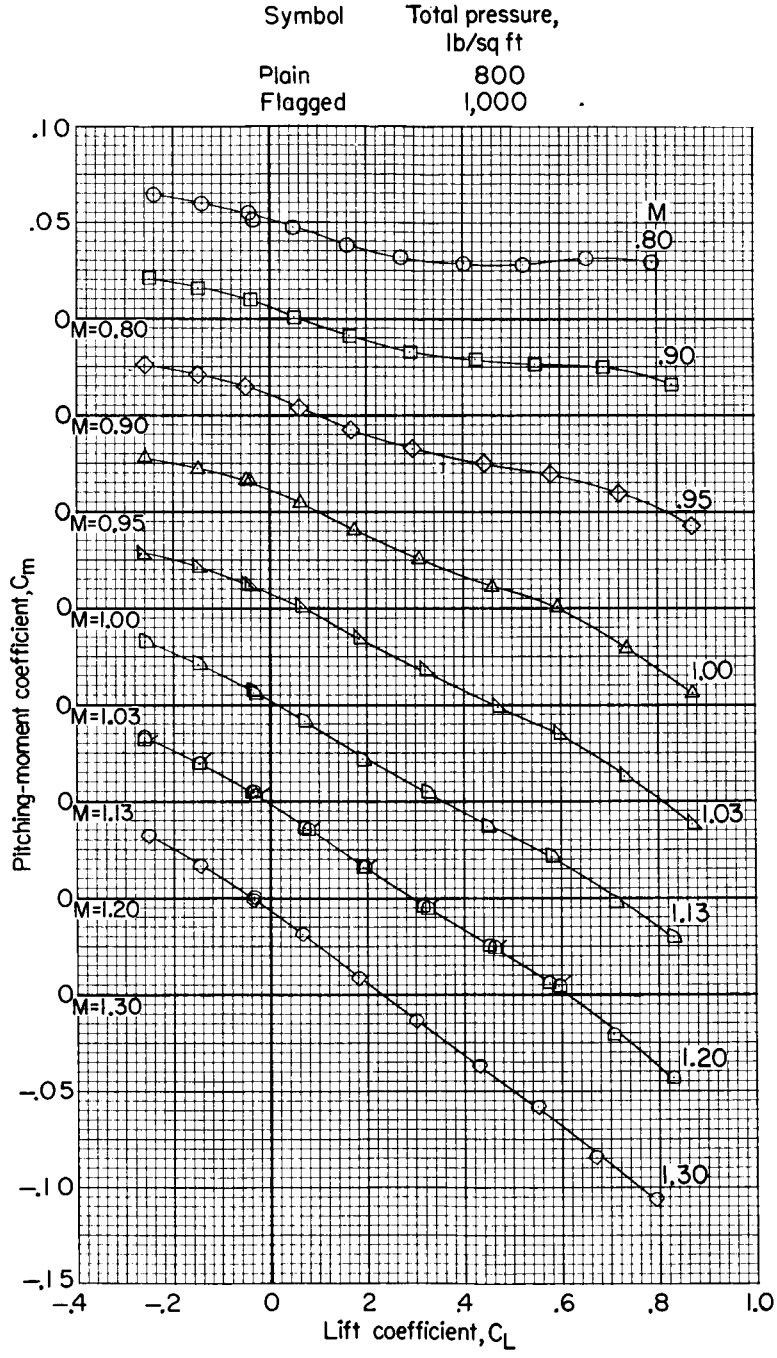

(b) C_m against C_L.

Figure 23.- Continued.

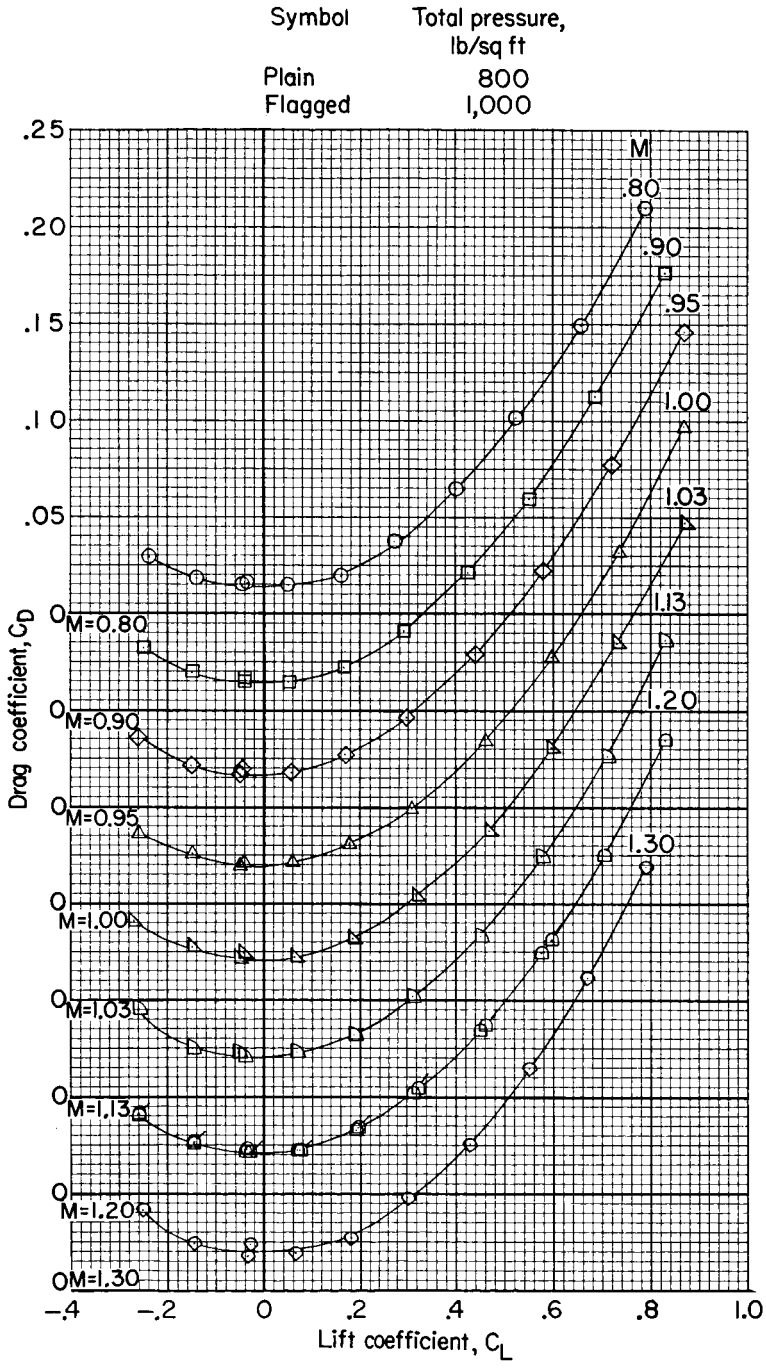

(c) C_D against C_L.

Figure 23.- Concluded.

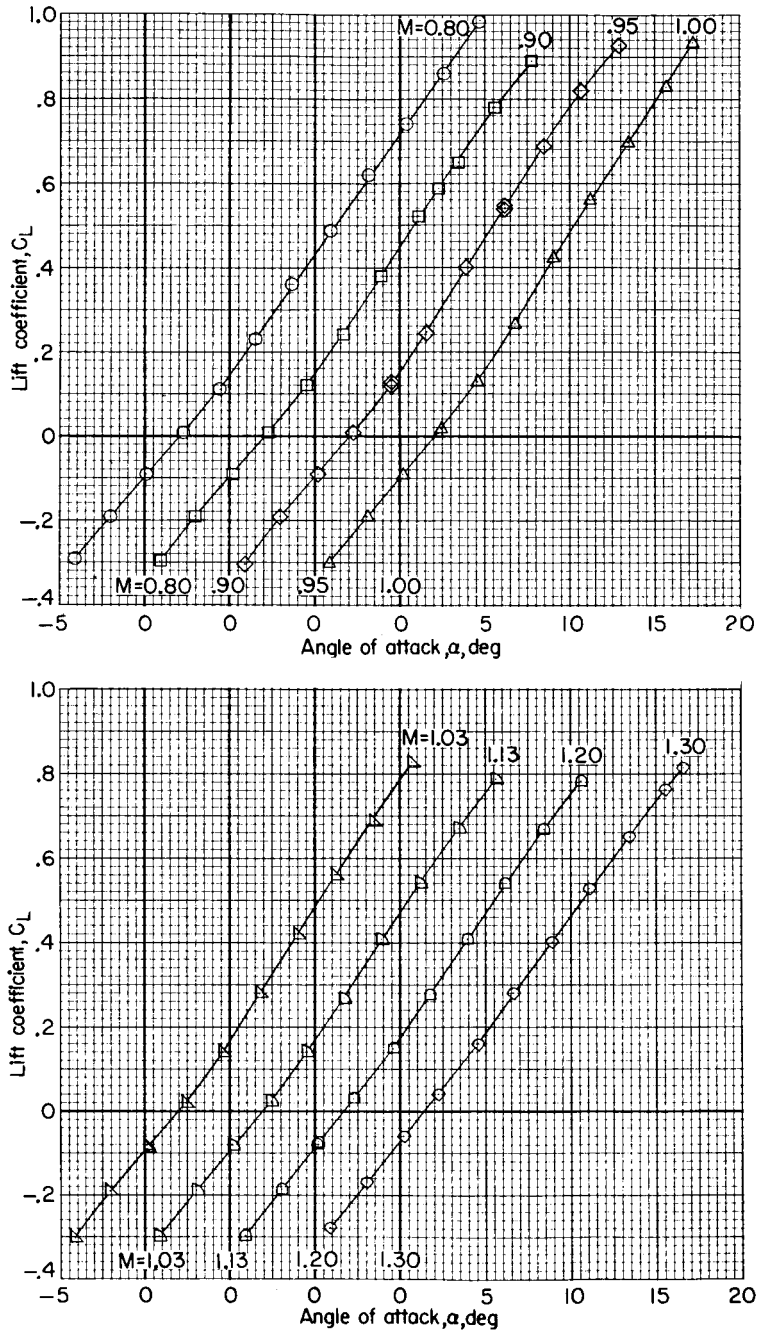

(a) C_L against α.

Figure 24.- Longitudinal aerodynamic characteristics. $\Lambda = 75^\circ$; $i_t = -10^\circ$; total pressure, 800 lb/sq ft; $\beta = 0^\circ$; 8-foot transonic pressure tunnel.

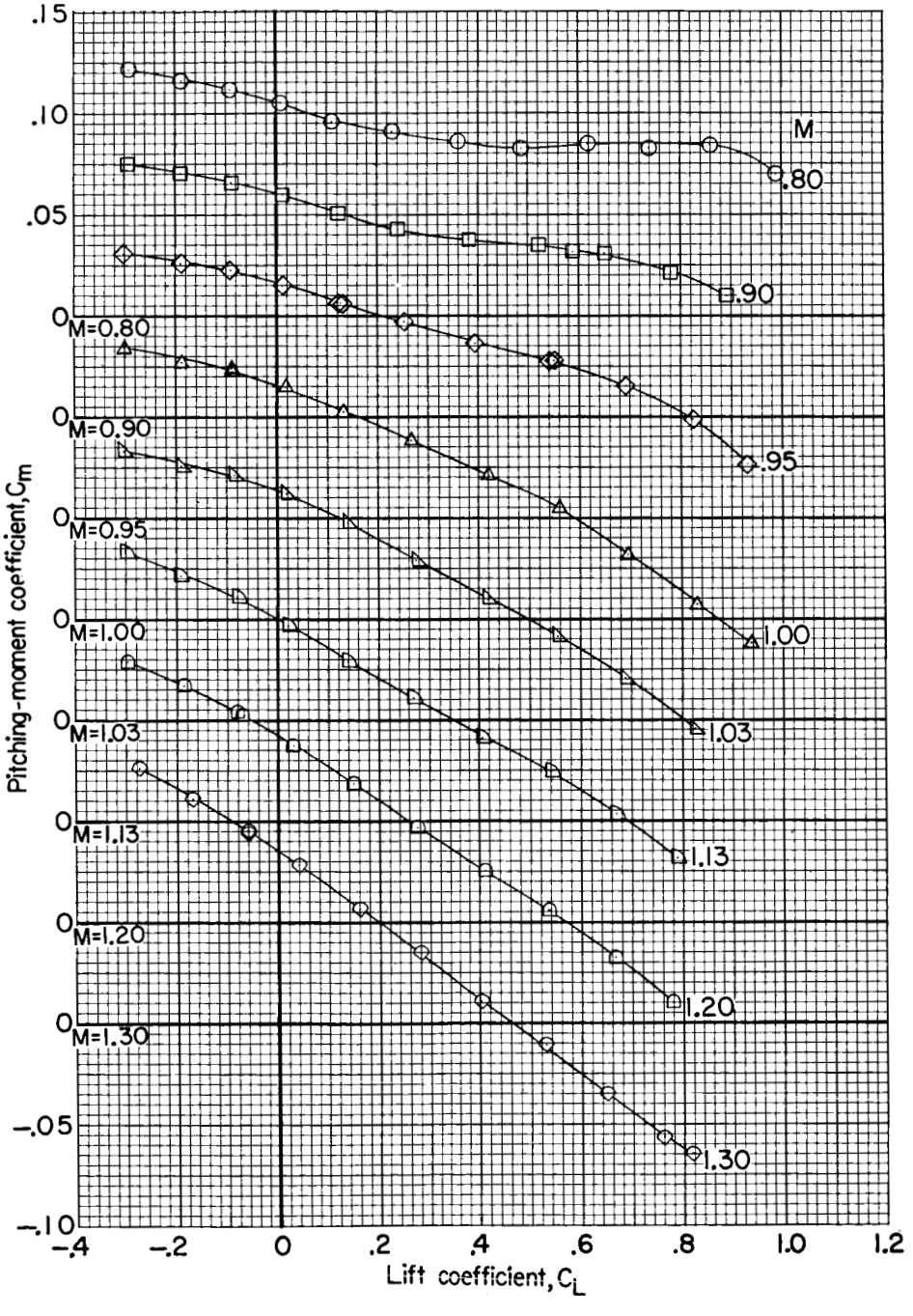

(b) C_m against C_L.

Figure 24.- Continued.

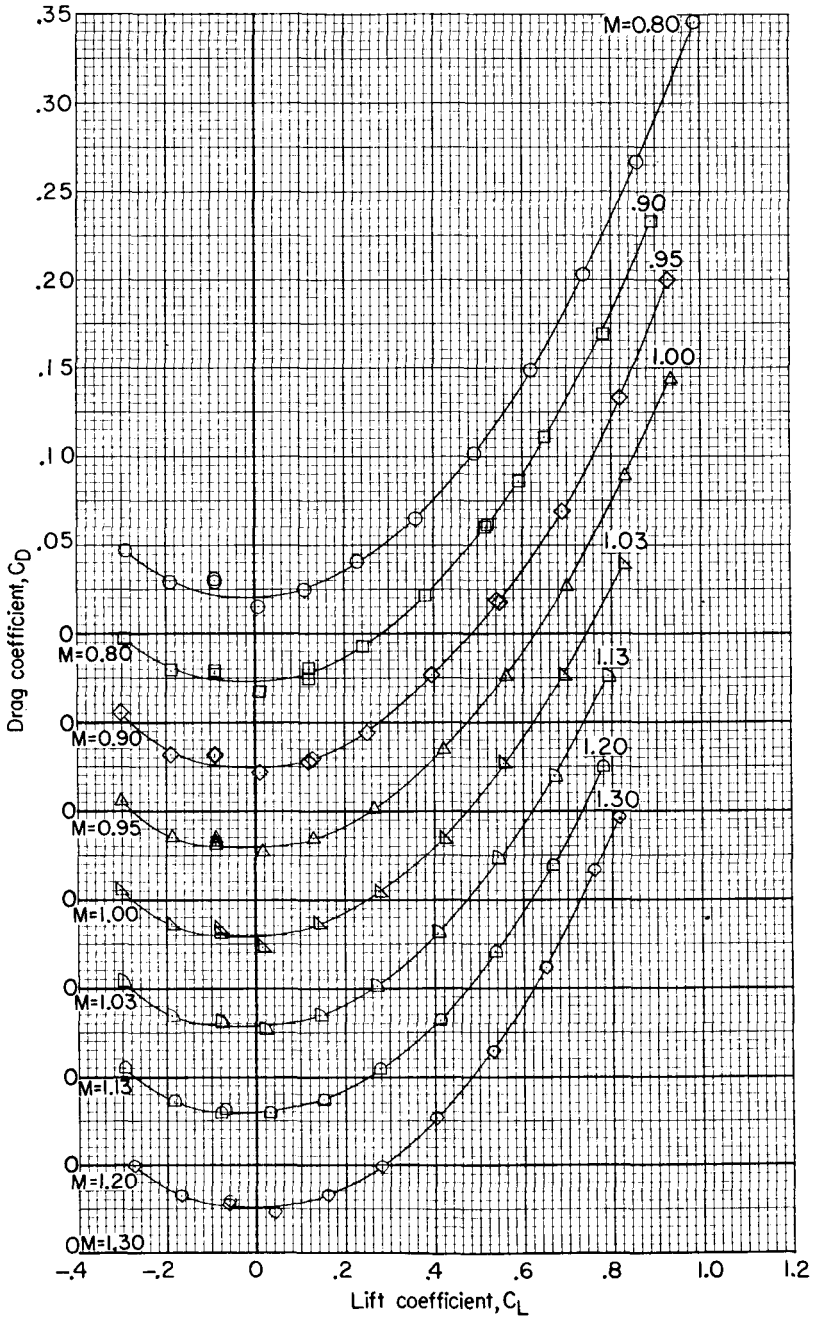

(c) C_D against C_L.

Figure 24.- Concluded.

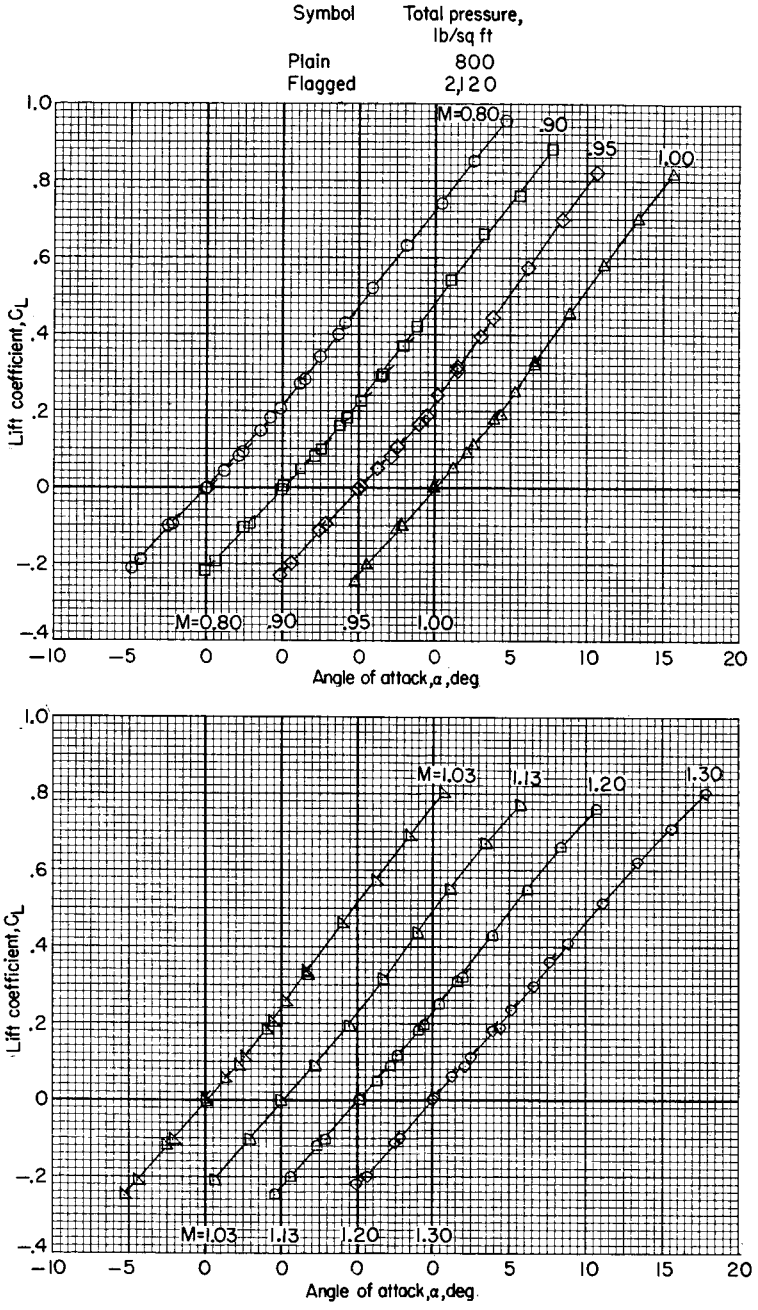

(a) C_L against α.

Figure 25.- Longitudinal aerodynamic characteristics. $\Lambda = 75^\circ$; horizontal tail off; $\beta = 0^\circ$; 8-foot transonic pressure tunnel.

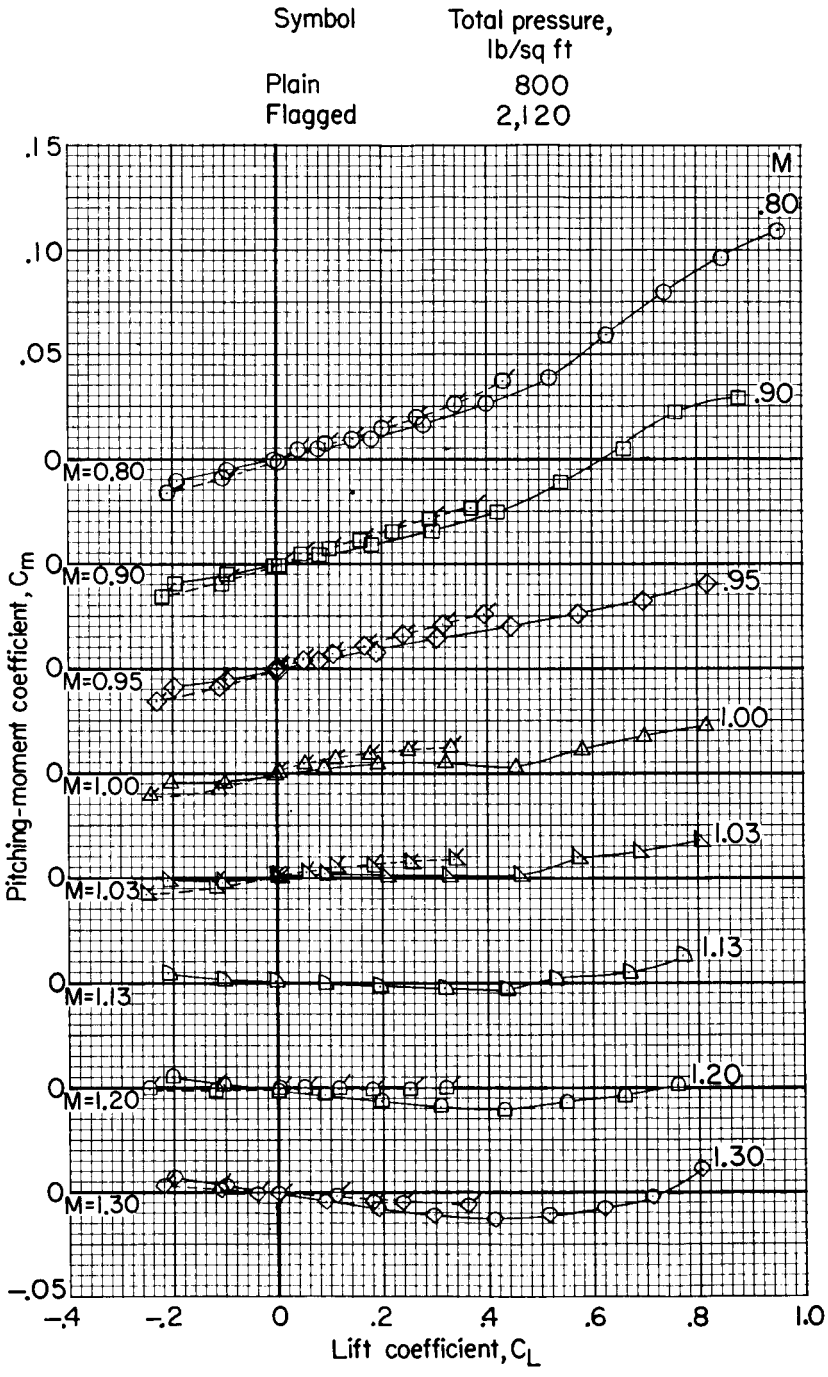

(b) C_m against C_L.

Figure 25.- Continued.

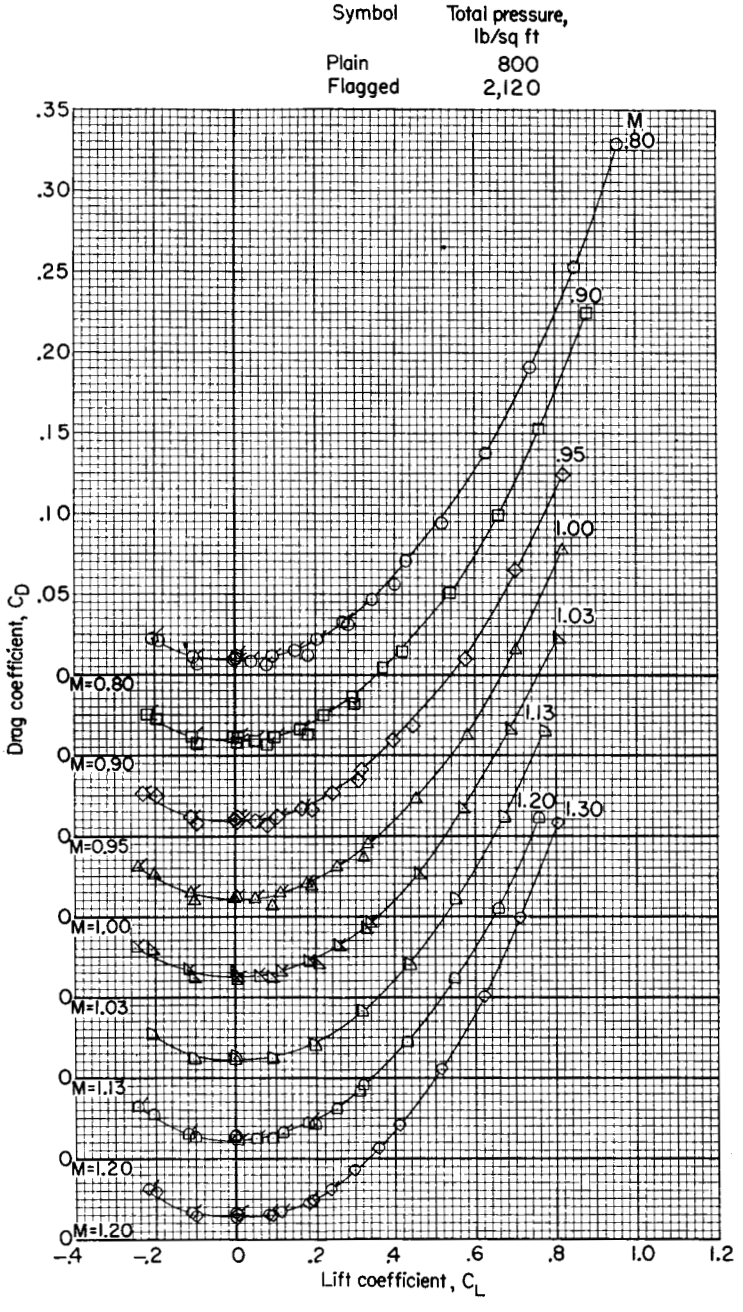

(c) C_D against C_L.

Figure 25.- Concluded.

[redacted]

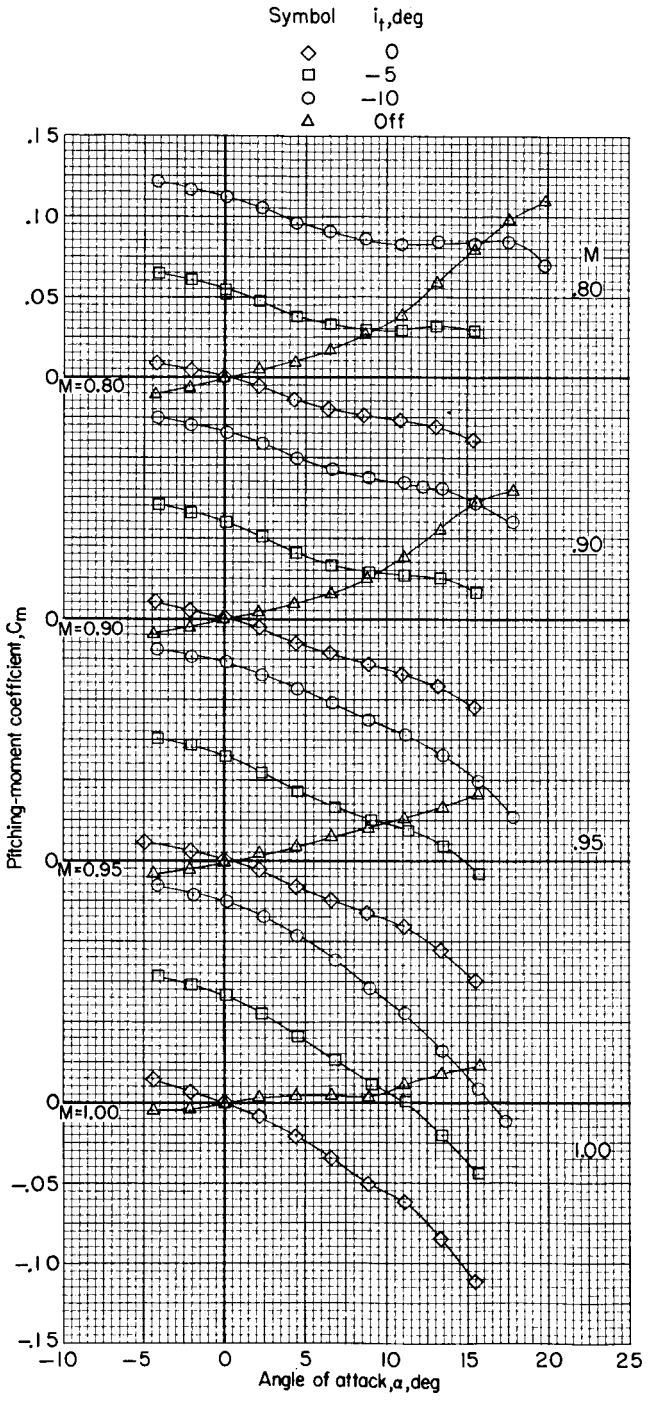

Figure 26.- Variation of pitching-moment coefficient with angle of attack at various horizontal-tail incidences. $\Lambda = 75^{\circ}$; $\beta = 0^{\circ}$; 8-foot transonic pressure tunnel.

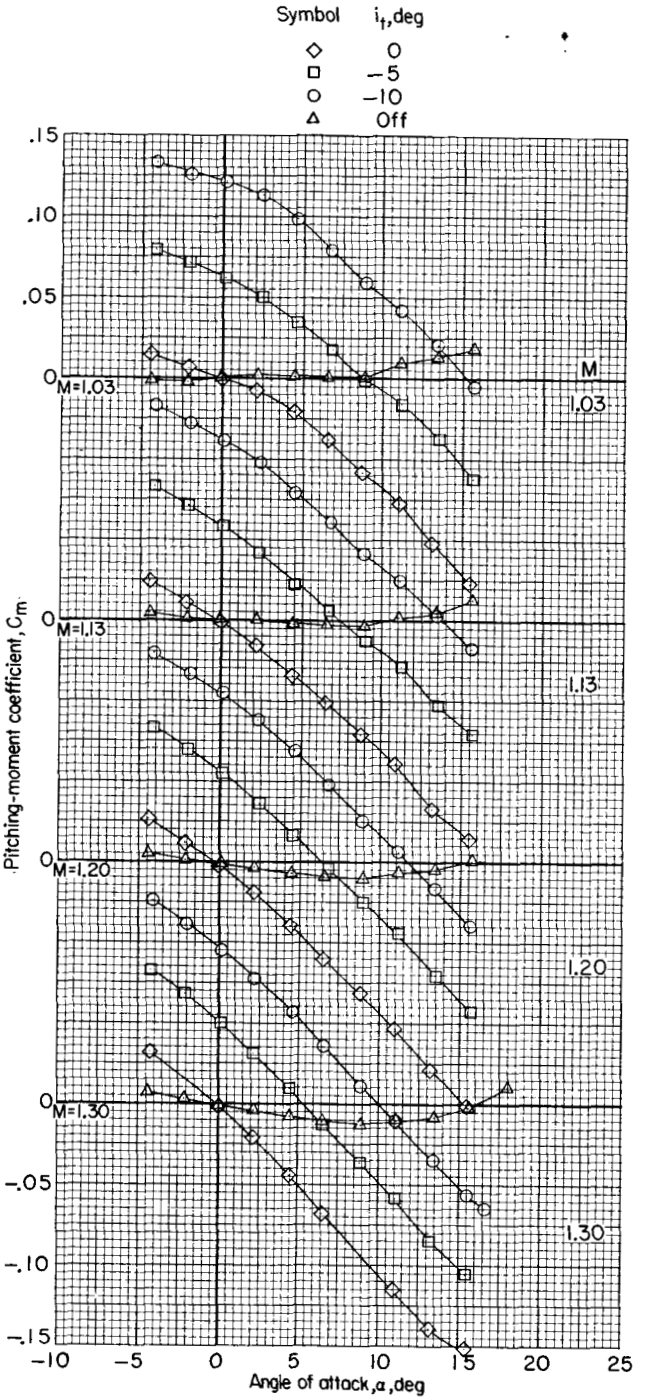

Figure 26.- Concluded.

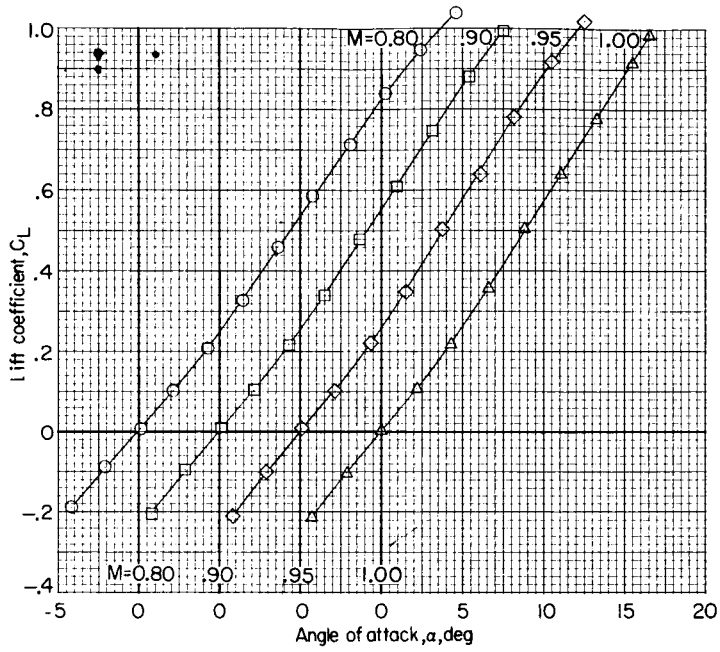

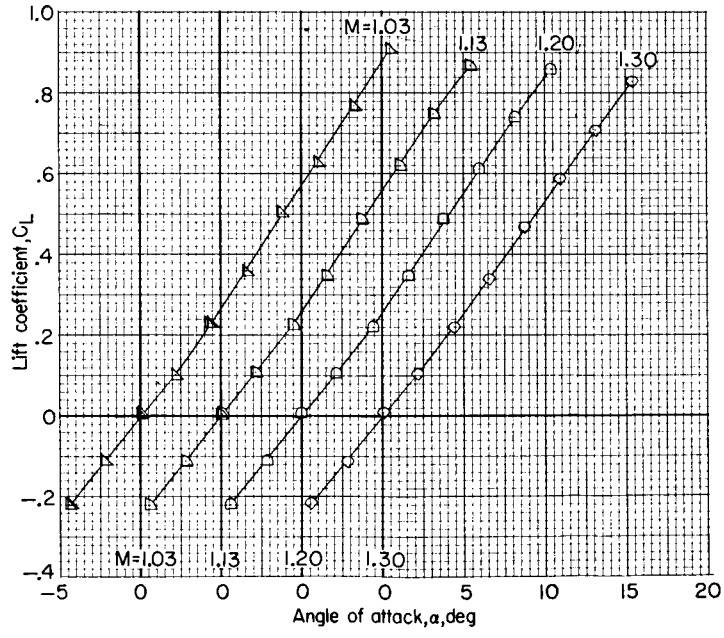

(a) C_L against α.

Figure 27.- Longitudinal and lateral aerodynamic characteristics. $\Lambda = 75^\circ$; $i_{t,L} = 5^\circ$; $i_{t,R} = -5^\circ$; total pressure, 800 lb/sq ft; $\beta = 0^\circ$; 8-foot transonic pressure tunnel.

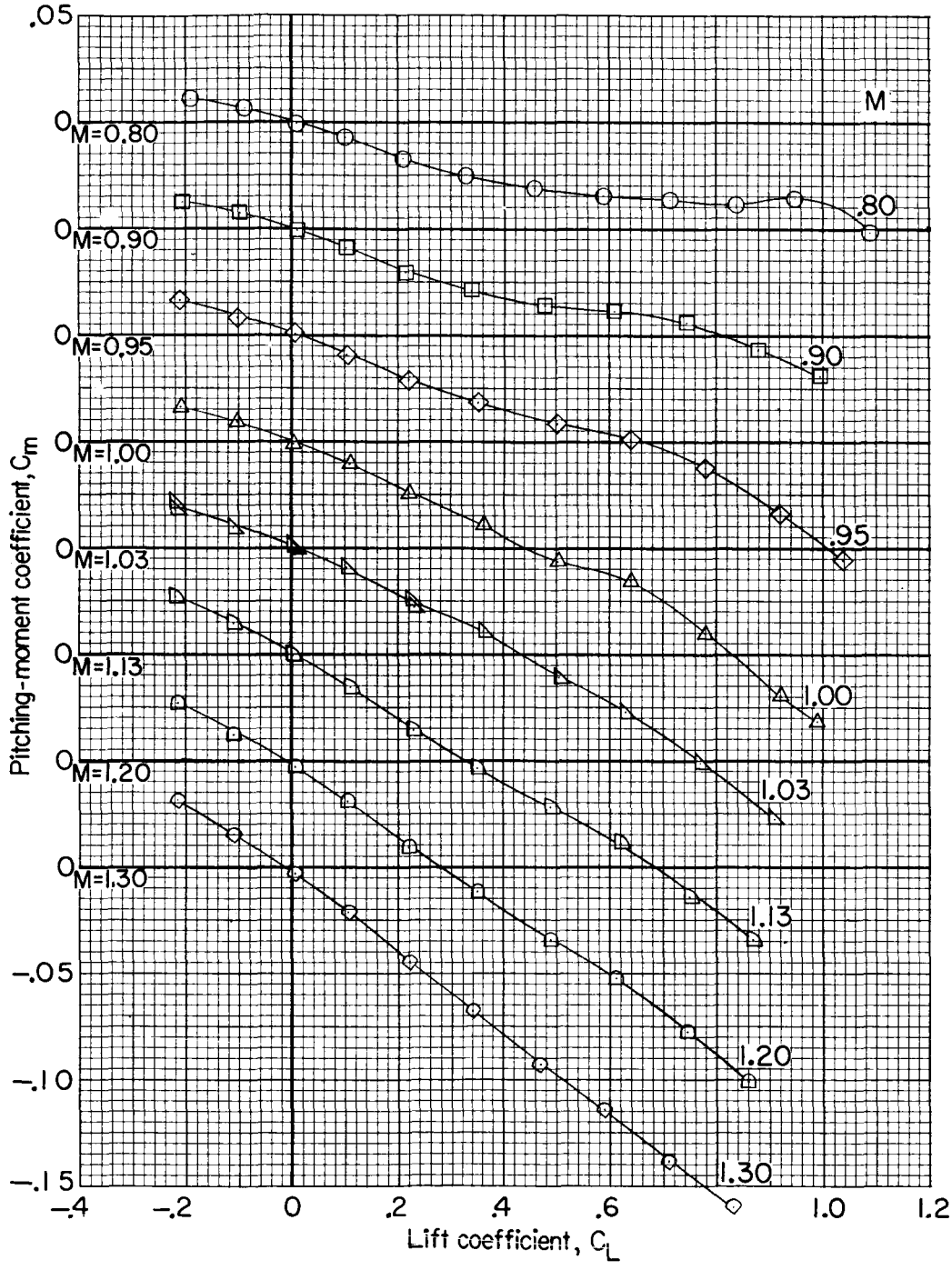

(b) C_m against C_L.

Figure 27.- Continued.

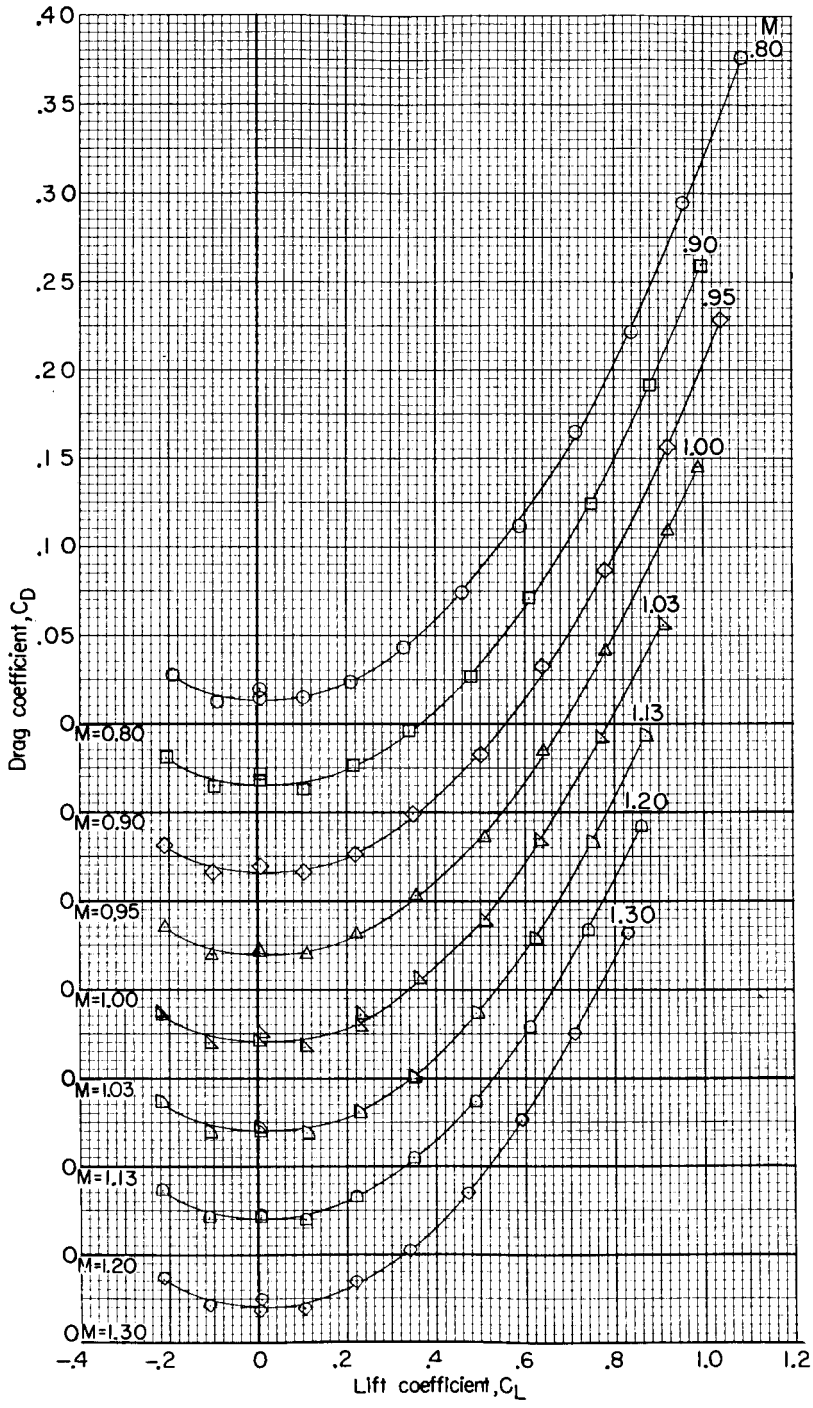

(c) C_D against C_L.

Figure 27.- Continued.

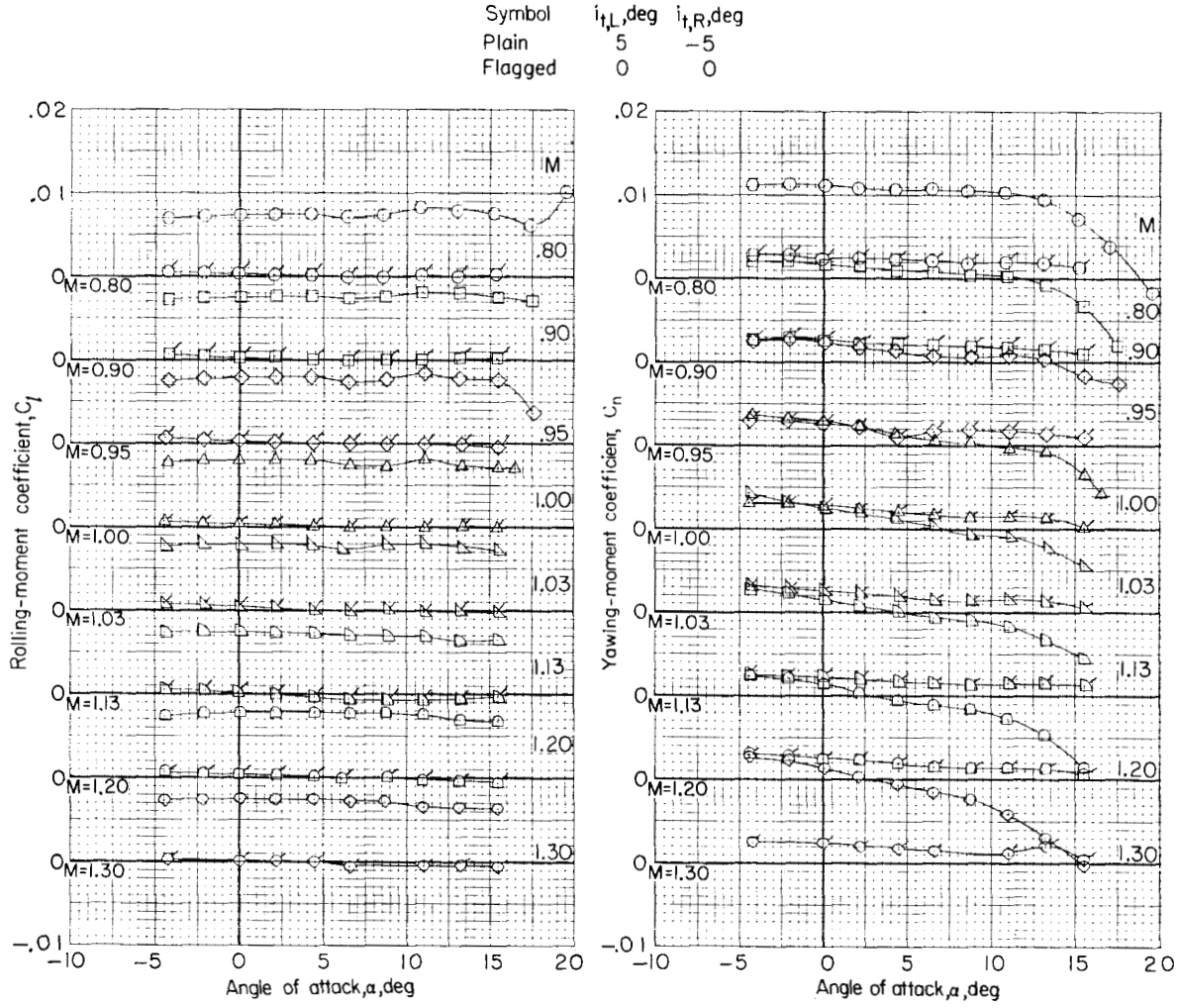

(d) C_l against α.

(e) C_n against α.

Figure 27.- Continued.

[redacted]

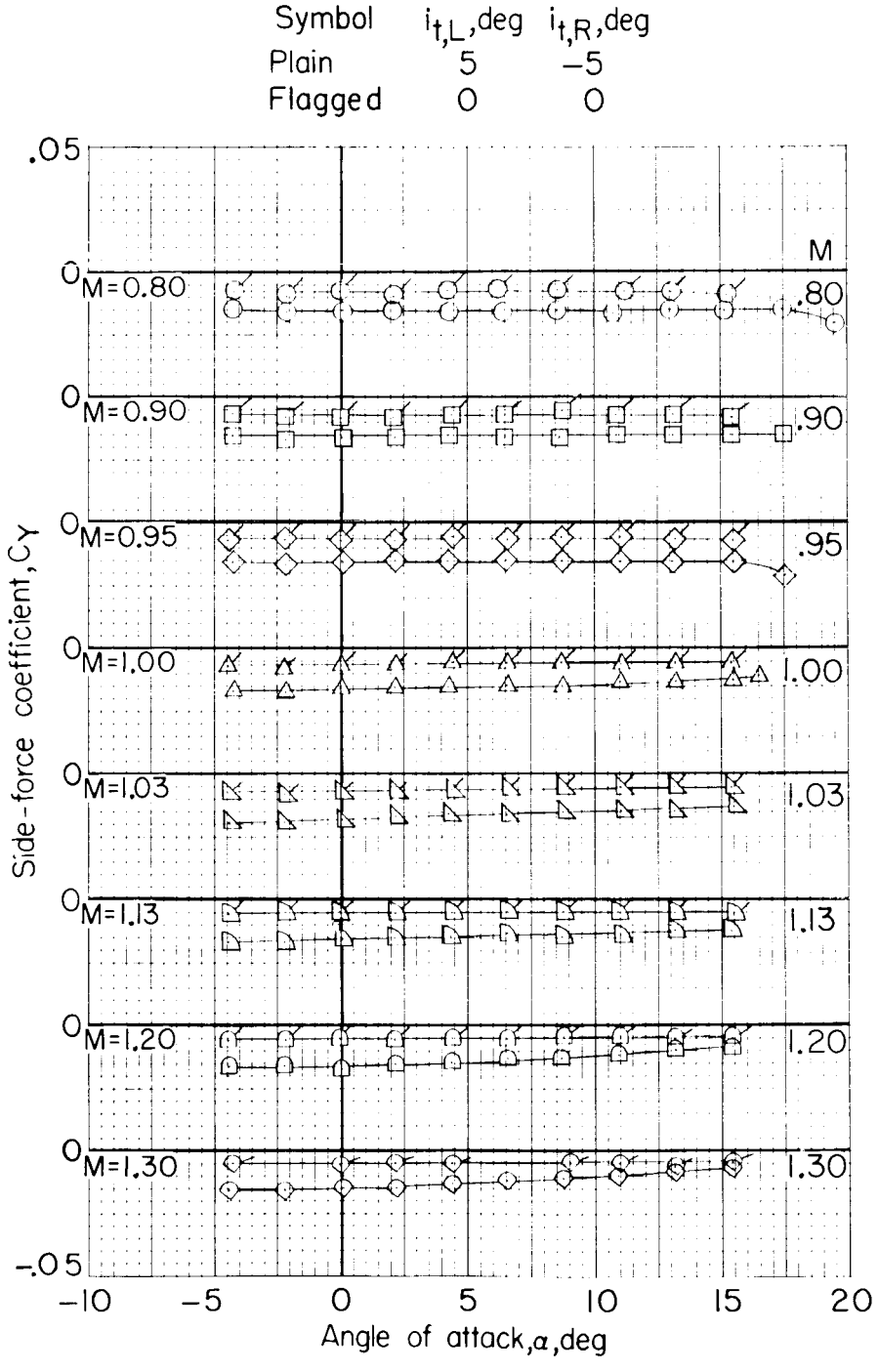

(f) C_Y against α.

Figure 27.- Concluded.

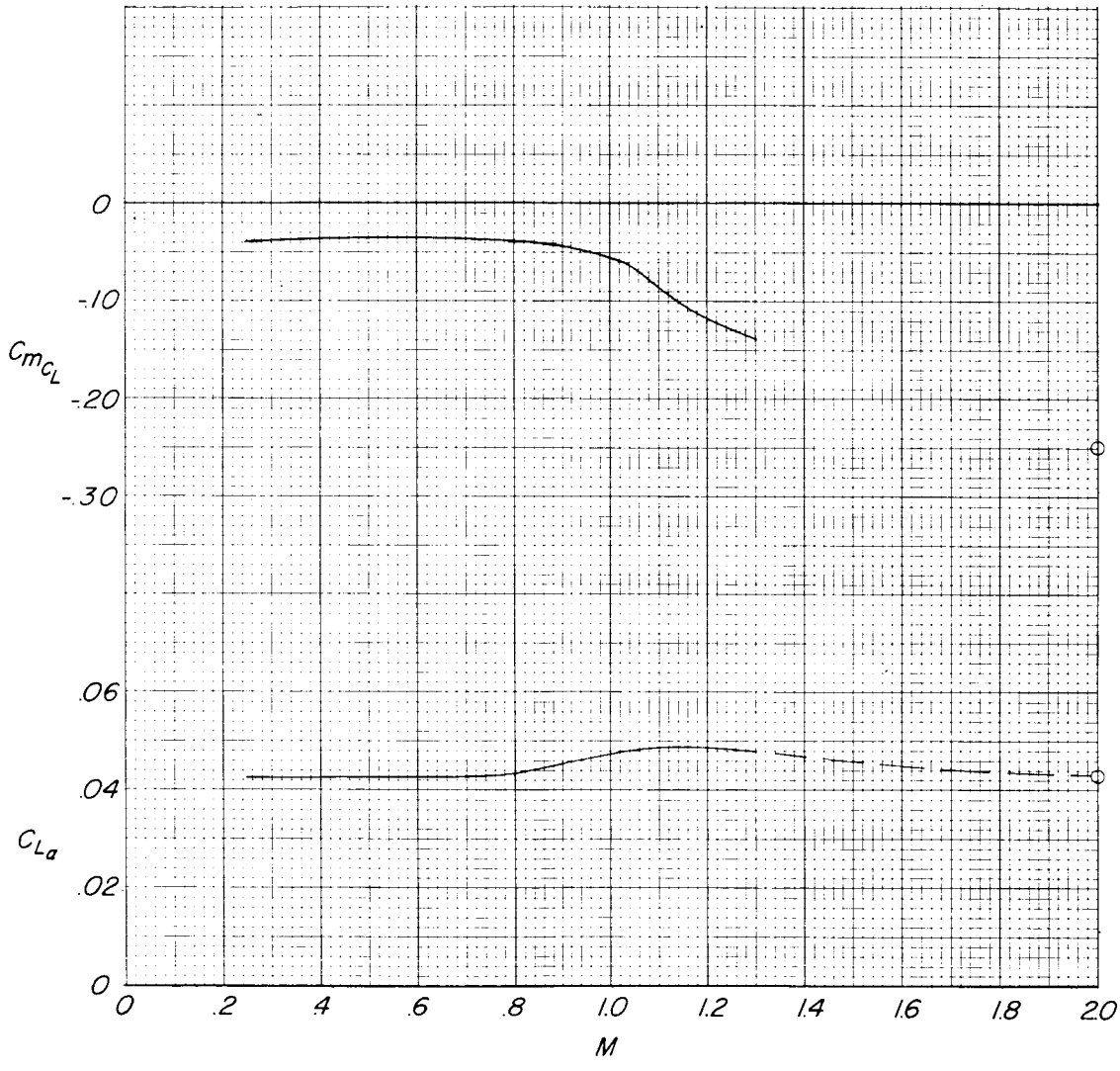

Figure 28.- Effect of Mach number on some of the longitudinal aerodynamic characteristics. $\Lambda = 75^{\circ}$.

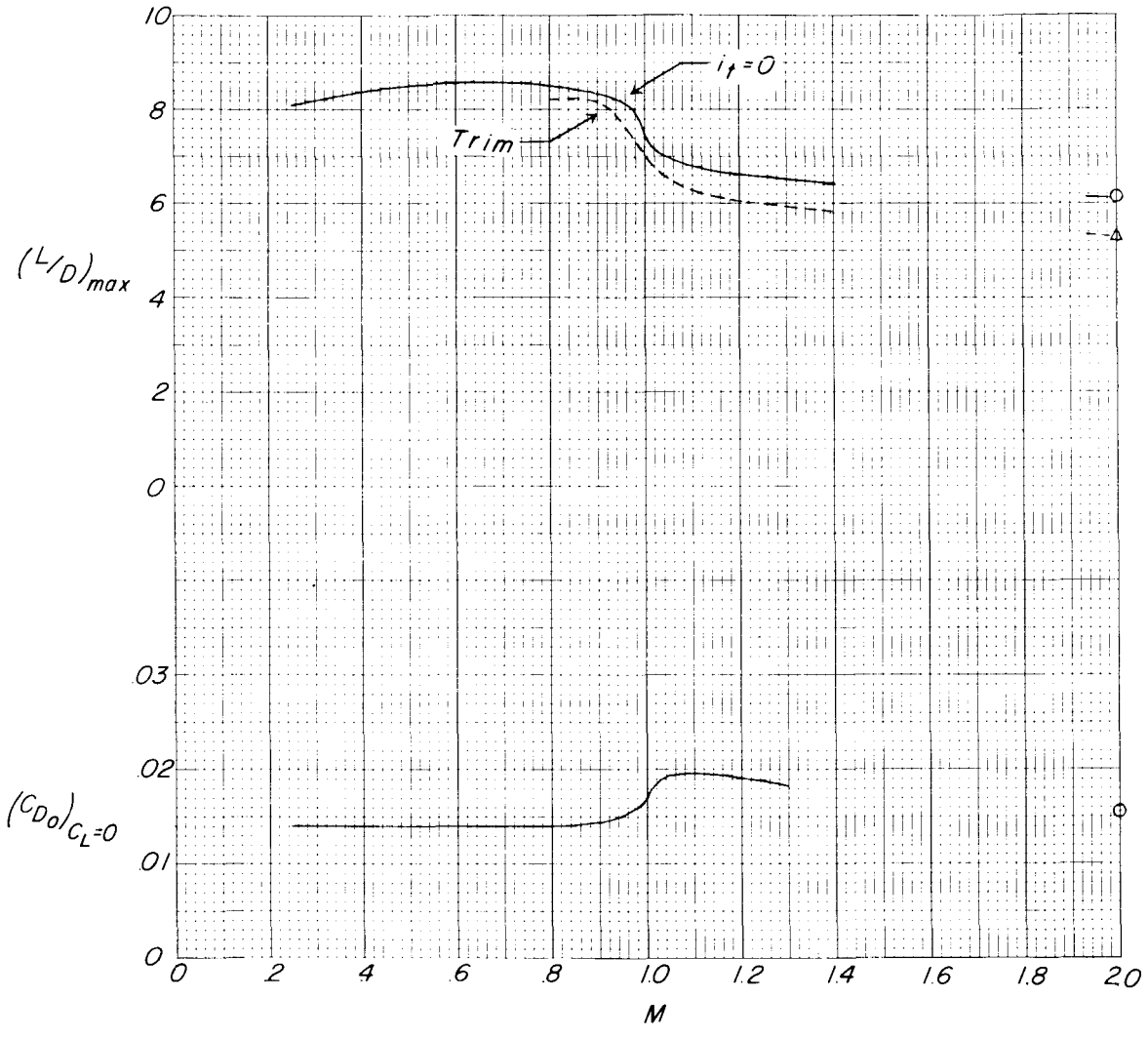

Figure 29.- Effect of Mach number on some of the longitudinal aerodynamic characteristics. $\Lambda = 75^{\circ}$.

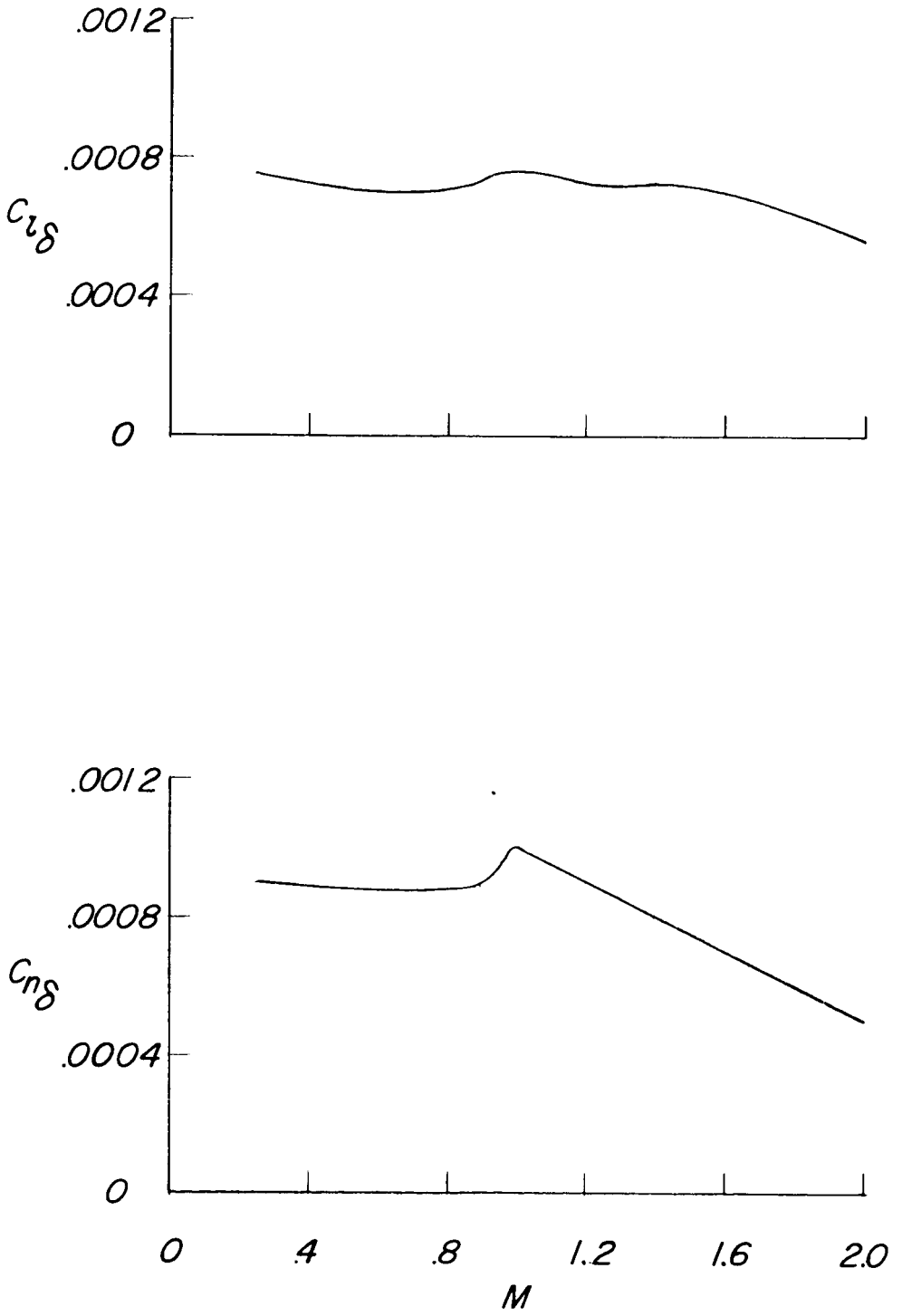

Figure 30.- Effect of Mach number on lateral control of differentially deflected horizontal tail. $\Lambda = 75^{\circ}$.